Production and Characterization of Bio-Oil and Biochar

from Fast Pyrolysis of Micro-Algae *Chlorella vulgaris*

A Thesis

Presented in Partial Fulfillment of the Requirements for the

Degree of Master of Science

with a

Major in Natural Resources

in the

College of Graduate Studies

University of Idaho

by

Farid Sotoudehniakarani

Major Professor: Armando G. McDonald, Ph.D.

Committee Members: Thomas M. Gorman, Ph.D.; Brian He, Ph.D.

Department Administrator: Charles Goebel, Ph.D.

December 2017

Authorization to Submit Thesis

This thesis of Farid Sotoudehniakarani submitted for the degree of Master of Science with a Major in Natural Resources and titled "Production and Characterization of Bio-Oil and Biochar from Fast Pyrolysis of Micro-Algae *Chlorella vulgaris*," has been reviewed in final form. Permission, as indicated by the signatures and dates below, is now granted to submit final copies to the College of Graduate Studies for approval.

Major Professor: _____ Date: _____
Armando G. McDonald, Ph.D.

Committee Members: _____ Date: _____
Thomas M. Gorman, Ph.D.

_____ Date: _____
Brian He, Ph.D.

Department
Administrator: _____ Date: _____
P. Charles Goebel, Ph.D.

Abstract

Microalgae cells are comprised of a complex mixture of compounds such as carbohydrates, lipids, and proteins. Their cellular structure makes microalgae suitable subjects for thermal conversion to bio-oil, synthesis gas, and biochar. In this work, commercial and University of Idaho cultured *Chlorella vulgaris* microalgae were pyrolyzed at various temperatures and their pyrolysis products were characterized and analyzed. The entire process was divided into three phases: (i) analysis of the biomass properties, (ii) thermochemical conversion of the biomass (pyrolysis), and (ii) analysis and characterization of the products. The thermal degradation behavior of algae was investigated using thermogravimetric analysis (TGA). Proximate, ultimate, fatty acid methyl ester and carbohydrates analyses, and pyrolysis-gas chromatography-mass spectrometry (GC-MS) were further employed to characterize the chemical components of algae. Pyrolysis was conducted at three different temperatures of 450, 500, and 550 °C. The highest biochar yield was 42% at 450 °C and the highest bio-oil yield was 47.7% at 550 °C.

The biochar physical and chemical properties were assessed using proximate and ultimate analysis, calorific values, specific surface area, butane absorption activity, Raman spectroscopy, and electron microscopy. Algae biochar was found to be mostly composed of condensed phenolic compounds and majorly disordered amorphous carbon. The bio-oil was characterized by the combination of GCMS, high-pressure liquid chromatography (HPLC), and electrospray ionization mass spectrometry (ESI–MS). Lipids (fatty acids), carbohydrates, nitrogen-containing compounds, and aromatic hydrocarbons were abundantly found in the algae bio-oil.

Acknowledgements

This accomplishment would have been impossible without all the support I have been given along the way. My deepest gratitude goes to my advisor, Dr. Armando McDonald. I feel very fortunate to have had the opportunity to work with him. I could not have asked for a more understanding, knowledgeable, and supportive advisor. I would also like to express my sincere appreciation to my committee members, Dr. Brian He and Dr. Thomas Gorman, who provided great insight and guidance during my academic journey. I would also like to acknowledge Timothy Jackson, who has provided me with unparalleled support both as a friend and as my non-academic supervisor. Last but not least, I would like to thank my wife, Hanieh, for her encouragement and support throughout this journey.

Table of Contents

List of Tables

List of Figures

Chapter 1: Introduction and Literature Review

1.1 Introduction

The human population has been rapidly growing in the past century. Because of this rapid growth, energy demand is projected to increase by 50% or more by the year 2030 [1]. The use of petroleum will not keep up with the current consumption rate, but it also is harmful to the environment through the release of greenhouse gas emissions that ultimately contribute to global warming [1]. To overcome these problems, researchers have focused on alternative renewable and sustainable energy technologies worldwide. Extensively researched alternatives to petroleum fuels include solar energy, wind energy, hydro energy, and biomass energy. Among all these alternatives, biomass energy has exhibited the most favorable and promising properties to replace petroleum-derived fuels [2].

Liquid fuels derived from biomass, also known as biofuels, are a potential alternative to reduce dependence on fossil fuels. Biofuels are renewable energy resources and contribute very little to the production of greenhouse gases. Identifying suitable biomass species and technologies that can provide high-energy outputs to replace conventional fossil fuels has become the focus of many researchers in recent years [3]–[5]. Biomass resources include wood, wood wastes, energy crops, aquatic organisms (algae and microalgae), agricultural crops and their waste by-products, municipal wastes, and animal wastes. Many methods are currently used and studied for the conversion of biomass to biofuels. These methods include biochemical conversion to ethanol in food crops such as wheat, biodiesel production through trans-esterification of triglycerides from vegetable oils, and thermochemical conversion methods such as pyrolysis, gasification, and liquefaction [6]–[15].

Biofuels obtained through thermochemical conversion of biomass have shown to be one of the most viable alternative renewable energy resources [16]. Among biofuels produced from various biomass resources, biofuels obtained from algae have exhibited properties that make them suitable to be the main source of renewable biodiesel that can potentially eliminate the worldwide demand for transport fuels [17].

Algae are among the quickest developing organisms on the planet, and up to 80 of their dry weight is made up of oil [18]. Their rapid growth and high carbon fixing efficiency make them promising feed-stocks for biofuels development [19]. The per unit zone yield of oil from the green growth of algae is assessed to be between 20,000 and 80,000 L per acre per year; this is 7–31 times more yield than the next best potential resource, palm oil [17]. While green growth that predominantly yields oil is used for biodiesel generation, green growth that yields sugar as its main product is used to deliver ethanol. Microscopic algae, from here on referred to as microalgae, can be converted to bio-oil, bioethanol, bio-hydrogen, and bio-methane using thermochemical and biochemical systems [20]. Due to their relatively high energy output, ease of production and manipulation, and photosynthetic efficiency, microalgae have proven to be a promising and desirable resource for future energy supply [21].

Microalgae can be converted to liquid bio-oil, biochar, and gaseous products through pyrolysis [22]. Pyrolysis of algae, in general, is a promising way to extract oil by converting protein and carbohydrate to biofuels. Fast pyrolysis can generate a greater amount of high-quality bio-oil by continuous processing of microalgae [16].

In recent years, fast pyrolysis of biomass has attracted a great deal of attention for maximizing liquid yields and has been the topic of much research. Through fast pyrolysis, the

production of bio-oil can be maximized up to a 72% yield. However, the main focus of most of the conducted research has been on fast pyrolysis of lignocellulosic materials rather than microalgae [23].

1.2 Literature Review

1.2.1 Algae

Macroalgae and microalgae are photosynthetic organisms that grow in aquatic environments. Macroalgae are classified according to their pigments into three main categories: green seaweed (*chlorophyceae*), brown seaweed (*phaeophyceae*), and red seaweed (*rhodophyceae*) [24]. They can grow quickly and reach a length of 60 min salt or fresh water [17]. Microalgae are primitive single cell photosynthetic organisms that are classified according to their life cycle, cellular structure, and pigmentation. They, also, are able to grow in marine and freshwater habitats [25]. Microalgae can grow in various cultivation conditions. In a photoautotrophic culture, microalgae use light as their energy source and inorganic carbon as their carbon source in order to photosynthesize. In heterotrophic cultures, microalgae grow in darkness and use organic carbon such as glucose or acetate as both their energy and carbon source for photosynthesis [17], [26]. Microalgae have a simple cellular structure with the ability to absorb lots of nutrients because of their large surface area-to-volume ratio. These small plant-like organisms are highly efficient in comparison to land-based plants due to their access to CO_2, nutrients, and water in an aquatic environment [27]. For optimal growth, microalgae need to have access to many essential inorganic elements such as iron, phosphorus, nitrogen, and silicon. Depending on the species, 2 to 40% of algae weight can be comprised of lipids that can be used as a source of energy [28]. The scientific

classification and microscopic image of microalgae used for this study, *C. vulgaris,* are shown in Table 1.1 [29], [30].

Table 1.1 Classification of *Chlorella* species and optical micrographs of *C. vulgaris* [29], [30]

SCIENTIFIC CLASSIFICATION		MICROSCOPIC IMAGES
Domain	Eukaryota	
Kingdom	Viridiplantae	
Division	Chlorophyta	
Class	Trebouxiophyceae	
Order	Chlorellales	
Family	Chlorellaceae	
Genus	Chlorella	
SPECIES		
Chlorella autotrophica		
Chlorella minutissima		
Chlorella pyrenoidosa		
Chlorella sorokiniana		
Chlorella variabilis		
Chlorella vulgaris		
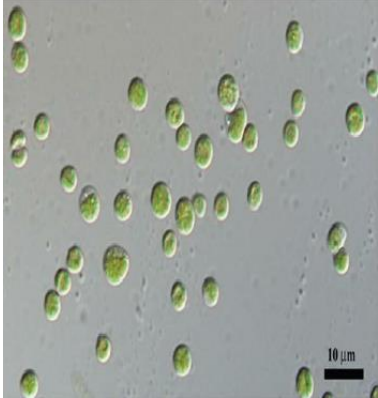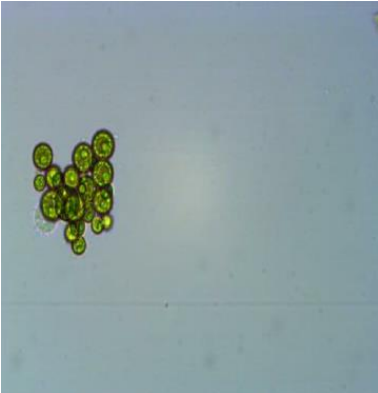
1.2.2 Algae production technology

According to Demirbas et al., a large portion of the algal species are phototrophs, hence requiring light for their development [17]. The phototrophic microalgae are most commonly developed in open lakes and photo-bioreactors. Biofuel generation expenses can

shift by altering the feedstock type and size and changing procedures. It is expected that green growth becomes the most viable biofuel source in the near future [17].

In order to mass-produce biofuels and improve production yield, it is necessary to have large amounts of pure strain algal biomass. Therefore, cultivating microalgae in controlled environments is the first crucial step. On an industrial scale, microalgae are produced in three type of reactors: open ponds, photo-bioreactors, and hybrid systems [17].

Figure 1.1 shows the algal biofuel production chain. The major concerns in this process are strain isolation, nutrient sourcing and utilization, production management, harvesting, coproduct development, fuel extraction, refining, and residual biomass utilization [31].
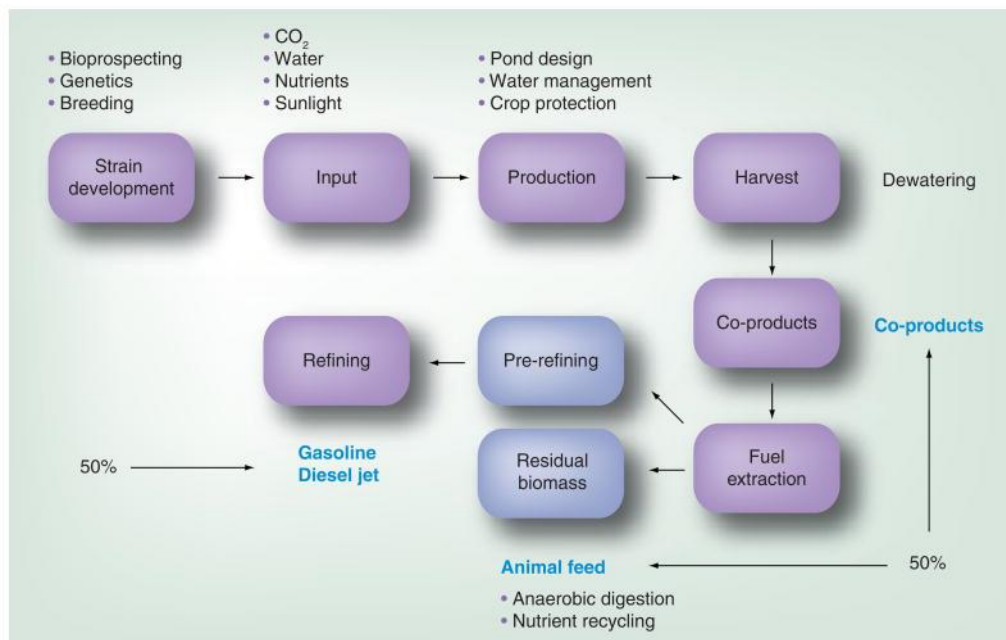
Figure 1.1 Algal biofuels production chain

1.2.2.1 Open Ponds

Open ponds are the most established and least complex framework for the mass production of microalgae. The pond is built in a raceway design (Figure 1.2), in which a

paddlewheel flows and blends the algal cells and supplements. The new feed is added in the

front of the paddlewheel, and the algal stock is collected behind the paddlewheel after it has

flown through the circle. Supplements can be given through spillover water from adjacent

areas or by directing the water from sewage or water treatment plants. Careful control of pH

and other physical conditions for introducing CO_2 into the ponds allow for greater utilization

of injected CO_2 (>90%). Since open ponds may become infested with other unwanted

organisms, ponds are cleaned and flushed on a regular basis. Open ponds can be considered as

batch cultures [17].
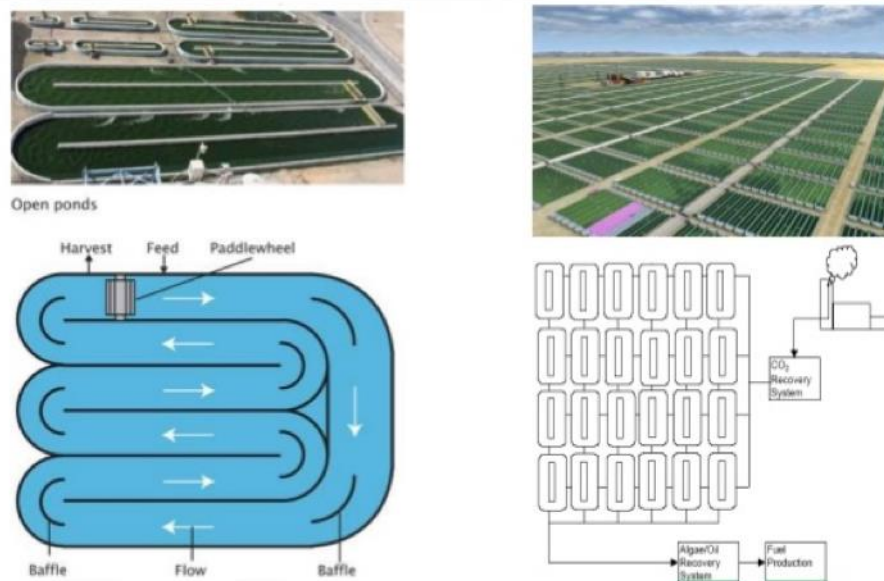
Figure 1.2 The structure of an open pond system used for large-scale production of microalgae [18]

1.2.2.2 Photo-bioreactors

Photo-bioreactors are closed systems to cultivate algae. Their construction is more

expensive than open pounds. However, since they allow for a better-controlled cultivation

environment, they are undoubtedly the preferred method for scientists. Photo-bioreactors

generally have controls for temperature, pH, and oxygen and CO_2 levels [28]. A distinguishing feature of these bioreactors is that they allow for growing one specific algae strain without interference or competition from other strains. In these safe, highly controlled environments algae can be cultured without the concern of being attacked by other micro-organisms [32]. Photo-bioreactors have higher effectiveness and biomass fixation (2–5 g/L), shorter harvest time (2–4 weeks), and the higher surface-to-volume ratio (25–125 m^{-1}) than open ponds [17]. Figure 1.3 shows the overall features of a tubular photo-bioreactor.
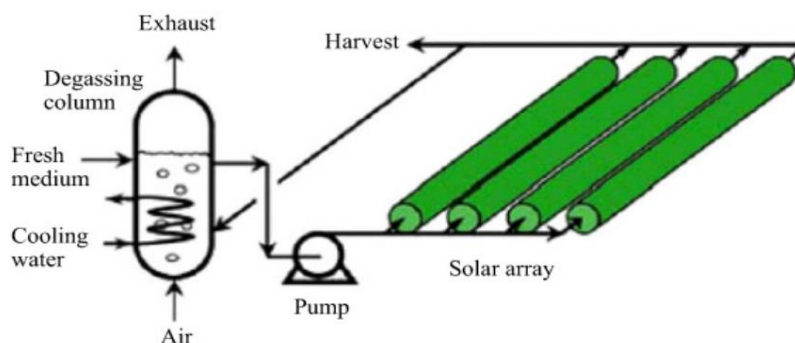
Figure 1.3 A tubular photo-bioreactor with parallel run used for large-scale production of specific strains of microalgae [18]

In a hybrid or mix system, open ponds and bioreactors are combined to improve cultivation results.

1.2.3 Harvesting microalgae

Harvesting algae is the most expensive step in the process of biofuel production from algae biomass. Cost of harvesting can reach up to 30% of the total cost of algae biomass production [33]. Starting with a dry biomass product is essential for processing the algae in bioreactors. If biomass contains any moisture, additional energy will be required to dry the biomass inside the bioreactor. Peng et al. mention that algae in cultures are highly diluted and

most of their moisture must be removed before they can be processed further into biofuel [34]. Considering the microalgae diameter, which is usually between 3 and 30 μm, the product is diluted up to 0.5 g/L [27]. As a result of the dilute product, harvesting algae and extracting bio-oil is a challenging and energy-intensive process. Microalgae harvesting can be performed by centrifugation, foam fractionation, flocculation, membrane filtration, and ultrasonic separation [35]. Type of species, cell density, and culture conditions are factors that dictate what method should be used for harvesting microalgae. It is too costly to use chemical methods to harvest algae for large operations. One commonly used method is interrupting the CO_2 supply in an algal system, which causes the algae to flocculate on its own. This process is called auto-flocculation. In another process called froth flotation, the water and algae are aerated into froth and algae is then removed from the water [17].

1.2.4 Selection of appropriate algal strain

As previously mentioned, algae contain lipids and fatty acids. Depending on the algae strain, these lipids and fatty acids can be membrane components, stored products, metabolites, and sources of energy. Choosing the appropriate strain of algae for the process is essential. In most of the recently conducted research, C. *protothecoides* has shown to have the most desirable features for biofuel production through thermochemical conversion. Hu et al. have shown that it is imperative to choose the right strain and that heterotrophic *C. protothecoides* cells can yield 3.4 times more bio-oil than autotrophic cells via fast pyrolysis [36]. The extracted bio-oil has a much lower oxygen content, with a higher heating value (41 MJ kg−1), and a lower density (0.92 kg) [36].

1.2.4.1 Biodiesel generation from heterotrophic microalgal oil

C. protothecoides is a microalga that can grow photoautotrophically or heterotrophically under different conditions. Heterotrophic development of *C. protothecoides* generates cells with a substantially high lipid content. Heterotrophic cells can be comprised of as much as 55.20% lipid. A large amount of microalgal oil can be removed from these heterotrophic cells by utilizing n-hexane, and the oil can be used to produce biodiesel similar to traditional diesel through acidic transesterification. It is reasonable to note that growing or bioengineering microalgae with a high lipid content is a promising route for future biofuel generation. [37].

1.2.5 Thermochemical Conversion

One of the most reliable processes to produce bio-oil, synthetic gas, and biochar is the thermochemical conversion of carbon-rich feedstock under controlled temperature and oxygen-absent or oxygen-lean environments. Generally, thermochemical conversion is divided into three main categories: (i) liquefaction at 250–350 °C and at pressure range of 700–3000 psi (to obtain liquid), (ii) pyrolysis at 200-600 °C in the absence of oxygen (to produce bio-oil, biochar, and some gases like CH_4, CO, and CO_2), and (iii) gasification at >800 °C (to produce synthesis gas or syngas) [38] Figure 1.4 depicts the various thermochemical conversion processes along with their products and product utilization. The properties of the final product are highly dependent on operating temperatures, pressure, oxygen content, and feedstock characteristics. Using thermochemical liquefaction and pyrolysis to generate bio-oil is an extremely intensive step in making algae biofuels. Due to algae's high moisture content, the drying process is very energy-intensive. However, biofuels obtained from the pyrolysis of biomass have lower levels of sulfur and nitrogen and emit less

gaseous pollutants than conventional diesel fuels, which makes them one of the most environmentally friendly resources of renewable energy.
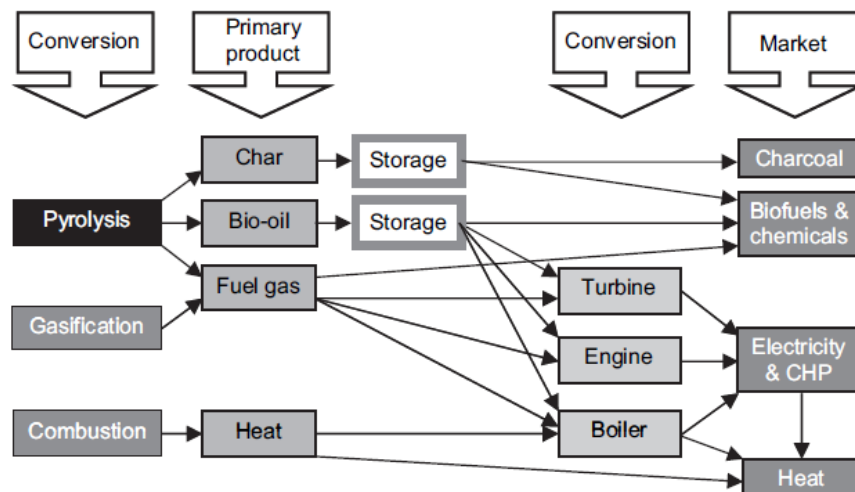
Figure 1.4 Various thermochemical conversion processes of biofuel production

Much of today's focus and interest has been on liquid production in pyrolysis centers. One important reason that biomass pyrolysis has received a great deal of attention, according to Grierson et al., is that this process can be used to maximize liquid yields [21]. The energy input in thermochemical conversion processes may decrease or increase based on the residence time. The residence time is defined as the time the biomass sample stays under high-temperature conditions inside the bioreactor. The longer residence times can cause secondary cracking of the primary products, reducing yield and adversely affecting bio-oil properties. In addition, a low heating rate and a long residence time may increase energy input [39]. Figures 1.4 and 1.5 present multiple pathways for thermochemical conversion of biomass.
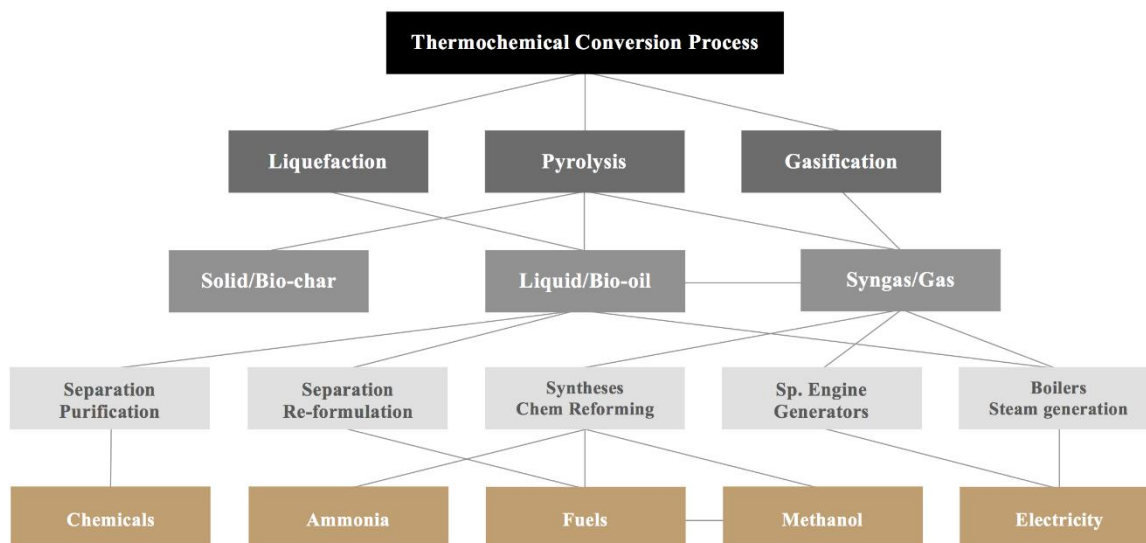
Figure 1.5 Various thermal conversion processes for biomass and their final products

1.2.6 Pyrolysis

Pyrolysis, in general, is the process of thermochemical decomposition of organic material at high temperatures and in the absence of oxygen. It is an irreversible reaction that results in a simultaneous change of chemical composition and physical phase or the organic material. Pyrolysis is considered the most effective procedure for biomass conversion when it comes to energy production [21]. It produces energy fuels with the high fuel-to-feed ratio, making it an efficient system suitable for supplanting non-renewable fossil fuel resources [21]. During pyrolysis, the temperature and heating rate must be controlled to optimize the production of bio-oil. The feed particles should also have a controlled moisture content to achieve optimal mass and heat transfer [23].

As previously mentioned, thermochemical conversion of carbon-rich feed-stocks, usually conducted at 400 to 600 ℃ and in the absence of oxygen, produces bio-oil, char, hydrogen, carbon monoxide, carbon dioxide, and methane. Proportions of products vary

according to pyrolysis conditions such as operating temperatures, pressure, oxygen content, and biomass characteristics.

Bio-oil yield from algae pyrolysis increases with higher temperature. The yield increases steadily with rising temperatures up to 477 ℃ and reaches a plateau at 502 ℃ [20]. Grierson et al. have used one alga sample, *Cladophora fracta*, and one microalgae sample to demonstrate that the yield of bio-oil from pyrolysis increases with higher temperatures [21].

Pyrolysis of algae produces biofuels with a high fuel-to-feed proportion, making it the most effective procedure for biomass conversion and one of the most promising routes to replace fossil fuels. The process can be adjusted to favor char, liquid (bio-oil), or gas production. Since bio-oil can be readily stored or transported and has lower nitrogen and sulfur content, much of the present interest in pyrolysis focus on optimizing bio-oil production. Depending on the temperature of the process and its residence time, biomass pyrolysis is divided into three major categories of (i) slow, (ii) fast, and (iii) flash pyrolysis.

The reactor is the most crucial component of fast pyrolysis. In the past couple of decades, various types of reactors have been designed to improve bio-oil yield. Table 1.2 summarizes the different types of reactors and lists their advantages and disadvantages.

Table 1.2 Different types of pyrolysis reactors

ABLATIVE PYROLYZER	CIRCULATING FLUID BED PYROLYZER

Advantages:	Disadvantages:	Advantages:	Disadvantages:
• Ability to process large particles • Good heat transfer	• Hard to scale up • Complex operation	• Require medium feed particle size • High bio-oil yield (up to 75%)	• High-level complexity in operation • High operating cost • Require large quantity of heat carrier
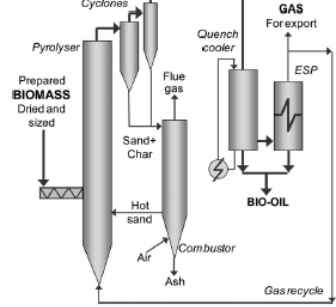
AUGER PYROLYZER	ROTATING CONE PYROLYZER
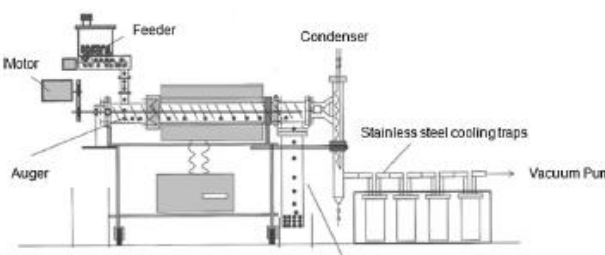
Advantages:	Disadvantages:	Advantages:	Disadvantages:
• Low carrier gas needed; • Simple construction and easy to operate	• Lower bio-oil yields • Long residence time	• Low heat carrier/sand requirement • Relatively simple construction and operation	• Very difficult to scale up • Limited scale/capacity; • Require fine feed particles
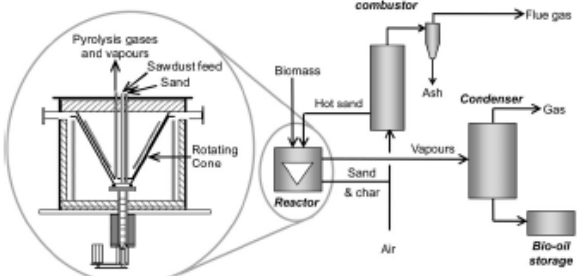
BUBBLING FLUID BED PYROLYZER

Advantages:	Disadvantages:
• High bio-oil yield (up to 75%) • Easy to scale up • Good heat transfer	• High operating cost • Require large quantity of inert gas • Require small particle feed sizes

1.2.6.1 Slow Pyrolysis

Slow pyrolysis predominantly produces gases, char, and bio-oil. This process is characterized by a long residence time (from 5 to 30 min), a medium or high reaction temperature (from 400 to 500 °C), and a low heating rate of 10 °C per second.

1.2.6.2 Flash pyrolysis

Flash pyrolysis generates gases, bio-oil, and little char. This process takes place with a very short residence time (about 500 °C/s) and/or very high temperature (1000 °C).

1.2.6.3 Fast pyrolysis

Fast pyrolysis conditions are in between slow and flash pyrolysis. The major products of fast pyrolysis are bio-oil, gases, and char. The residence time for the process is between 0.5 and 2 s, and the process is carried out under medium or high-temperature conditions (from 400 to about 650 °C) with a high heating rate of 100 °C/s.

In recent years, fast pyrolysis of biomass has attracted a great deal of attention for maximizing liquid yields. Fast pyrolysis saves energy by avoiding lower heating rates and longer residence times. Long residence times can adversely affect bio-oil quality [21]. Fast pyrolysis can also provide a commercial potential for large-scale production of liquid fuels from microalgae. It is more efficient and uses less energy compared to slow pyrolysis [23].

1.2.6.4 Advantages of fast pyrolysis

Delivering liquid fuels from microalgae through fast pyrolysis is an achievable and promising approach [23]. In a fast pyrolysis system, a greater amount of high-quality bio-oil can be directly produced from continuous processing of microalgae, fed at a rate of 4 g/min. Studies on fast pyrolysis of microalgae have shown multiple advantages for the process of

slow pyrolysis [34]. First, slow pyrolysis of microalgae does not directly produce flowing bio-oil products. The viscous compounds thought to be oils in slow pyrolysis were, in fact, organic extracts isolated from response blends by washing with dichloromethane and separating by filtration. These organic, viscous compounds have a rubber-like texture that makes them unsuitable to be used as liquid fuels. By contrast, fast pyrolysis can directly produce flowing bio-oil products from microalgae [34]. Second, slow pyrolysis can only process small quantities of algal cells and yields insignificant amount of low-quality bio-oil, whereas in fast pyrolysis it is possible to generate a large amount of high-quality bio-oil by continuously feeding microalgae to the system at a rate of 4 g/min [20]. Last but not least, slow pyrolysis is a very time-consuming and energy-intensive process. All these advantages suggest that fast pyrolysis is a promising process for the large-scale and commercial production of clean liquid fuels from microalgae [20].

1.2.7 Product yield

Miao et al. studied the essential features of a fast pyrolysis process and determined that these features are very high heating and heat transfer rates, carefully controlled pyrolysis reaction temperature of around 500 °C, short vapor residence times of less than 2 s, and rapid cooling of the pyrolysis vapor [23]. They used 500 °C in their study to investigate fast pyrolytic characteristics of microalgae and the resulting product yield. Figure 1.6 shows the product yields of fast pyrolysis of microalgae at this temperature, with a heating rate of 600 °C/s per second, nitrogen flow rate of 0.4 m^3/h, and a vapor residence time of 2 to 3 s.
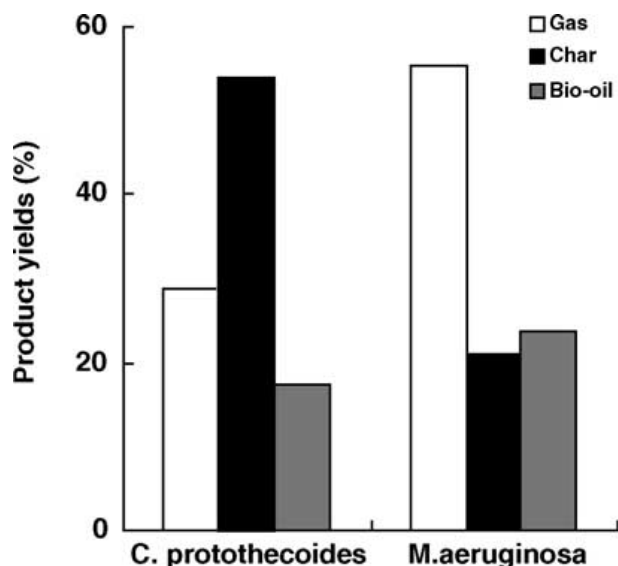
Figure 1.6 The product yields of fast pyrolysis of microalgae *C. protothecoides* and *M. aeruginosa* at 500℃.

The bio-oil yields from *C. protothecoides* and *M. aeruginosa* were 17.5 and 23.7%, respectively. Much of the microalgae powder adhered to the wall of the reactor, most likely due to electrostatic forces, which paralyzed the particles and resulted in the atypical high yield values for char. Furthermore, the pyrolysis vapor was not sufficiently dense, which resulted in uncharacteristically low bio-oil yields. The bio-oil yields could have improved by enhancing the mechanical assembly of the fast pyrolysis process. The above preparatory work shows that fast pyrolysis is a promising method to generate clean liquid fuels.

Hu et al. [36] demonstrate that there is a direct relationship between pyrolysis temperature and biofuel yield. Biofuel generation peaks at 900 °C with an astonishing 91.1% yield. Also, in the experiment, the optimal emission of CO and H_2 was accomplished at a pyrolysis temperature of 800 and 900 °C, respectively. The researchers are confident that in

fast pyrolysis, the biofuel yield of *C. Vulgaris* is higher at a higher temperature. Furthermore, assessment techniques based on heating values and energy consumption indicate that pyrolysis temperature significantly affects the generation of syngas. The optimal pyrolysis temperature to generate syngas was found to be 800 °C.

1.2.8 Biochar and synthetic gases

Biochar is the carbon-rich solid residue produced in the thermochemical conversion of biomass to biofuels. The increase in temperature results in cell rupture and coalescing, which leads to the production biochar. The yield for biochar is in 5-40% range and vary based on biomass origin and process conditions. Biochar is most commonly used as a soil amendment and carbon sequestration agent. When added to soil, biochar increases the organic matter content of the soil and its cation-exchange capacity. It also facilitates drainage and aeration, while decreasing the soil's bulk density. Moreover, its addition leads to less denitrification of the soil, N_2O emissions, and nutrient leaching.

The gaseous products of thermochemical conversion of biomass to biofuels include hydrogen, carbon monoxide, and methane. Carbon monoxide and hydrogen can be used as a primary ingredient to synthesize alcohol and aldehydes via oxo-synthesis and gasoline and diesel via Fischer tropsch (FT) synthesis. Furthermore, the hydrogen gas can be used in the hydrogenation of chemical processing.

1.2.9 Bio-oil

The oil-like liquid derived from bio-renewable feedstocks is called bio-oil. Bio-oil is typically obtained by heating biomass in the absence or low levels of oxygen. In early 2000s researchers found that the most efficient process to generate bio-oil is fast pyrolysis. In fast

pyrolysis, the biomass feedstock is heated at high temperatures and rapid rates, and the vapor is quickly condensed to yield bio-oil [40].

Bio-oil, also known as pyrolysis oil, is usually made up of 15 to 30% water by weight. At this level, sometimes phase separation can be observed. The water cannot be removed with methods like distillation. The high water content of the sample contributes to lower energy outputs and decreases the flame temperature of pyrolysis oil, which ultimately makes the ignition difficult. According to Demibas, the highest heating value of pyrolysis oil is 26 MJ/kg, which is considerably lower than the heating value of conventional petroleum, 45 ML/kg. Unlike petroleum oils that are hydrophobic (non-polar and water insoluble), biomass oils are hydrophilic (polar and water soluble) and can rapidly gain relatively large amounts of water [41].

Bio-oil characteristics vary depending on the biomass source it was derived from. For example, bio-oil derived from wood is a viscous dark red brown liquid with a density of about 1,200 kg/m^3, which is higher than the original biomass. Table 1.3 lists the properties of bio-oil, biodiesel, and conventional diesel.

Table 1.3 Properties of bio-oil, biodiesel, and conventional diesel

Property	Test method	ASTM D975 (Diesel)	ASTM D6751 (biodiesel, B100)	Pyrolysis oil (bio-oil)
Flashpoint	D 93	325 K min	403 K	-
Water and sediment	D 2709	0.05 max %vol	0.05 max %vol	0.01–0.04
Kinematic viscosity	D 445	1.3–4.1 mm^2/s	1.9–6.0 mm^2/s	25–1,000
Sulfated ash	D 874	-	0.02 max %wt	-
Ash	D 482	0.01 max %wt	-	0.05–0.01 %wt
Sulfur	D 5453	0.05 max %wt	-	-
Sulfur	D 2622/129	-	0.05 max %wt	0.001–0.02 %wt
Copper strip corrosion	D 130	No 3 max	No 3 max	-
Cetane number	D 613	40 min	47 min	-
Aromaticity	D 1319	-	35 max %vol	-
Carbon residue	D 4530	-	0.05 max %mass	0.001–0.02 %wt
Carbon residue	D 524	0.35 max %mass	-	-
Distillation temp	D 1160	555 K min	-	-
(90% volume recycle)		-611 K max		

Bio-oils contain a high percentage of alkylated compounds, especially methyl derivatives. These alkylated compounds may be hydrolyzed when temperature increases [42]. High concentration of oxygenated compounds in bio-oil produced through pyrolysis can lead to high viscosity, thermal and chemical instability, high rate of deterioration, and immiscibility with hydrocarbon fuels. However, these problems can be overcome by further processing the bio-oil to reduce its oxygen content [39] [40].

1.2.9.1 Bio-oil characteristics

Pyrolysis oil from microalgae is a complex organic mixture. It is comprised of amides, amines, n-heterocyclic compounds, carboxylic acids, ketones, phenols, and hydrocarbons [36]. Since bio-oils derived from different biomass sources vary in their physical and

chemical characteristics, it is essential to consider all of their specific properties for use in any application. Depending on the type of the feed material and its production and collection processes, the liquid obtained from biomass contains different amounts of water. This liquid forms a stable single-phase mixture and can have a water content ranging from 15 to 50% by weight [36].

There are some key properties of bio-oils that dictate how they can be used. An important property of bio-oil is its viscosity that affects the choice of bio-oil used in fuel applications [45]. Bio-oil viscosity can vary between 25 and 1000 m^2/s at 40 °C, depending on the feedstock, the water content and age of bio-oil, and the amount of liquid collected [36].

Another property of pyrolysis liquid is its ability to vaporize. They cannot be completely vaporized after they have been recovered from the vapor phase. The liquid rapidly reacts and eventually produces a solid residue that is approximately 50% of the original liquid by weight and some distillate containing volatile organic compounds and water [20]. While bio-oil can be stored for several years in normal storage conditions in steel and plastic drums without any deterioration and risk of oxidization, its viscosity increases gradually over time, making it unusable for current tests and applications. More recent samples distributed for testing have shown substantial improvements in consistency and stability, demonstrating the improvement in process design and control as the technology develops [37].

1.2.9.2 Chemical composition and characterization of bio-oils from fast pyrolysis of microalgae

Microalgae have shown great potential for use in the future energy supply chain due to. They are highly efficient in carrying out photosynthesis and are capable of removing CO_2 from the atmosphere, which can be a partial solution to global warming. Compared to other

energy crops, microalgae has a fast growth rate and can be cultivated in larger amounts, which leads to the production of more biomass in a shorter period [46]. The mentioned favourable properties microalgae have made them an attractive research topic in the area of renewable energy resource research.

Miao et al. have used chromatography on bio-oil samples derived from two strains of microalgae, *C. protothecoides* and *M. aeruginosa,* to demonstrate that they have similar chemical class compositions [37]. Both samples had a rather high asphaltenes content. Bio-oils of *C. protothecoides* and *M. aeruginosa* were 35.9% and 29.9% organic content by weight, respectively. The researchers highlighted that, on average, saturated and polar fractions accounted for 1.1% and 31.2% of the weight of bio-oils from microalgae, respectively, whereas in bio-oil derived from wood, the saturated and polar fractions accounted for less than 1% and 12% of the weight, respectively.

Miao et al. argue that the differences in chemical class compositions between the bio-oil produced by fast pyrolysis of microalgae and wood are most likely due to the differences in the main chemical components of the biomass source [23]. Proteins, lipids, and carbohydrates constitute more than 60% of microalgae components, whereas hemicellulose, cellulose, and lignin make up more than 95% of wood components.

The number of hydrocarbons that can be obtained from any component of biomass is limited by the percentage of carbon and hydrogen in the original samples. Therefore, lipids, proteins, and carbohydrates are preferable when it comes to conversion to hydrocarbons through pyrolysis, when compared to hemicellulose, cellulose, and lignin [37]. The analysis of saturated fractions of the extracted bio-oils indicates that the straight-chain alkanes range from C_{10} to C_{30} in *C. protothecoides* sample and from C_{10} to C_{28} in *M. aeruginosa* sample. A

maximum number of chains was found to be in the C_{17} to C_{18} range in both samples. These results are similar to straight-chain alkane profile of diesel fuel.

Elemental compositions and heating values for fast pyrolysis of oils derived from *C. protothecoides* and *M. aeruginosa* are shown in Table 1.4. The differences between the main chemical components of microalgae and wood lead to the production of bio-oils that are not only different in chemical class compositions, but also have different elemental compositions. Highest quality bio-oils are obtained from fast pyrolysis of microalgae. Bio-oil extracted from microalgae has a higher carbon and hydrogen content and a lower oxygen content than the bio-oil from wood. On average, the hydrogen-to-carbon and oxygen-to-carbon molar ratios are 1.72 and 0.26 for bio-oil derived from microalgae, and 1.38 and 0.37 for bio-oil derived from wood, respectively.

Table 1.4 Elemental compositions (wt. %) of bio-oils from fast pyrolysis of *C. protothecoides* and *M. aeruginosa*

Bio-oils	C	H	O	N	H/C	O/C	Heating value (MJ.kg^{-1})
C. protothecoides	62.07	8.76	19.43	9.74	1.72	0.24	30
M. aeruginosa	60.99	8.23	20.95	9.83	1.71	0.27	29

Miao et al. state that the lower oxygen content of bio-oil extracted from microalgae is one of its most fundamental characteristics that makes it a promising candidate for replacing of transport fuels [23]. Bio-oil products from *C. protothecoides* and *M. aeruginosa* also have high heating values of 30 MJ/kg and 29 MJ/kg due to their higher carbon and hydrogen content and lower oxygen content. Chlorophyll and proteins contribute to the high nitrogen contents of bio-oils from microalgae.

As previously mentioned, fast pyrolysis of biomass is a complicated process [39]. The process consists of a large number of reactions that happen both in parallel and in series. The steps and variables of the pyrolytic processes are unique for each type of biomass, which lead to even more complexity and a unique bio-oil product. The key properties of bio-oil products are viscosity, heating value, density, and stability. These properties dictate the extent that a bio-oil product can be used as a fossil-fuel alternative.

Among bio-oils derived from different biomass sources, bio-oil from microalgae seems to be the most favorable for use as a fuel. As indicated in Table 1.5, it has a lower oxygen content than the bio-oil from wood, which makes it more stable. It also has a higher heating value, lower viscosity, and lower density. Compared to the bio-oils from lignocellulosic materials, bio-oil from microalgae is more suitable to be used as fuel due to its mentioned physical properties [23].

Table 1.5 Comparison of typical properties of fossil oil and bio-oils from fast pyrolysis of wood and microalgae

Properties	Typical value		
	Bio-oils		Fossil Oil
	Wood	Microalgae	
C	56.4%	61.52%	83.0-87%
H	6.2%	8.50%	10.0-14.0%
O	37.3%	20.19%	0.05-1.5%
N	0.1%	9.79%	0.01-0.7%
S	Not determined	Not determined	0.05-5.0%
Density	1.2 kg/L	1.16 kg/L	0.75-1.0 kg/L
Viscosity (Pa s)	0.04-020 (at 40℃)	0.10 (at 40℃)	2-1000 (depending on temperature, density, and contents)
Heating value	21 MJ/kg	29 MJ/kg	42 MJ/kg
Stability	Not as stable as fossil fuels	Not as stable as fossil fuels but more stable than the bio-oil from wood	

1.2.9.3 Comparison of microalgae and wood bio-oils

As previously mentioned, the physical properties of pyrolysis oil from microalgae make it a more appropriate fit for fuel oil than the bio-oils from lignocellulosic materials. The lower oxygen content of the bio-oil from microalgae makes it more stable compared to the bio-oil from wood [47]. Additionally, a study conducted by Miao *et al.* [23] suggests that bio-oil from microalgae has higher heating value, lower viscosity, and lower density in comparison to the bio-oil from wood [23]. Microalgae's high carbon and hydrogen content and low oxygen content contribute to its higher heating values. The heating value of bio-oil from microalgae is 29 MJ/kg on average, which is about 1.4 times more than the bio-oil from wood.

The differences in chemical class compositions between the bio-oil produced by fast pyrolysis of microalgae and wood are most likely due to the differences in the main chemical components of the biomass source [23]. Microalgae are mainly made up of proteins, lipids, and carbohydrates, whereas wood is almost entirely made up of hemicellulose, cellulose, and lignin [20]. Since the number of hydrocarbons that can be obtained from any component of biomass is limited by the percentage of carbon and hydrogen in the original samples and lipids, proteins, and carbohydrates have a higher percentage of carbon and hydrogen in their compositions, microalgae biomass is preferred for pyrolytic processes [37]. The bio-oils from microalgae and wood also vary in their elemental compositions.

These distinguishing characteristics of microalgal bio-oils contribute to their higher quality compared to wood bio-oil and make them a more promising candidate for fossil fuel substitution. Furthermore, the lower oxygen content of microalgal bio-oil makes it a more attractive contender for production of transport fuels compared to bio-oil derived from higher plants such as wood [48], [49].

1.2.9.4 Comparison of microalgal bio-oils and fossil oils

Bio-oils have a higher concentration of oxygenated compounds than fossil oils. This contributes to their high viscosity, thermal and chemical instability, high rate of deterioration, and immiscibility with hydrocarbon fuels. Bio-oils' characteristics can alter quickly during condensation and under storage conditions. Most of the bio-oil issues associated with their higher oxygen content can be overcome using existing treatments [43], [44].

Bio-fuels have lower sulfur and nitrogen contents than do fossil fuels such as coal and petroleum. This makes the bio-oil from microalgae cleaner and friendlier to the environment. Microalgae bio-oils have the potential to be used in many applications as green alternatives to

conventional fuels [21], [34]. In order to optimally utilize bio-oils as fuels or sources of chemical feedstock, their storage stability and heating values have to be improved.

Typical properties of fossil oil and bio-oils obtained by fast pyrolysis of wood and microalgae are shown in Table 1.5.

1.3 Research Objectives

The objective of this work is to explore the kinetic and thermal behavior of *C. vulgaris* and to characterize its pyrolysis products obtained under various pyrolysis temperatures. The effect of temperature on product yields and quality was studied while keeping all other pyrolysis conditions constant. The *C. vulgaris* biomass and its pyrolysis products will be compared to other types of biomass, including lignocellulosic biomass and residual bacterial biomass, to better understand potential areas of use.

The following two chapters of this thesis are organized into the three distinct phases of the project including pre-operation, operation, and post operation. During the pre-operation phase, the chemical composition of C. vulgaris biomass was investigated using TGA, analytical pyrolysis, proximate and ultimate analysis, and FAME and carbohydrate analysis. During the second phase, pyrolysis was performed at three different temperatures of 450, 500, and 550 ℃. In the last phase, the pyrolysis products of *C. vulgaris* biomass (bio-oil and biochar) were characterized. The biochar characteristics were investigated by proximate and ultimate analysis, calorific value, surface area, butane activity, Raman spectroscopy, and electron microscopy. The bio-oil was analyzed using ESI-MS, HPLC, GC-MS, and FTIR.

Chapter 2: Materials and Methods

2.1 Materials

University of Idaho algae (UIA) and commercial *C. vulgaris* algae (CCA) (Zokiva Nutritionals) were used in this study.

UIA was produced from polyhydroxyalkanoate bioreactor effluent which was fed fermented dairy manure using an outside open raceway (14 m x 1 m, with a flowrate of 114 L min^{-1}) and operated by Mr. Nick Guho in June-July 2017, inoculated from a seed mainly comprised of *C. vulgaris* together with *Scenedesmus obliquus* and *Synechococcus leopoliensis* and obtained from Dr. Kevis Feris, Boise State University [50]. Figure 2.1 shows actual photos of the raceway open pond used in the production process. The UIA was then harvested and freeze-dried.

Figure 2.1 Photos of the University of Idaho algae raceway fed dairy manure waste.

2.2 Methods of *C. vulgaris* characterization

2.2.1 Thermogravimetric analysis (TGA)

In order to determine the activation energy and the thermal degradation behavior of *C. vulgaris*, TGA was performed on raw microalgae samples using a PerkinElmer TGA-7 instrument. Samples (3-5 mg) were heated from 30 to 900 °C at rates of 10, 20, 30, 40, and 50 °C/min under 30 mL/min nitrogen. The percent of original weight was recorded at different temperatures. Pyris v8 software was used to analyze the differential thermogravimetric data (DTG).

The kinetic equation for the decomposition rate in solid-state can be expressed as a product of Arrhenius' expression and a function of the extent of conversion [51].

$$\frac{d\alpha}{dt} = A exp^{\left(\frac{-E}{RT}\right)} f(\alpha) \qquad\qquad \text{Equation 2.1}$$

where *A* is the pre-exponential frequency factor (1/min), *E* is the activation energy (J/mol), R is the gas constant (8.314 J/mol·K), *T* is the absolute temperature (K), α is the extent of conversion and *f(α)* is the reaction model which is a function of conversion.

Thermal decomposition of microalgae comprises a series of simultaneously occurring complex reactions involving various compounds. This makes kinetic modelling a challenge. Model-free techniques, which rely on a set of TGA experiments based on various heating rates at a particular fraction of conversion, are more reliable and can be applied for the determination of apparent *E*. This way the need for a reaction model and 'compensation

effect' in the determination of kinetic parameters is eliminated [51]. The models deliver fairly accurate results when compared with some other model-fitting techniques [52].

At constant linear heating rate $\beta = dT/dt$, integration of Equation 2.1 by separating variables gives

$$\int_0^\alpha \frac{d\alpha}{f(\alpha)} = g(\alpha) = \frac{A}{\beta} \int_{T_0}^T exp^{(-\frac{E}{RT})} dt \qquad \text{Equation 2.2}$$

If T_0 falls below the temperature at which the rate of decomposition cannot be measured, the lower limit of the integral form disappears. Letting $x = -\frac{E}{RT}$, Equation 2.2 becomes

$$g(\alpha) = \left(\frac{AE}{\beta R}\right)\left\{-\frac{exp^x}{x} + \int_0^\infty \left(\frac{exp^x}{x}\right) dx\right\} = \left(\frac{AE}{\beta R}\right) p(x) \qquad \text{Equation 2.3}$$

The term $p(x)$ symbolizes the temperature integral and does not have an exact analytical solution.

There are two model-free techniques that have been previously applied to TGA data of biomass, Flynn-Wall-Ozawa's (FWO) method [53] and Starinks method [54]. No significant differences have been observed between the results of the two methods in the literature [55]. Flynn-Wall-Ozawa's (FWO) approximation, explained below, was adopted for this study.

The FWO method is commonly used to determine kinetic parameters. The FWO method uses Doyle's empirical approximation [56] to linearize the temperature integral in Equation 2.3 as shown in Equation 2.4.

$$\log p(x) \cong -2.315 + 0.457x \qquad\qquad\qquad \text{Equation 2.4}$$

Combining with Equation 2.4 with logarithm of Equation 2.3 gives the FWO expression in Equation 2.5.

$$\log \beta = \log \frac{AE}{g(\alpha)R} - 2.315 - 0.457\frac{E}{RT} \qquad\qquad \text{Equation 2.5}$$

A series of TGA experiments at heating rates β_1 β_2 … β_i can be performed and a temperature $T_{j,i}$ can be recorded at a conversion ratio, α_j, and heating rate β_i. Then a plot of log β against $T_{i,j}$ $^{-1}$ for each of j conversion ratios, α_1, α_2, ..., α_i will give j iso-conversional lines for which the slopes can be calculated from Equation 2.6 [53].

$$Slope \cong 0.457\frac{E}{R} \qquad\qquad\qquad\qquad \text{Equation 2.6}$$

Therefore, the E at each conversion step can be calculated from the plot of log β vs. the reciprocal of absolute temperature.

2.2.2 Fatty acid methyl ester (FAME)

Algae samples (4 g, in duplicate) were Soxhlet extracted using dichloromethane for 16 h to determine the lipid (extractives) content gravimetrically according to ASTM D1108-96. The identity of the lipids was determined by FAME analysis. The extracts (2 mg) were converted to their FAME derivatives by heating the sample in a sealed vial for 90 min at 90°C in a mixture of $CH_3OH/H_2SO_4/CHCl_3$ (1.7:0.3:2.0 v/v/v, 2 mL). $CHCl_3$ contained 1-naphthaleneacetic acid as an internal standard (200 µg/mL). The tube was cooled and water

added to the mixture, shaken vigorously, and the organic layer collected and dried over anhydrous sodium sulfate. The FAME compounds were analyzed by GC–MS using a FOCUS-ISQ system at a temperature gradient of 40 ℃ (1 min) to 320 ℃ at 5 °C/min equipped with a ZB-5MS (30 m, 0.25 mmØ) capillary column. The eluted compounds were identified with authentic C_{12} to C_{20} fatty acid standards and by spectral matching with the 2008 NIST mass spectral library.

2.2.3 Carbohydrate analysis

The lipid-free algae (200 mg) were hydrolyzed with 72% sulfuric acid (2 mL) and incubated for 60 min, then diluted to 4% sulfuric acid and subjected to a secondary hydrolysis (120℃ for 30 min) in an autoclave. Once cooled the hydrolysate was transferred to a volumetric flask (250 mL). An aliquot portion of the hydrolysate (5 mL) was transferred to a centrifuge tube to which internal standard (inositol, 1 mL, 0.5 mg/mL) and $PbCO_3$ (0.16 g) were added, mixed well, centrifuged, and the supernatant (4 mL) deionized (column of Amberlite IR-120 H^+ (0.5 mL) and Amberlite IRA35 OH^- (0.5 mL) resins) and filtered (0.45 µm) into HPLC vials. Monosaccharides were the quantified by HPLC using two RPM columns in series (7.8 mm × 30 cm, Phenomenex) at 85 °C equipped with differential refractive index detector (Waters Associates model 2414) on elution with 0.5 mL/min water. Data analysis were done using an N200 software package.

2.2.4 Pyrolysis–gas chromatography-mass spectrometry (Py–GCMS)

Py–GCMS was performed on microalgae samples (<0.1 mg) at 500 °C in helium with a Pyrojector II unit (SGE Analytical Science) coupled with a FOCUS-ISQ GC-MS (Thermo Scientific). The compounds were separated on the ZB-5MS capillary column (30 m × 0.25

mm Ø, Phenomenex) at a temperature range of 50 to 250 °C at 5°C/min. The eluted

compounds were identified using their mass spectra, authentic standards, and NIST 2008

library matching. The relative abundance of each compound was calculated in relation to the

CO_2 peak.

2.3 Pyrolysis

CCA was pyrolyzed at three different temperatures of 450, 500, and 550 °C with a 0.5

kg h^{-1} feeding rate using a K-Tron loss-in-weight feeder. UIA was only pyrolyzed at 550 °C.

A custom built auger reactor (Ø 5 cm x 90 cm) was used to perform the pyrolysis experiments

with an N_2 purge (5 L/min). Auger speed was adjusted to achieve an 8-s residence time. All

the vapors were condensed by first passing through a 450 °C transfer tube and then passing

through a two-stage ice-water-cooled tube and shell condenser. At the end of the process,

biochar and bio-oil were collected to determine gravimetric yields and for further

characterization. Figure 2.2 shows a schematic representation of the pyrolysis reactor used in

this work.
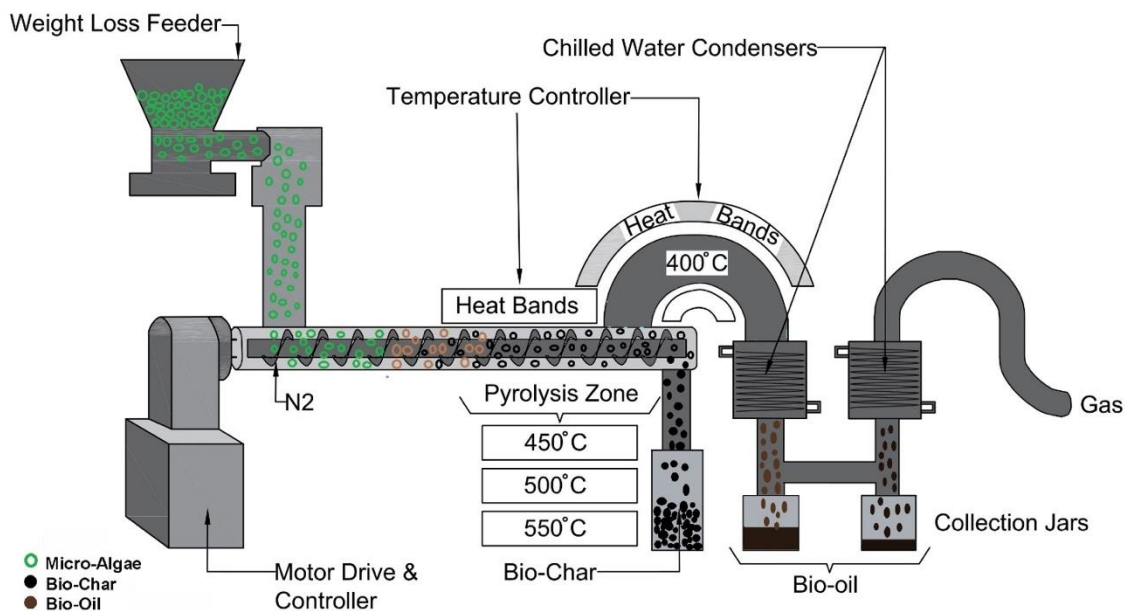
Figure 2.2 Schematic representation of a pyrolysis reactor.

2.4 Methods used for biochar characterization

2.4.1 Proximate and ultimate analysis

Proximate analysis was performed on algae and biochar according to ASTM E870-82 standard. In order to obtain the percentage of volatile matter (VM), samples were combusted at 950 °C in a muffle furnace for 7 min. The ash content was kept at a temperature of 600 °C for at least 16 hours. The obtained values for fixed carbon (FC) content, VM, and ash content were recorded as a percentage of the total sample weight. C and N contents were determined using a Costech ESC 4010 elemental analyzer.

2.4.2 Calorific value

The calorific values of algae and biochar (in duplicate) were determined by bomb calorimetry using a Parr oxygen bomb calorimeter (model no. 1261) in accordance with

ASTM D5865-04. Pre-dried samples (1.0 g) were pressed into pellets (6 mm Ø) using a

Carver Laboratory hydraulic press (1500 MPa) for analysis.

2.4.3 Surface area

The specific surface areas (S_{BET}) of all degassed biochar samples (0.25 g, in duplicate)

were measured using 30% N_2 in He to obtain an N_2 adsorption-desorption isotherm at -196°C

on a Micromeritics ChemiSorb 2720 instrument according to ASTM D6556-10.

2.4.4 Butane activity

The butane activity (BA) of biochar was determined in accordance with ASTM

D5742-95. Dry biochar (16.7 ± 0.05 mL of known weight) was placed in a test tube in a water

bath (25 ± 0.2 °C) and flushed with butane (250 ± 5 mL/min) until a constant weight was

obtained and the sample no longer absorbed the butane. Activated charcoal (plant cell culture

grade, Sigma-Aldrich) was used as a reference standard.

2.4.5 Raman spectroscopy

The biochar was analyzed by Raman spectroscopy on 5 replicates on an Alpha 300 R

confocal Raman microscope (Witec) spectrometer with 532 nm excitation, 0.5 s integration

time and 5 scans. The spectra were averaged and baseline corrected using Omnic v9

(ThermoScientific) software. The ratio of D (disordered, 1380 cm^{-1})/G (graphitic, 1605 cm^{-1})

band intensities (I_D/I_G) was used to calculate an estimation of disordered carbon in the sample

[57], [58].

2.4.6 Imaging

Scanning electron microscopy (SEM) of algae and biochar samples were examined on a HITACHI TM3030 instrument at 15 kV.

2.5 Methods of *C. vulgaris* bio-oil characterization

2.5.1 Electrospray ionization mass spectrometry (ESI-MS) of bio-oil

Molar masses of fresh bio-oil samples were determined by negative and positive ion ESI-MS using a Finnigan LCQ-Deca instrument (Thermoquest). The bio-oil samples were dissolved in methanol containing 1% acetic acid and then subjected to ESI–MS (*m/z* 100–2,000) at a flow rate of 10 μL/min. The ion source and capillary voltages were 4.48 kV and 47 V at 275°C, respectively. The data were analyzed according to the calculation of number average molar mass (M_n) as $M_n = \sum N_i M_i / \sum N_i$ and the weight average molar mass (M_w) as $M_w = \sum N_i M_i^2 / \sum N_i M_i$ where N_i is the intensity of ions and M_i is the mass after accounting for the charge. The PDI was calculated as $PDI = M_w / M_n$.

2.5.2 Fractionation of bio-oil

The pH of the bio-oils was measured using an Orion 3-Star Plus Dissolved Oxygen portable meter (Thermo Scientific). Bio-oil fractionation was performed using the method outlined by Sipila et al [59]. Bio-oil (5 g) was mixed with water (10 g), centrifuged for 30 min at 5000 rpm, and the water-soluble (WS) supernatant and water-insoluble (WI) bottom fraction collected. The water-soluble fraction was further fractionated by extraction with diethyl ether (4 volumes) to obtain an ether-soluble (ES) and aqueous (AQ) fractions. Figure 2.3 shows the fractionation process for bio-oil.
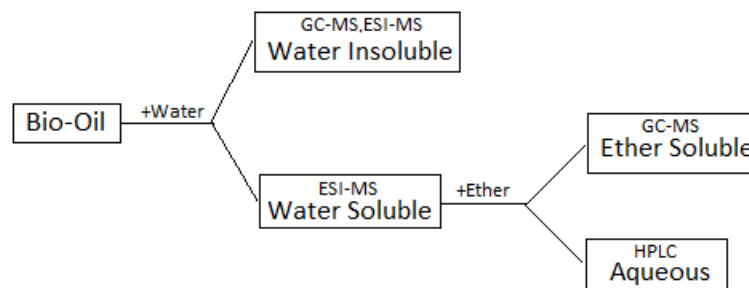
Figure 2.3 Bio-oil fractionation

2.5.3 High-performance liquid chromatography (HPLC) of AQ fraction

The AQ fraction was analyzed for organic acids by HPLC, in triplicate, using a Rezex ROA organic acid column (7.8 × 30 cm, Phenomenex) equipped with a differential refractive index detector (ERC-5710, ERMA), on elution with 0.005 N aqueous sulfuric acid (0.5 mL/min) at 65 °C. N2000 chromatography software (Science Technology Inc., China) was used to acquire and analyze the data.

2.5.4 GC-MS of ES fraction

The ES fraction was analyzed by GCMS using FOCUS-ISQ GC-MS instrument (Thermo Scientific). 1 mg of bio-oil was mixed with 1 mL of chloroform containing anthracene (100 µg/mL) as an internal standard, in triplicate. Separation was achieved on ZB-5MS capillary column (30 m × 0.25 mm Ø, Phenomenex) using a temperature gradient of 40 °C (1 min) to 320 °C at 5 °C/min.

2.5.5 Fourier-transform infrared spectroscopy (FTIR) analysis

FTIR spectra were obtained for the bio-oil using a Thermo-Nicolet iS5 equipped with a ZnSe attenuated total reflection (iD5 ATR) accessory. Igor Pro version 6.03 was used to perform peak fitting analysis.

Chapter 3: Results and Discussion

Multiple techniques have been used to characterize algae and the pyrolysis products, biochar and bio-oil. This chapter summarizes the results obtained from characterization methods explained in the previous chapter.

3.1 Kinetic characterization of *Algae*

3.1.1 Thermogravimetric analysis (TGA)

TGA was conducted on the algae samples to determine their thermal degradation behavior. The weight loss and differential thermograms (DTG) at several heating rates (β) are shown in Figures 3.1 and 3.2. Thermal degradation of both algae samples occurred in multiple stages between 30 and 900 °C. The small peak at under 100 °C corresponds to the release of moisture and possibly the liberation of some low molar mass organic compounds at the beginning of the TGA process. The main devolatization peak appears between 200 °C and 500 °C for CCA and between 200 °C and 420 °C for UIA. The DTG curve in Figure 3.1 (b) shows that this stage happened in two sub-stages for the CCA sample, with an intensified second sub-stage at higher heating rates. This devolatilization stage is generally attributed to carbohydrate and protein devolatilization [60]. Another significant degradation peak appears around 570 °C for the commercial samples and 525°C for the UIA sample. Some researchers associated this stage with devolatilization of lipids [34] and others have proposed a connection with mineral matter decomposition [61]. The third peak has a higher intensity at higher temperature rates and is thought to be linked to the solid residue (char) devolatilization [34], [62], [63] or degradation of chemical compounds that may have been formed during previous steps of thermal decomposition [64]. A noticeably less intense fourth devolatilization

rate peak appeared in the interval 620 to 800 °C for the UIA sample only and led to a complete conversion of the material. It is noteworthy that the intensity of all peaks increased with an increase in β. An increase in β also tends to slightly postpone the thermal decomposition process of microalgae samples without significantly changing their thermal profiles. This thermal decomposition trend emphasizes that the reaction rate is dependent on the temperature and the decomposition mechanism is independent of β [65].

(a)

(b)
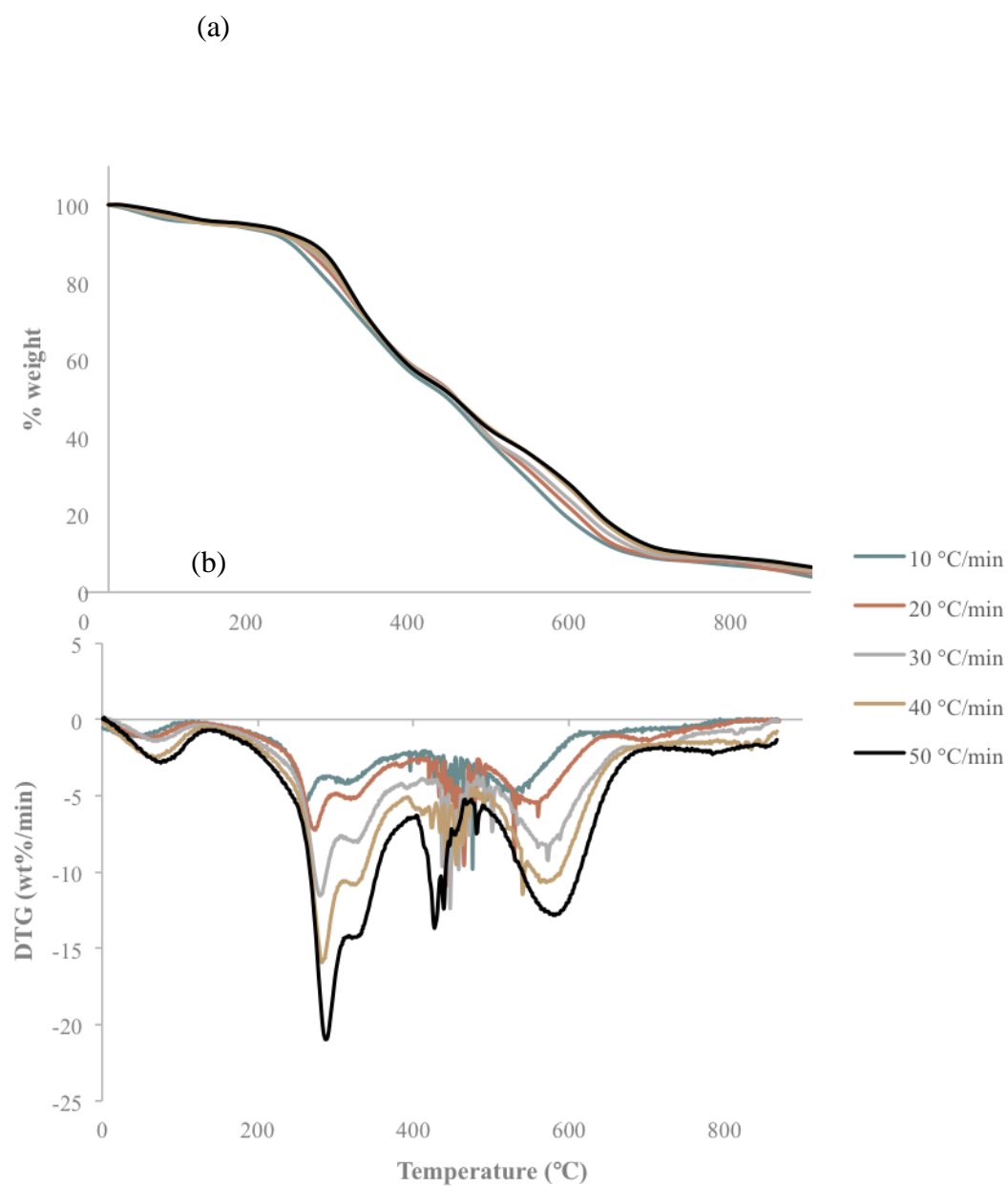
Figure 3.1 (a) TGA thermograms curves of commercial *C. vulgaris* algae (CCA) at different heating rates (β) and (b) DTG thermograms of CCA at different β.
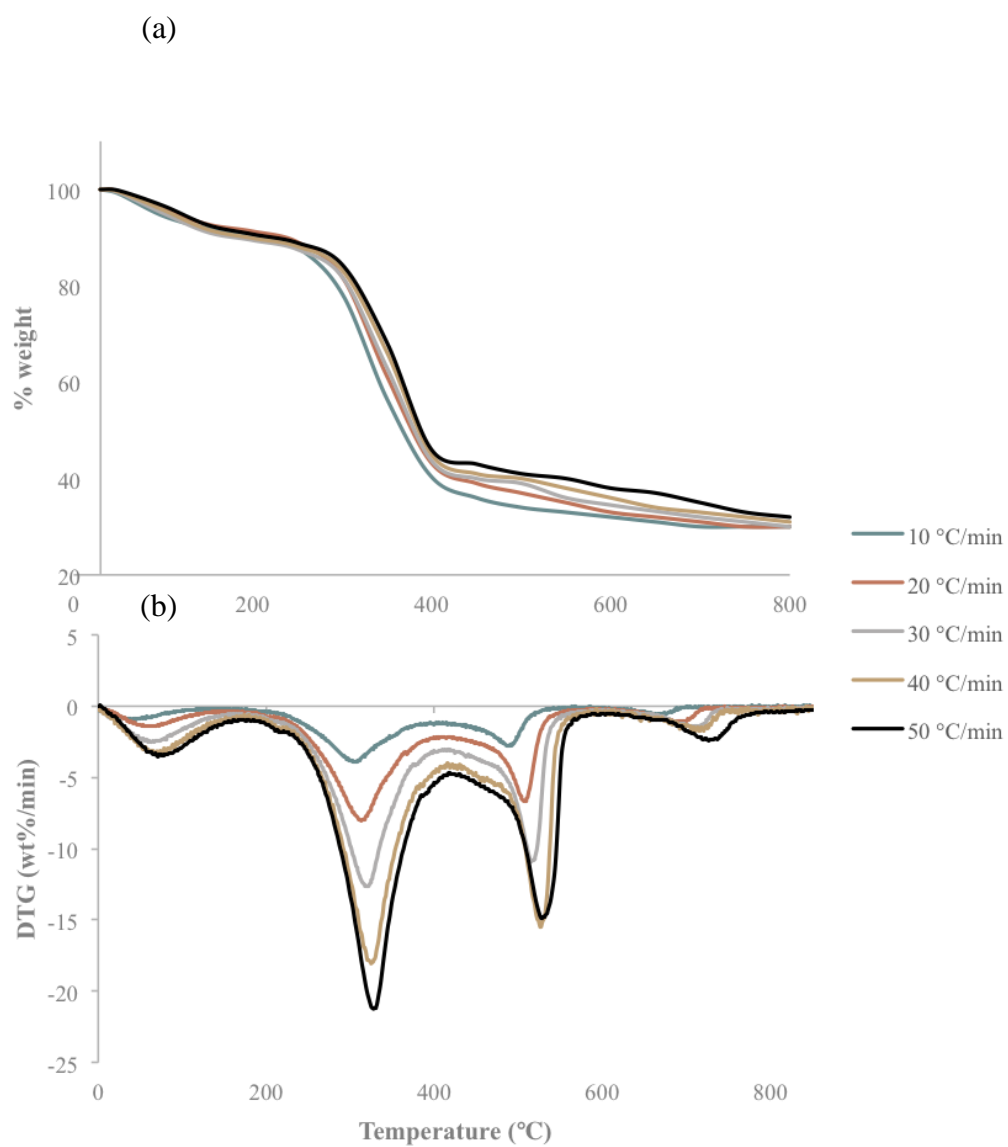
Figure 3.2 (a) TGA thermograms of U of I algae (UIA) at different heating rates (β) and (b) DTG thermograms of UIA at different β.

3.1.2 *C. vulgaris* **activation parameters**

The plots of iso-conversional lines in Figures 3.4 and 3.5 were derived from the application of Equations 2.6 to the TGA data. Figures 3.4 and 3.5 depict the correlation between the logarithmic function containing heating rate (β) and 1/T at α ratios of 0.1 to 0.90 for FWO method for UIA and CCA, respectively. Table 3.1 presents the values of activation energy (E) calculated from the individual slopes of the α ratio for CCA and UIA. At lower stages of conversion (smaller α), the reaction is mainly physical (moisture release) and cannot be defined by the current devolatilization kinetic models accurately. A moisture diffusion mechanism to achieve a more accurate result for the drying stage has been suggested in the literature [66].

The E values varied greatly for different conversions in both *C. vulgaris* samples, emphasizing the presence of a multi-step reaction. E increases to 540 kJ/mol at α level of 0.40 for CCA and 259 kJ/mol at α level of 0.50 for UIA (Figure 3.3), which corresponds to the third peak observed in both DTG plots in Figures 3.1 (b) and 3.2 (b). With the progression of thermal decomposition reactions, a dense carbonous structure (char) is formed through either a cross-linking of polymer chains, polycondensation, or cyclisation reaction of side chains. The higher energy required to degredate the char may have caused the spike in E. The E value range obtained in this work were lower in comparison with ranges reported in the literature for microalgae [34], [67].

Table 3.1 Activation energy (*E*) for conversion range of 0.1 - 0.9 using FWO method on CCA and UIA from TGA data.

Conversion (α)	E (kJ/mol) CCA	E (kJ/mol) UIA
0.1	385.1	20.2
0.2	281.9	155.4
0.3	471.4	183.2
0.4	540.6	222.7
0.5	414.9	258.6
0.6	249.1	182.3
0.7	216.0	158.7
0.8	202.6	174.7
0.9	202.0	203.3
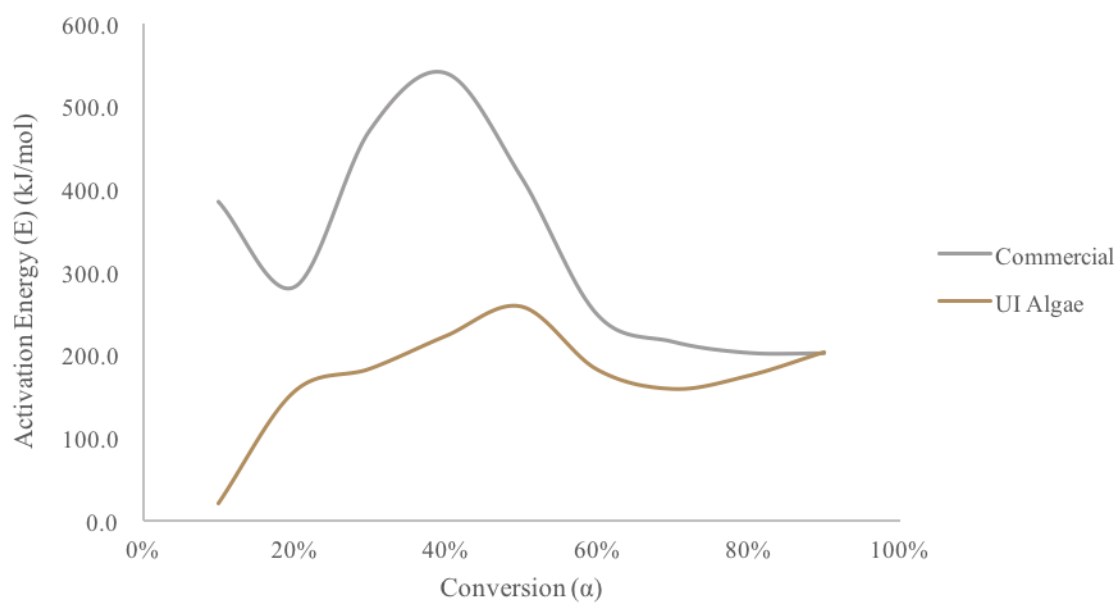
Figure 3.3 Activation energy (*E*) vs. conversion ratio (α) of CCA and UIA.
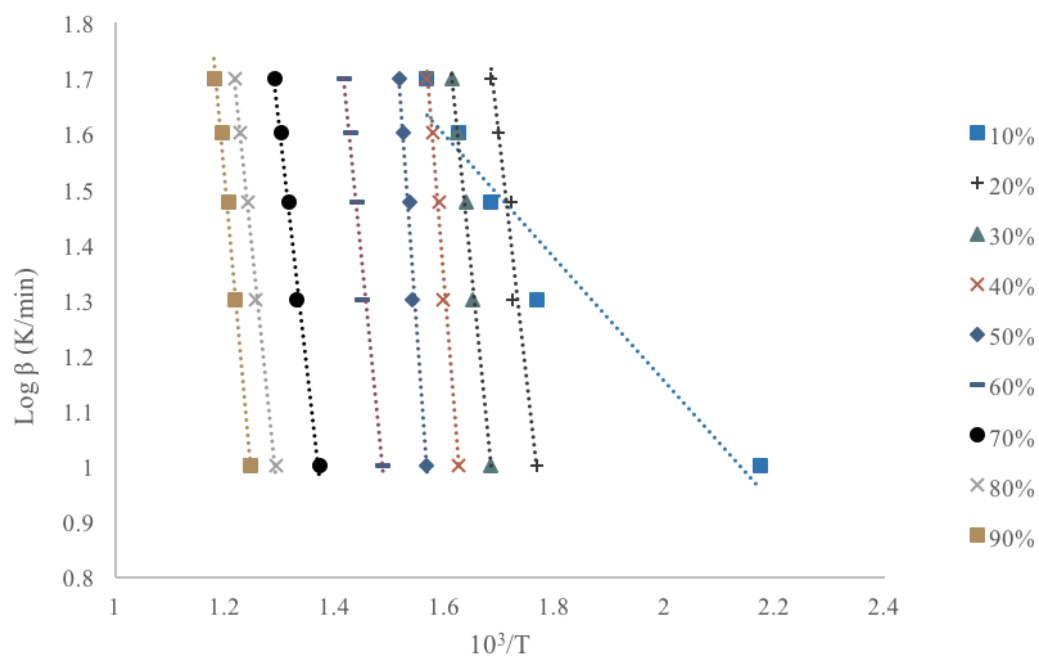
Figure 3.4 Determination of *E* according to FWO method at heating rates (β) of 10, 20, 30, 40, and 50 °C/min for UIA
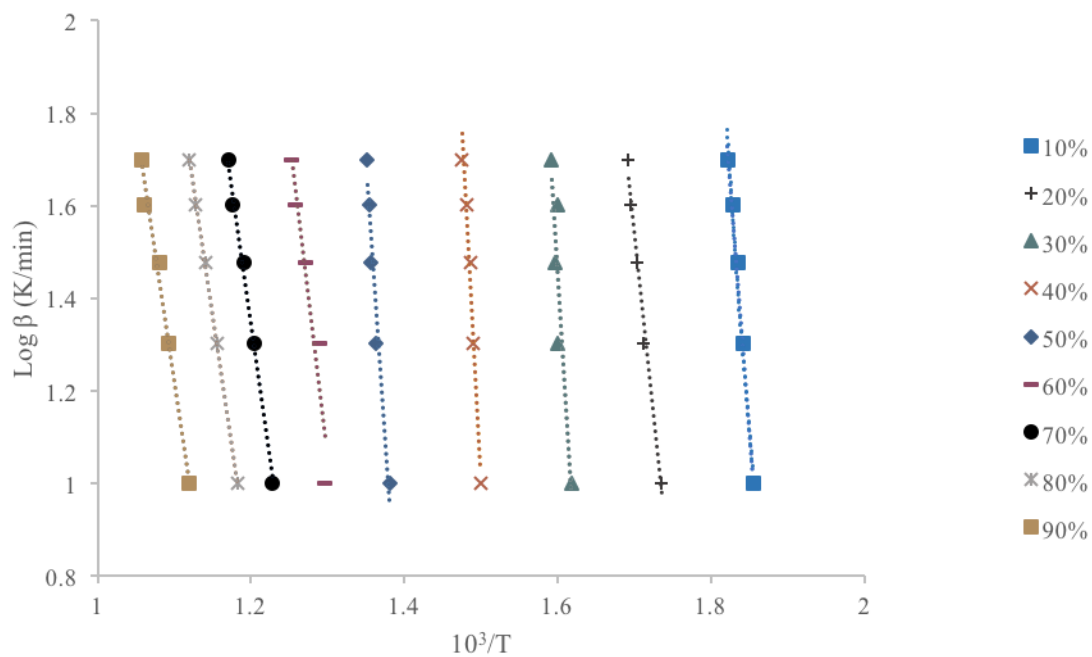
Figure 3.5 Determination of *E* according to FWO method at heating rates (β) of 10, 20, 30, 40, and 50 °C/min for CCA

3.2 Proximate analysis, calorific value, butane activity, and surface area of *C. vulgaris* biomass and biochar

Proximate analysis was performed on algae samples and their biochar obtained at various temperatures to acquire information on the FC, VM, and ash contents. The ultimate analysis was conducted to determine the C and N contents. The calorific value, butane activity, and BET were also evaluated for all samples. The results of all these analyses are given in Table 3.2.

Major differences could be observed between CCA and UIA samples. The FC was much higher for CCA (26.6%) compared to UIA (9.4%), which also resulted in UIA having a higher VM than CCA. The FC's for both microalgae samples are well within the range reported for *C. vulgaris* in the literature [68]–[70], however, FC for UIA was on the lower side. Generally, biomass has a much higher VM content than solid fossil fuels like coal and peat, which makes it more suitable for pyrolytic oil production [71]. The ash content was much higher in UIA (30%) than the CCA sample (4.4%). Since ash is mainly composed of inorganic materials, the high ash content in the UIA sample was most likely due to dust and dirt falling on the open raceways during a windy summer and accumulating in the algae. Another possibility is an accumulation of minerals from the dairy manure-derived effluent feed. The higher ash content could explain the lower FC values for UIA and will likely have a positive influence on biochar yields, depending on metal ions and anions present [40]. Das et al. [72] observed that ash in biomass has a significant influence on the quality of organic yield. Furthermore, it has been reported in the literature that low ash and high C contents contribute significantly to high heating values for biomass samples [73]. The ash content acts as a catalyst in fast pyrolysis, promoting the production of gas and char, at the expense of bio-

oil; it may also cause operational problems in pyrolyzers [74], [75]. Therefore, biomass resources with relatively lower ash content may be more suitable for pyrolysis.

Both algae samples had a high N content (9.1% for CCA and 5.9% for UIA), as expected for microalgae due to their high protein content. Both samples had C and N contents close to those reported in the literature for *C. vulgaris* [68], [69], [76].

The calorific value of CCA (23 MJ/kg) was 33 % higher than that of UIA (17.22 MJ/kg). Both were close to calorific values reported for *C. vulgaris* in the literature [77], [78]. The calorific values are comparable to those reported for RBB [79] and hardwoods [80], but higher than those for seaweed algae samples [81]. According to Illman et al., an increase in calorific value in algae is associated with an increase in their lipid content rather than change in other cell components such as carbohydrates and proteins [82].

Compared to their parent biomass feedstocks, the biochars had lower C and N content. The lower C/N ratio was most likely caused by the denitrogenation via deamination of proteins and amino acids during pyrolysis [79]. The biochar from UIA had a very high ash contents (70.51 %) at the expense of carbon content. This high ash content puts the biochar at a disadvantage compared other biochars for most applications [83]. The BET surface areas were very low for CCA biochar samples, with little variation caused by pyrolysis temperature. The BET surface area for UIA was 3 times higher, however, it was still low compared to other biochar surface areas reported in the literature [83].

BA is an indirect measure of surface area and organic compound adsorption. The BA values for all CCA biochar samples were less than 1%. The low BA value corroborates the low SA values obtained for this biochar. The BA value was higher for UIA (2.51%), which is

consistent with the sample's higher total surface area. Higher pyrolysis temperatures would likely increase the BA [84].

The surface area and BA results for biochar samples suggest that *C. vulgaris* biochar obtained in this work would not work well as a soil amendment and carbon sequestration agents. The lower surface area would adversely affect the ability of biochar to increasing cation-exchange capacity and facilitating drainage and aeration. However, they can still be used as a nutrient source due to their high nitrogen content.

Table 3.2 Proximate and ultimate analysis results for CCA and UIA algae and biochar.

Sample ID	CCA	UIA	CCA 450 °C Biochar	CCA 500 °C Biochar	CCA 550 °C Biochar	UIA 550 °C Biochar
% N	9.51	5.9	5.65	6.12	5.81	2.893
% C	58.16	36.7	32.46	36.05	30.65	21.572
% Ash	4.4	30.03	8.5	10.1	12.6	70.51
% Fixed carbon	26.6	9.4	35.6	38	46.5	14.01
Calorific value (MJ/kg)	23.0	17.2	26.0	28.0	32.0	7.83
% Butane absorption	0	0	1	0.65	0.59	2.51
Surface Area (m^2/g)		0	2.9	2.8	2.2	6.8

3.3 FAME and carbohydrate analysis of *C. vulgaris*

FAME and carbohydrate analyses were conducted to further assess the composition of *C. vulgaris* algae as a renewable energy source.

3.3.1 FAME analysis

The results of the GC-MS on the extracted lipids are presented in Figure 3.6. The tabulated results are shown in Table 3.4. In the CCA sample, palmitic acid (C16:0), physetoleic acid (C16:1), oleic acid (C18:1), and stearic acid (C18:0) were most abundantly found. These four fatty acids were also found in the UIA sample, however, to a much lesser extent. The difference in abundance can be attributed to different cultivation regimes.

The chain length of fatty acids was between C_{14} and C_{26} in this study, which is consistent with previous findings [85]–[91]. The results of this work are also in accordance with previously reported findings that C16:0, C16:1, and C18:1 are the major fatty acids present in *C. vulgaris* lipid extracts [86].

It has been reported that microalgae store high amounts of neutral lipids and stearic acids as a protection mechanism [92]. Furthermore, Petkov et al. have stated that fatty acid composition of *C. vulgaris* is of a higher quality compared to other green algae [87]. Considering that fatty acids with chain lengths of C_{14}–C_{24} is the most abundant fatty acids in biodiesel, *C. vulgaris* is a promising contender for production of high-quality bio-oil.
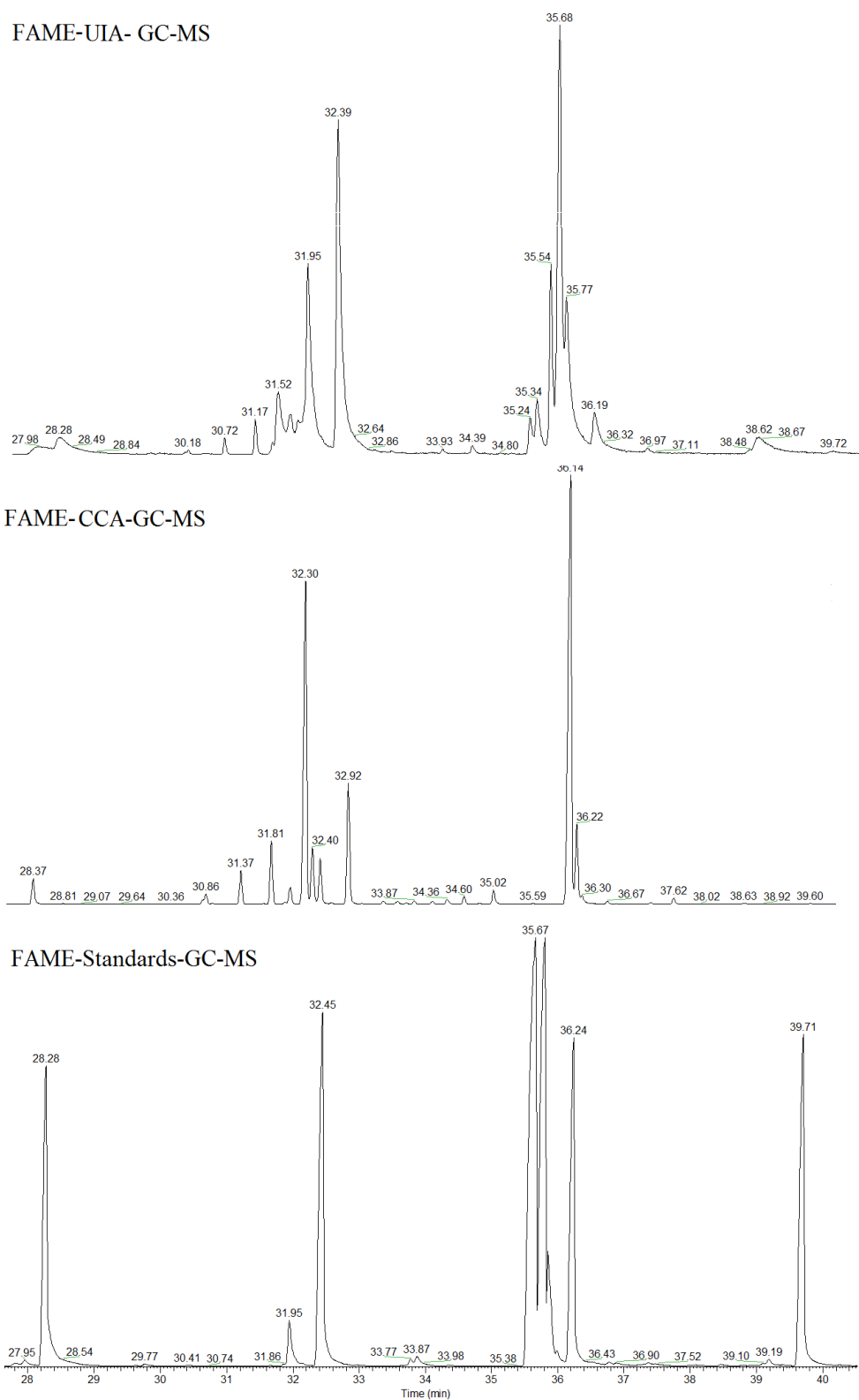
Figure 3.6 GC-MS profile of FAME components in UIA and CCA samples.

Table 3.3 Fatty acid methyl esters identified and quantified (% of extract) in CCA and UIA samples.

Name	Apex RT	M+	FAME	CCA	UIA
Myristic acid	28.85	228	C:14	1.12%	1.39%
Pentadecanoic acid	30.72	242	C15	0.91%	0.15%
physetoleic acid	30.99	268	C16:1	9.18%	1.16%
Palmitic acid	31.45	270	C16:0	34.95%	6.50%
α-Eleostearic acid	32.91	278	18:03	0.80%	
γ- Linolenic acid	33.37	278	C18:3	0.53%	
α-Linolenic acid	33.58	278	C18:3	0.32%	
Linoleic acid	34.62	294	C18:2b	1.12%	2.10%
Oleic acid	34.73	296	C18:1	12.94%	1.89%
Stearic acid	35.19	298	C18:0	9.30%	0.53%
Eicosapentaenoic acid (EPA)	42.78	302	C20:5	1.58%	
Arachidonic acid	44.23	304	C20:4	2.31%	
Arachidic acid	45.63	304	C20:0	3.24%	0.45%
Docosahexaenoic acid (DHA)	46.97	328	C22:6	3.97%	
Behenic acid	48.28	354	C:22	2.98%	
Petacosanoic acid	49.54	396	C:25	2.11%	
Hexacosanoic acid	51.95	410	C:26	0.61%	

3.3.2 Carbohydrate analysis

The carbohydrate composition of CCA was determined after hydrolysis by HPLC. The carbohydrate composition is given in Table 3.4. The three most abundant sugars were glucose (12.1%), arabinose (7.1%), and galactose (4.3%) with a minor amount of xylose.

Since carbohydrates derived from microalgae do not require pretreatment and can easily be sacharificated compared to carbohydrates derived from lignocellulosic materials, they are considered a competitive feedstock for ethanol production [93]. The carbohydrate productivity can be increased by understanding and modifying carbohydrate metabolic pathways in microalgae. Factors such as light, nutrients, temperature, and CO_2 can be manipulated to improve carbohydrate productivity [94].

The abundance of glucose has been linked to the high amount of starch in microalgae [95]. The profusion of starch in microalgae makes them highly suitable for fermentation to ethanol. Another study has found galactose to be the most prominent monosaccharide in *C. vulgaris* [96]. Galactose can be obtained from large concentrations of galactolipids that make up the photosynthetic membranes in actively growing microalgae cells [97] or from β(1-6) linked galactans on the cell wall glycoproteins [98].

Table 3.4 Carbohydrate analysis of CCA

Name	Original dry algae basis (%)
Glucose	11.94
Xylose	0.17
Galactose	4.19
Arabinos	7.01
Mannose	2.12

3.4 Py-GCMS of *C. vulgaris*

Analytical Py-GCMS was performed to identify potential pyrolysis products of CCA and UIA (Figure 3.8). 154 peaks were observed in pyrolyzed CCA and UIA at 550 °C (Table 3.5).

Compared to lignocellulosic material, fewer oxygenated compounds were present in the pyrolysis products of *C. vulgaris.* This outcome was consistent with previous findings in the literature [8], [43]. The most abundant compounds were identified as CO_2 (13%), palmitic acid at (13%), and linoleic acid (5%) in CCA and linoleic (8%), oleic acid (6%), and 2-pyridinecarboxylic acid (6%) in UIA. The abundance of fatty acids in pyrolysis products of *C. vulgaris* is correlated with the high lipid content of this biomass.

Compounds such as 3-methyl-2-cyclopentene-1-one, 1-methanol-2-cyclopentane, 2,5-dimethylfuran were found by pyrolysis of the carbohydrates fraction. About 25% of the total peak area of both CCA and UIA is associated with the peak area for these compounds, which falls within the range reported for microalgae in the literature [68]. Low molecular weight compounds, such as acetic acid and acetic anhydride, were generated by fragmentation reactions [68]. These C_2–C_4 class compounds identified in pyrolysis products of *C. vulgaris* were the result of cracking reactions of higher molecular weight molecules such as carbohydrates. These compounds account for about 25% of the biomass.

High molecular weight compounds such as long-chain fatty acids, aldehydes, alcohols, and saturated and unsaturated linear hydrocarbons were generated by the decomposition of lipids during pyrolysis [99], [100]. As anticipated by the FAME analysis results reported earlier in this chapter, fatty acids such as palmitic acid, oleic acid, and linoleic acid were abundantly found in both *C. vulgaris* samples.

Mono-aromatic hydrocarbons such as xylene, styrene, phenols, and guaiacol were present in *C. vulgaris* pyrolysis products. The presence of these aromatic hydrocarbons is attributed to the presence of amino acids that contain aromatic rings in microalgae proteins [99], [101]–[103]. They most likely have originated from aromatic amino acids such as phenylalanine and tyrosine during thermal decomposition of proteins in pyrolysis [68]. As shown in Figure 3.7, aromatic compounds can also be produced from Diels-Alder cyclization of unsaturated lipids [68]. In addition to the production of phenolic compounds, the pyrolysis of protein fraction also produces a variety of nitrogenous compounds such as indoles, pyrroles (3-methyl-1H-pyrrole) and nitriles (benzenepropanenitrile). The indole derivatives were possibly formed from thermal decomposition of tryptophan during pyrolysis, whereas pyrrole derivatives were formed from serine and asparagine. Pyrrole, indole, and their derivatives have also been observed in pyrolytic oil from sewage sludge [104], [105]. Previous studies have reported that mono-aromatic content increased at higher temperatures, and the formation of nitriles was associated with the dehydration of amides that were originally present in algae proteins [106].
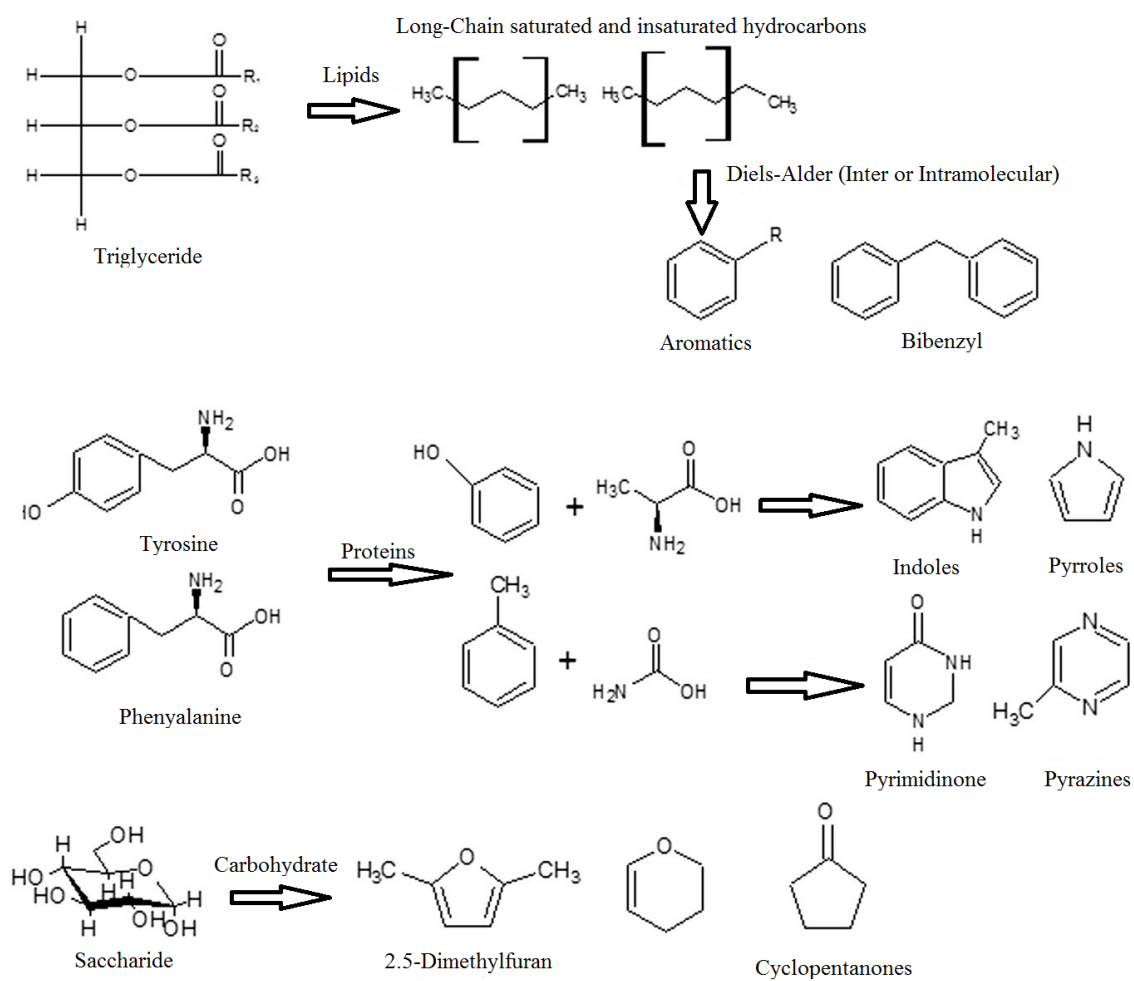
Figure 3.7 Proposed pathway for pyrolysis products of *C. vulgaris.*
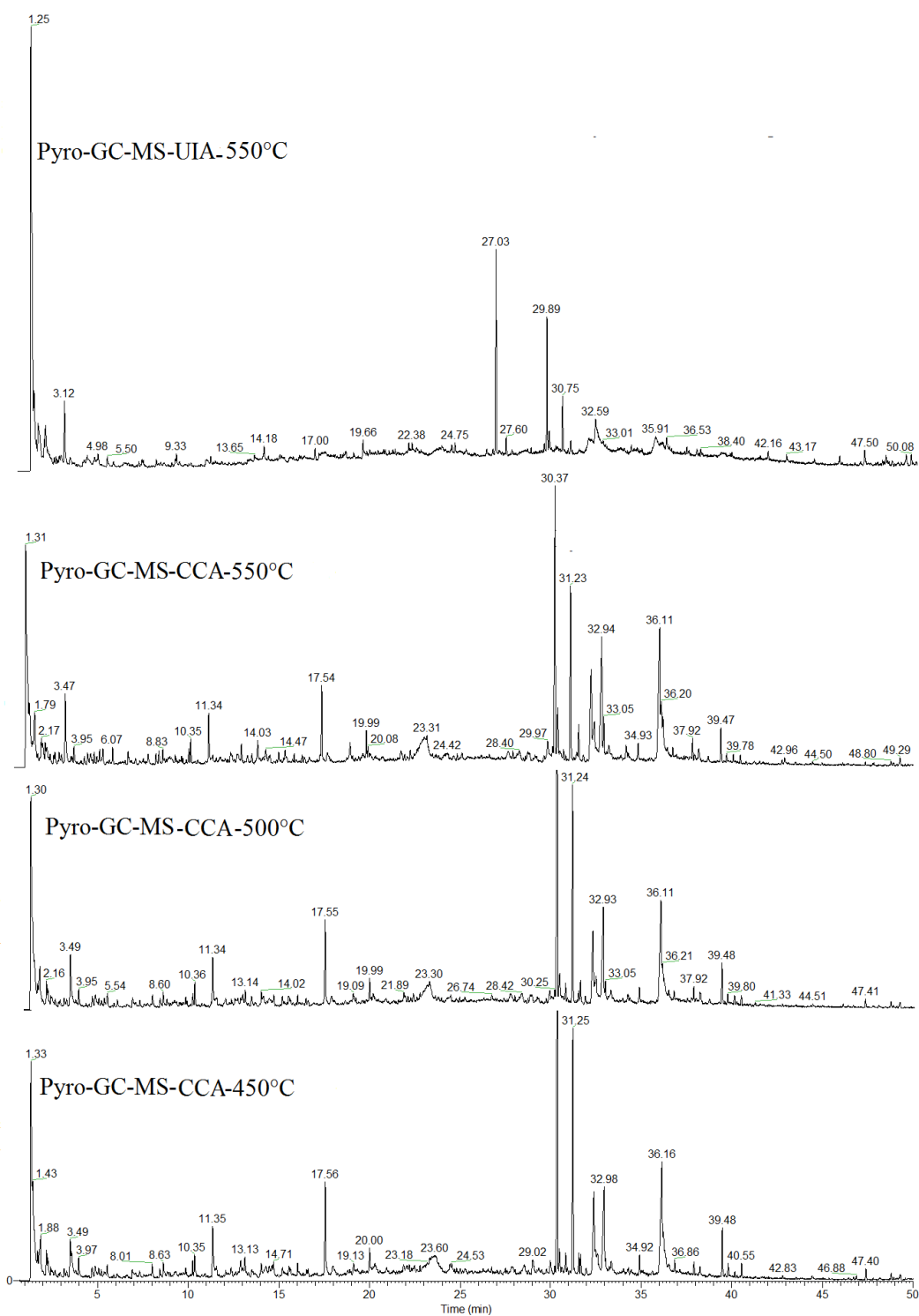
Figure 3.8 Py-GCMS profiles of UIA and CCA pyrolyzed at different temperatures

Table 3.5 Potential pyrolysis products of CCA, pyrolyzed at (450, 500, and 550 °C) and UIA (pyrolyzed at 550 °C).

GC-MS	Compound	Formula	RT	M+	CCA 450 °C	CCA 500 °C	CCA 550 °C	UIA 550 °C
1	Carbon dioxide	CO_2	1.24	44	12.52	14.82	11.40	3.68
2	Furfuran	C_4H_4O	1.47	68			1.42	1.72
3	Acetic acid, anhydride with formic acid	$C_3H_4O_3$	1.72	88	1.25	1.44	1.76	2.51
4	Isovaleraldehyde	$C_5H_{10}O$	2.11	86	1.33	0.38	0.43	2.88
5	Butanal, 2-methyl	$C3H6O2$	2.21	86		0.55	0.29	
6	Pentene-diol	$C_5H_{12}O_2$	2.36	102	0.19	0.55	0.85	
7	Furaldehyde	$C_5H_4O_2$	2.61	96	0.12	0.27	0.18	
8	2,5-dimethylfuran	C_6H_8O	2.8	96			0.19	
9	3-Methyl-3-buten-2-one	C_5H_8N	2.88	84			0.23	1.37
10	2-Pyridinecarboxylic acid	$C_6H_5NO_2$	3.11	79	0.22	0.23	0.21	5.81
11	Pyrrole	C_4H_5N	3.23	97	0.20	0.25	0.21	0.32
12	Toluene	C_7H_8	3.43	92	2.30	2.77	2.61	
13	Methyl pyruvate	$C_3O_3CH_6$	3.74	102	0.07	0.17	0.35	
14	3-methylpyridine	C_6H_7N	3.92	93	0.51	0.49	0.44	
15	2-methylpyrazine	$C_9H_6N_2$	4.33	81		0.07	0.08	
16	Methyl urea + 1,3-Octadiene	$C_2H_6N_2O/C_8H_{14}$	4.46	103/110			0.24	1.88
17	4-Cyclopropyl-1-butene	$C_5H_4O_2$	4.63	96	0.34	0.34	0.40	
18	5-pyrimidinol	$C_4H_4N_2O$	4.79	96	0.49	0.65	0.54	1.05
19	1H-Pyrrole, 2-methyl-	C_5H_7N	5.01	80	0.21	0.19	0.31	0.66
20	Furfuryl alcohol	$C_5H_6O_2$	5.16	98	0.21	0.16	0.20	0.54
21	Xylene	C_8H_{10}	5.31	106	0.18	0.16	0.31	
22	Benzylnitrile	C_7H_5N	5.46	103	0.19	0.39	0.43	1.25
23	4-Pentanoic acid	$C_5H_8O_2$	5.86	100		0.11	0.10	0.54

GC-MS	Compound	Formula	RT	M+	CCA 450 °C	CCA 500 °C	CCA 550 °C	UIA 550 °C
24	Styrene	C_8H_8	6.02	104	0.19	0.24	0.46	
25	2(5H)-furanone	$C_4H_4O_2$	6.62	84	0.19	0.15	0.01	
26	2,5 dimethylpyridine	C_7H_9N	6.88	107	0.66	0.37	0.54	
27	2-Pyrroline, 1,2-dimethyl-	$C_6H_{11}N$	7.27	98	0.22	0.25	0.16	
28	3-furfuryl alcohol	$C_5H_6O_2$	7.52	98	0.13		0.12	1.08
29	Propyl benzene	C_9H_{12}	7.72	120		0.19	0.08	
30	Hexahydro-3,6-pyridazinedione+5-methyl-2-furaldehyde (2-Furancarboxaldehyde, 5-methyl)	$C_4H_6N_2O_2/C_6H_6O_2$	7.97	110	0.39	0.56	0.29	0.51
31	2-Methyl-2-cyclohexene-1-ol	$C_7H_{12}O$	8.38	110	0.31	0.30	0.36	
32	Phenol	C_6H_6O	8.57	94	0.57	0.46	0.33	
33	Pyrimidine	$C_5H_6N_2O$	8.77	96		0.29	0.31	0.54
34	(2Z)-2-Nonenoic acid	$C_9H_{16}O$	8.88	127	0.22		0.07	
35	4-piperidinemethanamine	$C_6H_{14}N2$	8.97	114	0.11	0.07	0.09	
36	2-Propylfuran + 4-hydroxy-5,6-dihydro-(2H)-pyran-2-one	$C_7H_{10}O/C_5H_6O_3$	9.08	109		0.57	0.52	
37	2,3,4-trimethylpyrrole	$C_7H_{11}N$	9.15	109	0.45			
38	Maltol (3-Hydroxy-2-methyl-pyran-4-one)	$C_6H_6O_3$	9.46	126		0.13	0.26	1.63
39	Cyclotene (2-Hydroxy-1-methyl-1-cyclopenten-3-one)	$C_6H_8O_2$	9.81	112		0.15	0.15	
40	2-Hydroxy-3-methyl-2-cyclopenten-1-one	$C_6H_8O_2$	9.91	117	0.27		0.09	
41	1-Amino-2,6-dimethylpiperidine	$C_7H_{16}N_2$	10.21	128	0.40	0.32	0.32	
42	3-methyl-tetrahydrofuran-2,4-dione + 2,3-dihydro-benzofuran	$/C_8H_8O$	10.3	109	0.72	0.59	0.65	
43	2-methylphenol	C_7H_8O	11.28	108	1.82	1.66	1.53	0.48
44	2-furoic acid methyl ester + 4-hydroxy-2,5-dimethyl-3(2H)-furanone	$C_6H_6O_3/ C_6H_8O_3$	11.53	126+128	0.26	0.25	0.11	
45	Guaiacol	$C_7H_8O_2$	11.73	124	0.07		0.09	

GC-MS	Compound	Formula	RT	M+	CCA 450 °C	CCA 500 °C	CCA 550 °C	UIA 550 °C
46	Thiazole-5-methanol (5-Hydroxymethyl-2-furaldehyde)	C_4H_5NOS	11.88	126	0.13	0.40	0.33	
47	5-methoxy-2-methylsulfanyl-pyrimidin-4-ol	$C_6H_8N_2O_2S$	12.47	126	0.37	0.10	0.65	0.13
48	4(1H)-pyridone + 3-Pyridinecarbonitrile	$C_5H_5NO/C_6H_4N_2$	12.7	95+104		0.65	0.07	0.59
49	1-Hydroxymethyl-2-methyl-1-cyclohexene (overlapped with phenolic compound)	$C_8H_{14}O_2$	12.81	126	0.45	0.55	0.58	
50	Benzene, 1-isocyano-2-methyl+Cyclohexylidencyanoacetic Acid	$C_9H_{11}NO_2$	13.08	117	0.43	0.43	0.47	
51	Anhedro-pento-furanose		13.27	144		0.12		
52	2 4 dimethyl-phenol	$C_8H_{10}O$	13.4	122		0.45	0.32	0.25
53	Benzene, 1-chloro-4-methoxy-		13.64	142			0.25	0.78
54	Pentyl propionate (Propionic acid, pentyl ester)	$C_8H_{16}O_2$	13.9	144	0.34	0.20	0.79	
55	1-dodecene	$C_{12}H_{24}$	14.28	168			0.07	0.80
56	1,5-anhydro-arabinofuranose + 3,5-dihydroxy-2-methyl-4-pyrone	$C_5H_8O_4/C_6H_6O_4$	14.38	132+142		0.44	0.48	0.27
57	Veratrol (methyl guaiacol)	$C_8H_{10}O_2$	14.6	138		0.25	0.37	
58	1H-Pyrrole, 2-ethyl-3,4,5-trimethyl	$C_{10}H_{15}NO_2$	14.67	137	0.23			
59	3,5-Diethylpyridin-4-amine (3,5-Diethyl-4-pyridinamine)	$C_9H_{14}N$	15	150			0.10	0.34
60	1,4:3,6-dianhydro-hexopyranose	$C_6H_8O_4$	15.14	144	0.34	0.24	0.26	0.23
61	2,3-dihedrobenzofuran	C_8H_8O	15.4	120		0.05	0.08	
62	2-ethylphenol	$C_8H_{10}O$	15.49	122	0.53	0.23	0.52	
63	Unknown		15.89				0.08	
64	Benzenepropanenitrile, 4-(dimethylamino)-	$C_{11}H_{14}N_2$	15.99	131	0.32	0.26	0.18	
65	Uknown		16.08				0.13	
66	Phenol, 3-ethyl(3-Ethyl phenol)	$C_8H_{10}O$	16.39	122		0.21	0.26	
67	Homovanillin	$C_9H_{10}O_3$	16.54	166	0.33	0.18	0.26	
68	Indole	C_8H_7N	16.79	117			0.18	

GC-MS	Compound	Formula	RT	M+	CCA 450 °C	CCA 500 °C	CCA 550 °C	UIA 550 °C
69	4-ethyl guaiacol + 1,5-anhydro-xylofuranose	$C_9H_{12}O_2$/ $C_5H_8O_4$	17.25	152			0.07	1.49
70	Indolizine	C_8H_7N	17.47	117	3.12	2.26	1.89	0.31
71	2-Hydroxymethyl-5-hydroxy-2,3-dihydro-(4H)-pyran-4-one	$C_6H_6O_4$	17.77	144		0.41	0.64	0.15
72	4-vinylguaiacol	$C_9H_{10}O_2$	18.03	150	0.02	0.08	0.06	
73	3,6-Diazahomoadamantan-9-one	$C_9H_{14}N_2O$	18.43	166				0.14
74	Phenol, 3,5-dimethoxy	$C_8H_{10}O_3$	18.98	154		0.37	0.63	
75	3,6-Diazahomoadamantan-9-one	$C_{10}H_{16}O$	18.53	152				0.14
76	Anhydro-hexo-furanose		19.34	174		0.10	0.08	
77	Naphthalene, 1,2-dihydro-2,5,8-trimethyl	$C_{13}H_{16}$	19.51	172	0.49		0.21	
78	1-undecanol	$C_{11}H_{24}O$	19.74	172			0.18	1.66
79	Skatole(3-methyl-1H-indole)	C_9H_9N	19.92	131	0.78	0.58	0.73	0.24
80	Guaiacol, 4-ethyl (4-Ethylguaiacol)	$C_9H_{12}O_2$	20.05	152		0.05	0.23	
81	Creosol(guaiacol,4-methyl)	$C_8H_{10}O_2$	20.13	138		0.27		0.67
82	Benzeneacetic	$C_8H_8O_3$	20.4	152	0.70	0.05	0.13	
83	Uknown		21.81	166	0.24	0.66	0.52	
84	Guaiacol, 3-ethyl	$C_9H_{12}O_2$	22.03	152	0.17	0.15	0.20	
85	Unknown		22.16	152	0.13	0.16	0.20	0.50
86	Cis-isoeugenol	$C_{10}H_{12}O_2$	22.36	164	0.11	0.31	0.31	
87	6-methoxy-1-indanone	$C_{10}H_{10}O2$	22.56	166		0.09	0.07	
88	Coniferyl alcohol (trans)	$C_{10}H_{12}O_3$	22.65	180	5.61	3	4.94	
89	Propioguaiacone (3-Methoxy-4-hydroxypropiophenone)	$C_{10}H_{12}O_3$	23.59	180		0.07	0.07	
90	Unknown		23.7	166		0.07	0.05	
91	Unknown		23.78	166		0.08	0.09	
92	Laevoglucose	$C_6H_{10}O_5$	23.89	162		0.10	0.08	

GC-MS	Compound	Formula	RT	M+	CCA 450 °C	CCA 500 °C	CCA 550 °C	UIA 550 °C
93	Ethinamate	$C_9H_{13}NO_2$	24.11	167			0.21	
94	Coniferaldehyde	$C_{10}H_{10}O_3$	24.33	178	0.85	0.78	0.32	
95	Cyclotridecane	$C_{13}H_{26}$	24.67	182	0.14	0.22	0.27	
96	1-tridecene	$C_{13}H_{26}$	24.91	182	0.18	0.13	0.18	
97	Dihydroconiferil alcohol	$C_{18}H_{23}NO_3$	25.16	182	0.32	0.19	0.21	
98	Unknown		26.22	182		0.13	0.11	
99	Ohdppd	$C_{20}H_{14}O_4$	26.68	194	0.15	0.20	0.12	
100	Unknown		27.19	192		0.09	0.06	
101	Unknown		27.36	194		0.18	0.09	
102	Unknown		27.66	182		0.64	0.63	
103	Undecenoic acid	$C_{11}H_{20}O_2$	28.01	182	0.08	0.13	0.20	
104	Trans-isoeugenol	$C_{10}H_{12}O_2$	28.24	180	0.05	0.93	0.84	
105	Unknown		28.6	208		0.07	0.06	
106	Unknown		28.71	185		0.11	0.12	
107	Myristic	$C_{14}H_{28}O_2$	28.81	228		0.77	0.70	
108	Hexadecenoic acid	$C_{16}H_{30}O_2$	29.23	254	0.87	0.49	0.08	
109	Unknown		29.89	278		0.48	0.86	
110	Palmitic acid	$C_{16}H_{32}O_2$	30.29	256	14.07	13	12.31	
111	Unknown		30.45	280	0.85	0.95	1.51	
112	Pentadecanoic		31.62	242		0.55	0.76	
113	5,10-Diethoxy-2,3,7,8-tetrahydro-1H,6H-dipyrrolo[1,2-a:1',2'-d]pyrazine	$C_{14}H_{22}N_2O_2$	32.23	194	6.33	3.05	3.90	1.81
114	Unknown		32.43	194		0.61	1.02	
115	Linoleic acid	$C_{18}H_{32}O_2$	32.75	280	5.27	4.44	5.73	7.51
116	N-Hexadecanoic acid	$C_{16}H_{32}O_2$	33.01	256		0.38	0.84	
117	Unknown		34.23	221		0.30	0.43	

GC-MS	Compound	Formula	RT	M+	CCA 450 °C	CCA 500 °C	CCA 550 °C	UIA 550 °C
118	Unknown		34.35	207		0.08	0.14	
119	Unknown		34.87	280	0.55	8.41	0.44	
120	Oleic acid(C18:2)	$C_{18}H_{34}O_2$	35.93	280	9.53		5.06	6.33
121	Stearic acid	$C_{18}H_{36}O_2$	36.5	284	0.16	0.28	0.13	1.20
122	Unknown		36.78	330	0.24	0.12	0.27	0.45
123	Unknown		37.99	280	0.33	0.12	0.28	
124	Sinapaldehyde	$C_{11}H_{12}O_4$	38.21	208	0.36	0.69	0.44	
125	Unknown		38.7	269	0.12	0.20	0.27	
126	1-eicosene	$C_{20}H_{40}$	39.39	280	1.33	1.28	1.01	1.44
127	Linoleic acid ethyl ester	$C_{20}H_{36}O_2$	39.73	279	0.46	0.27	0.22	
128	(3S,8as)-3-Benzylhexahydropyrrolo[1,2-a]pyrazine-1,4-dione	$C_{14}H_{16}N_2O_2$	40.09	244	0.15	0.30	0.21	
129	9,12-Octadecadienoic acid, methyl ester, (E,E)-	$C_{19}H_{34}O_2$	40.5	294	0.35	0.29	0.26	
130	Unknown		41.18	264	0.05	0.29	0.23	
131	1H-Indene, 1-hexadecyl-2,3-dihydro-	$C_{25}H_{42}$	41.71				0.14	0.43
132	Eicosapentaenoic(EPA)	$C_{16}H_{22}O_4$	42.76	302	0.14	0.14	0.14	0.10
133	Arachidonic		44.43	304	0.21	0.21	0.09	
134	Arachidic acid	$C_{43}H_{88}$	46.1	304		0.03	0.07	0.27
135	Squalene	$C_{30}H_{50}$	46.37	410	0.15	0.05	0.07	
136	Docosahexaenoic (DHA)	$C_{28}H_{42}$	47.33	328	0.31	0.31	0.09	
137	Nonadecane	$C_{19}H_{40}$	47.5				0.01	0.72
138	Cholesta-3,5-diene	$C_{27}H_{44}$	47.83	365			0.04	0.21
139	Behenic	$C_{29}H_{48}$	48.73	354	0.23		0.11	0.42
140	3α,5-Cyclo-5α-ergosta-6,8(14).22t-triene	$C_{28}H_{42}$	48.88	378	0.05		0.09	
141	Steroid	$C_{27}H_{42}O$	49.2	382	0.23		0.28	

GC-MS	Compound	Formula	RT	M+	CCA 450 °C	CCA 500 °C	CCA 550 °C	UIA 550 °C
142	Petacosanoic		49.54	396	0.03		0.03	
143	Stigmastan-diene	$C_{29}H_{48}$	50.02	396	0.01	0.01	0.04	0.44
144	Steroid	$C_{29}H_{46}$	50.17	394	0.05	0.05		
145	Stigmastan-diene	$C_{29}H_{48}$	50.33	396	0.04	0.04	0.06	0.36
146	Steroid	$C_{29}H_{46}$	50.63	394	0.02	0.02	0.01	
147	Vitamin E	$C_{29}H_{50}O_2$	50.86	430	0.10	0.10	0.08	
148	Hexacosanoic	$C_{28}H_{44}O$	51.55	410	0.32	0.32	0.01	0.34
149	Cholesta-3,5-dien-7-one	$C_{27}H_{42}O$	0.02				0.27	
150	Beta-Sitosterol	$C_{29}H_{50}O$	52.82	400	0.13	0.13	0.11	
152	C-sitosterol	$C_{29}H_{50}O$	53.5	280	0.03		0.03	
153	Hexadecyl-palmitate	$C_{32}H_{64}O_2$	53.77	480	0.12	0.12	0.06	
154	Hexacosanoic	$C_{29}H_{46}O$	54.77	397				

3.5 *C. vulgaris* pyrolysis product yield

The bio-oil, biochar, and syngas yields for CCA and UIA are presented in Figure 3.9. The highest bio-oil yield (47.7%) was obtained from the CCA algae sample pyrolyzed at 550 ℃. Reported bio-oil yields vary greatly in literature and pyrolysis conditions affect the yields significantly, however, a 47.7% yield is considered high compared to many yields reported in the literature [23], [107]. Studies show that by optimizing the pyrolysis process, the yield can be considerably increased [39], [108]. The bio-oil yields for other three samples fall well within the range of reported yields for *C. vulgaris*. The results are in agreement with previous studies that indicated an increase in temperature causes an increase in bio-oil production [36].

The highest biochar yield was observed in the CCA sample pyrolyzed at 450℃ (42.5%), followed closely by UIA (40%). The high biochar yield for the CCA was attributed to the low pyrolysis temperature, and the high biochar yield for the UIA was due to the high ash content of the original biomass. The biomass nature, the heat transfer rate, and pyrolyzer efficiency can affect bio-oil and biochar yields [84]. The transfer tube efficiency can be improved to increase condensation and potentially recover more bio-oil. *C. vulgaris* pyrolysis product yields can further be optimized by altering the pyrolysis parameters such as residence time and temperature [79].

Bio-oil and biochar yields of CCA at 550 ℃ were promising and similar or better compared to other biomass resources. For example, the bio-oil and biochar yields for residual

bacterial biomass were 28% and 46% [79], for hybrid poplar were 40% and 15%, and for

potato peel waste were 26% and 32 %, respectively [84].
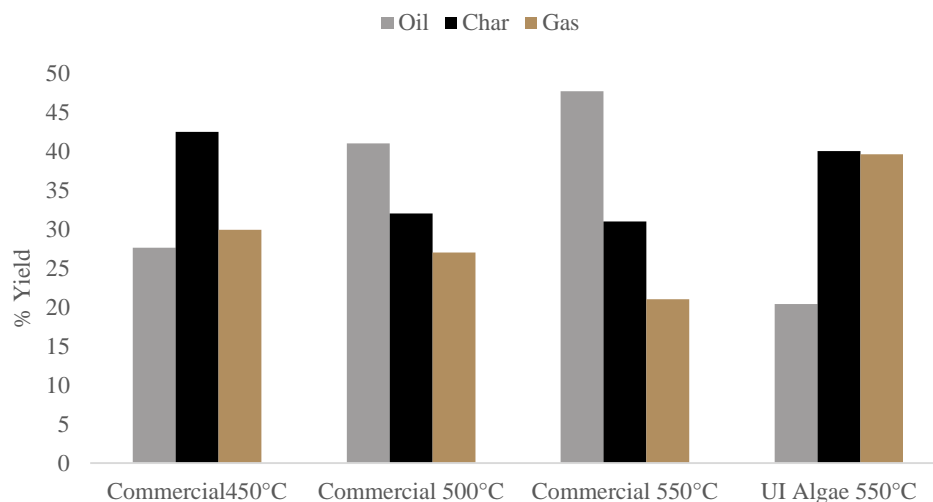
Figure 3.9 Pyrolysis product yields for CCA and UIA.

3.6 *C. vulgaris* **bio-oil properties**

Table 3.6 lists some basic properties of the bio-oil samples obtained from CCA

pyrolyzed at various temperatures (450, 500, and 550 °C). The UIA pyrolysis bio-oil was of

very low quality (high water content), and data is not presented. In general, the increase in

pyrolysis temperature improved the quality of the produced CCA bio-oil. The bio-oil

generated at 550 °C had the lowest moisture content and the highest calorific value, both of

which are desirable traits for bio-oils. The acidity of all three samples of bio-oil was low

(pH>9) compared to lignocellulosic biomass pyrolysis bio-oils reported in the literature [109].

This basicity was most likely a result of the high nitrogen content of the *C. vulgaris* samples

(due to the abundance of proteins in their structure), which was released during pyrolysis as

amines. Similar to other bio-oils with low acidity such as residual bacterial biomass bio-oil, *C.*

vulgaris bio-oil may be suitable for direct use as boiler fuel, as compared with low-protein lignocellulosic biomass bio-oils [79].

Table 3.6 Properties of bio-oil obtained from CCA pyrolyzed at various temperatures.

Sample ID	%Moisture Content	Calorific Value (MJ/kg)	pH
CCA 450 °C Bio-oil	64	27	9.62
CCA 500 °C Bio-oil	58	31	9.9
CCA 550 °C Bio-oil	55	32	10.13

3.7 *C. vulgaris* biomass and biochar SEM images

Figure 3.10 shows examples of SEM visualization of CCA and biochars obtained at three different pyrolysis temperatures (450, 500, and 550 °C). As depicted in Figure 3.10, an increase in pyrolysis temperature causes a drastic rupture and fusion of cell walls. The biochars generated from pyrolysis of CCA at 550 °C were more structurally disintegrated. The disintegration was most likely caused by thermal cracking of their parent biomass during pyrolysis. It is worth mentioning that the obscurely-porous structures of *C. vulgaris* biomass and biochar samples are consistent with the low surface area analysis results presented earlier. Furthermore, a high degree of cell wall decomposition in the biochar sample obtained at 550 °C is in agreement with the GC-MS results that show a greater variety of compounds for the bio-oil obtained at 550 °C.
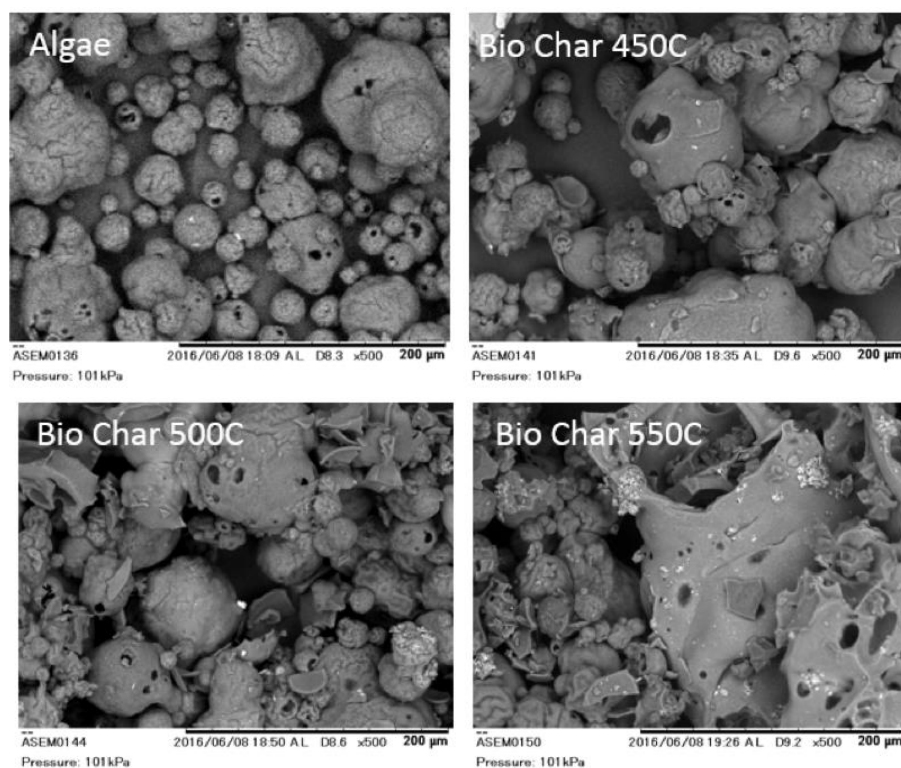
Figure 3.10 SEM micrographs of CCA and biochar obtained from CCA pyrolyzed at various temperatures.

3.8 Raman spectroscopy of *C. vulgaris* biochar

To evaluate the chemical structure of algal biochar, particularly the distribution and state of aromatic carbons, Raman spectroscopy was performed. Raman spectra of CCA and UIA biochars are presented in Figure 3.11. The spectra showed two peaks at Raman shifts of 1355 cm^{-1} and 1585 cm^{-1} for both microalgae samples. The former is assigned to the D-band (amorphous or disordered C), and the latter is assigned to the G-band (graphitic crystallites) of carbon [110]. The I_D/I_G values for CCA biochar pyrolyzed at 450, 500 and 550°C were respectively, 0.88, 0.93 and 0.95. These results show that pyrolysis temperature influenced biochar carbon structure. The I_D/I_G value obtained were 0.95 for CCA and 0.86 for UIA biochar pyrolyzed at 550 °C (Figure 3.11). These results fall within the range of values (0.8-1.5) reported for most biochars obtained from various biomass sources pyrolyzed at 500 °C [111]. These results show that the algal biochar has a reasonable amount of disordered amorphous carbon. This amorphous character promotes mineralization by bacteria and fungi, which is essential for nutrient turnover processes and aggregate formation.
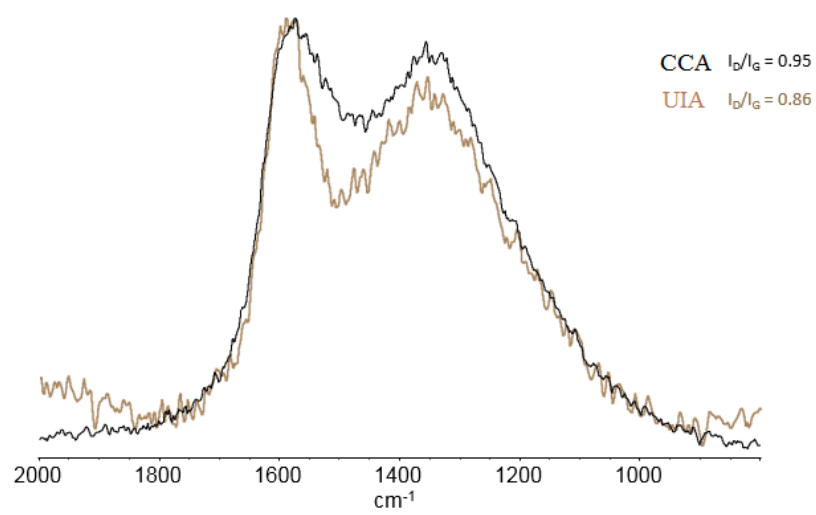
Figure 3.11 Raman spectra of CCA and UIA biochar samples pyrolyzed at 550 °C.

3.9 FTIR analysis of *C. vulgaris* biomass, biochar, and bio-oil

FTIR spectroscopic analysis was performed to investigate the chemical structure of *C. vulgaris* algae biochar and bio-oil samples. The algae samples were also analyzed for comparison. Figure 3.12 and 3.13 show FTIR results for CCA and UIA and their corresponding biochars. Figure 3.14 shows FTIR results for CCA bio-oils (obtained at 450, 500, and 550 °C) and UIA bio-oils (obtained at 550 °C). The band assignments are summarized in Table 3.7 for algae and biochar and in Table 3.8 for bio-oils. The broad bands in the region of 3600–3200 cm^{-1} are associated with the O−H (e.g., water, alcohol, and phenol) and N−H (amines) stretching vibrations [112]. The O−H and NH stretching vibrations were only observed in CCA and UIA biomass and bio-oil samples. The results indicate that the N-containing proteins were mostly converted into bio-oil products [79], which could explain the increase in the pH of the bio-oil generated at higher temperatures reported earlier. Furthermore, the relatively intense peaks in bio-oil samples between 3360 cm^{-1} and 3399 cm^{-1} suggest that a rather large amount of water was present in the samples, which is in agreement with the previously reported moisture content measurements of the bio-oil samples.

Aliphatic bands C−H (CH_3 and CH_2) stretching vibrations between 2950 cm^{-1} and 2850 cm^{-1} were present in the biomass samples, all CCA biochar samples, and bio-oil samples obtained at 500 and 550 °C. The broad bands at approximately 1650 cm^{-1} in all samples, except for UIA biochar, were ascribed to Amide I. Another band at 1532-1557 cm^{-1} was only observed in UIA and CCA biomass samples and CCA bio-oil samples. This band was attributed to the C−N stretching and N−H in-plane bending absorption due to Amide II of secondary amide in protein [79]. The bands between 1300 and 1500 cm^{-1} in the CCA and UIA biomass, all biochar, and bio-oil samples are associated with the deformation of CH_2 and CH_3

groups. The carboxylic acids C−O stretching vibrations showed up at around 1040 cm^{-1} in the biomass samples and UIA biochar.

UIA biochar had a very little absorbance in wavenumbers of higher than 1600 cm^{-1}, which could be attributed to its very high ash content reported earlier. The CCA bio-oil samples obtained at 500 and 550 °C had a very similar FTIR profile, which was significantly different from that of the bio-oil obtained at 450 °C. This is likely caused by the thermal decomposition of more chemicals in the biomass structure at higher pyrolysis temperatures. The results also indicate that the intensity of existing peaks decreases for biochar samples as the pyrolysis temperature increases. This, too, is associated with decomposition of easily degradable compounds. It is worth mentioning that most of the peaks that are present in the CCA biomass spectrum are also present in both biochar and bio-oil spectra, however, with diminished intensity. This further emphasizes that the type of biomass can greatly affect the properties of pyrolysis products.

Table 3.7 FTIR analysis results for CCA biomass and biochar obtained at various temperatures.

Band assignment	CCA	450 °C CCA Biochar	500 °C CCA Biochar	550 °C CCA Biochar	UIA	550 °C UIA Biochar
	Wavenumber (cm^{-1})					
O–H stretching vibration	3280				3307	
C–H (CH$_3$, CH$_2$) stretching vibration	2924	2924	2925	2923	2920	
C-H symmetric stretching	2854	2854	2854	2852	2851	
Amide I band	1644	1668	1661	1650	1644	
Amide II band	1531				1538	
Deformation of CH, CH$_3$, and CH$_2$	1454	1447	1453	1454	1454	1417
O–H or C–H bending	1393	1374	1375	1375		
C–C and C–O stretching in guaiacol	1230					
C–O stretching and O–H bending	1175	1099	1169	1170		
Silicate; C–O stretching	1033				1041	1052
Adjacent aromatic C–H deformation		745	744	699		
Phenol O–H out of plane deformation /=C–H bending	700				666	

Table 3.8 FTIR analysis results for bio-oil obtained from pyrolysis of CCA at various temperatures.

Band assignment	450 °C CCA Bio-oil	500 °C CCA Bio-oil	550 °C CCA Bio-oil	550 °C UIA Bio-oil
	Wavenumber (cm^{-1})			
O-H stretching	3374	3394	3399	3360
C-H asymmetric stretching		2955	2955	
C–H (CH3, CH2) stretching vibration		2924	2924	
C-H symmetric stretching		2853	2853	
Amide I band	1650	1660	1651	1644
Amide II band	1557	1557	1557	
Deformation of CH, CH3, and CH2	1454	1455	1455	1454
Adjacent aromatic C–H deformation		729	729	702
Phenol O–H out of plane deformation /=C–H bending	698			
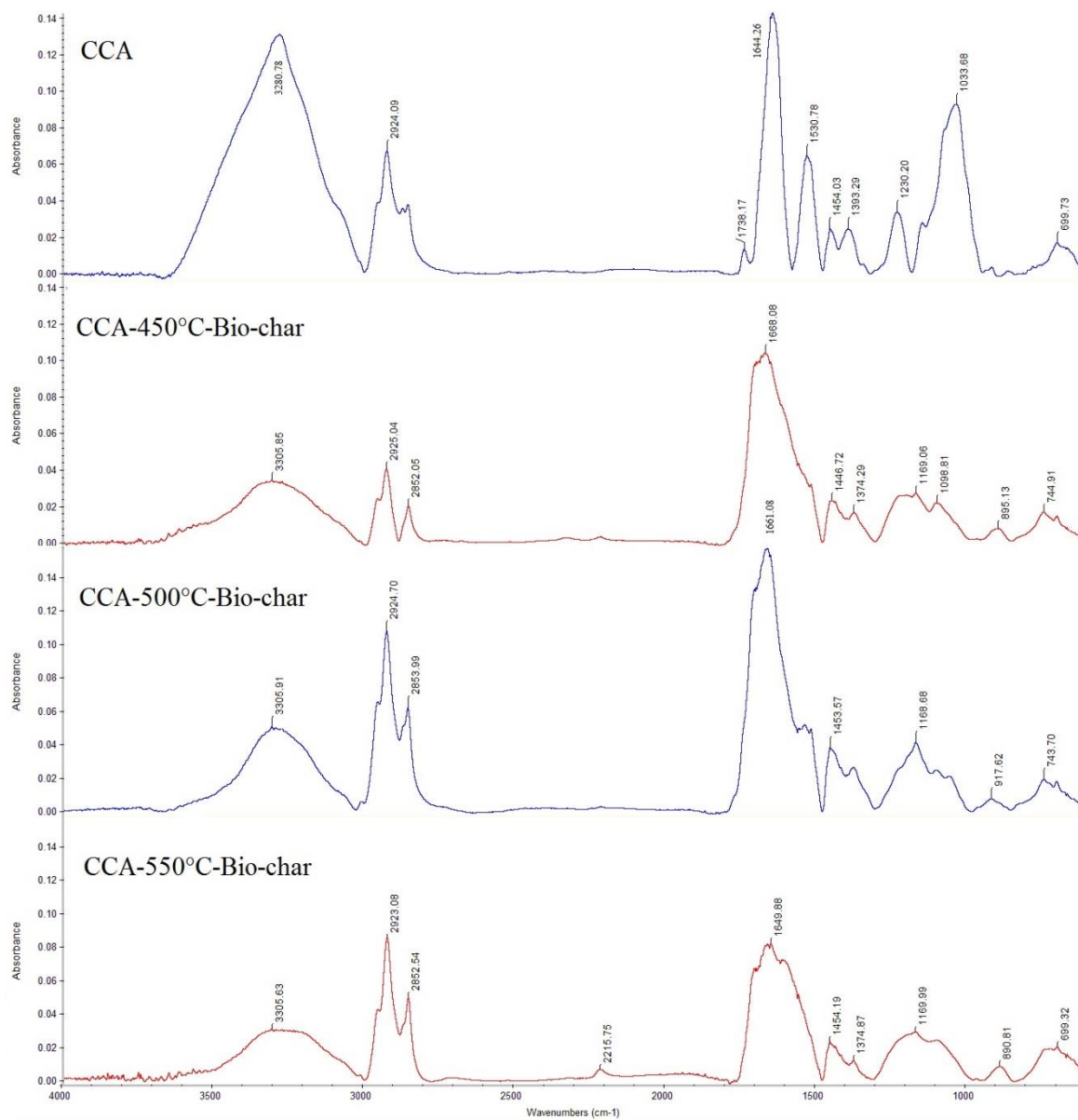
Figure 3.12 FTIR analysis of CCA and biochar obtained at 450, 500, 550 °C.
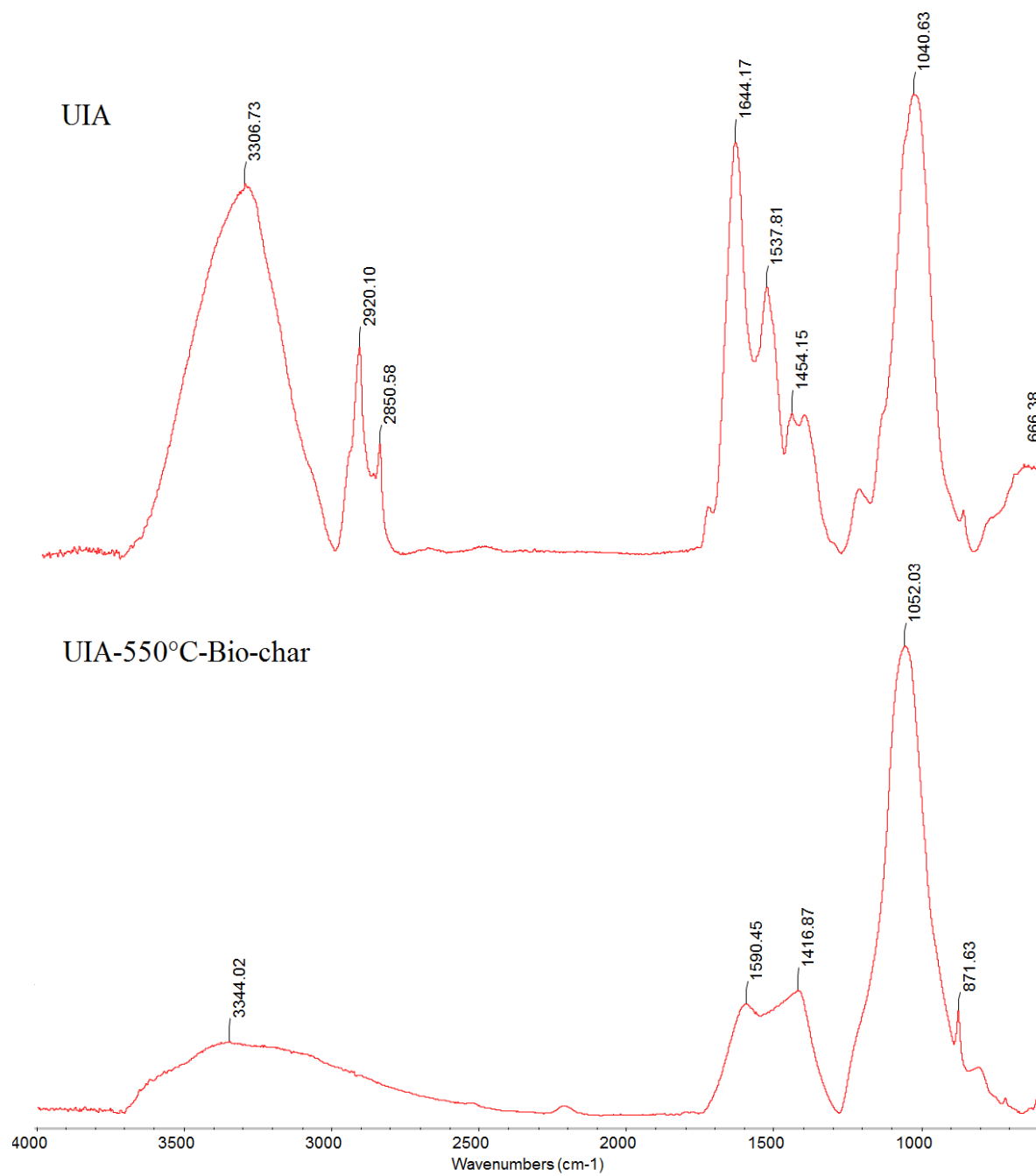
Figure 3.13 FTIR analysis of UIA and biochar obtained at 550 °C.
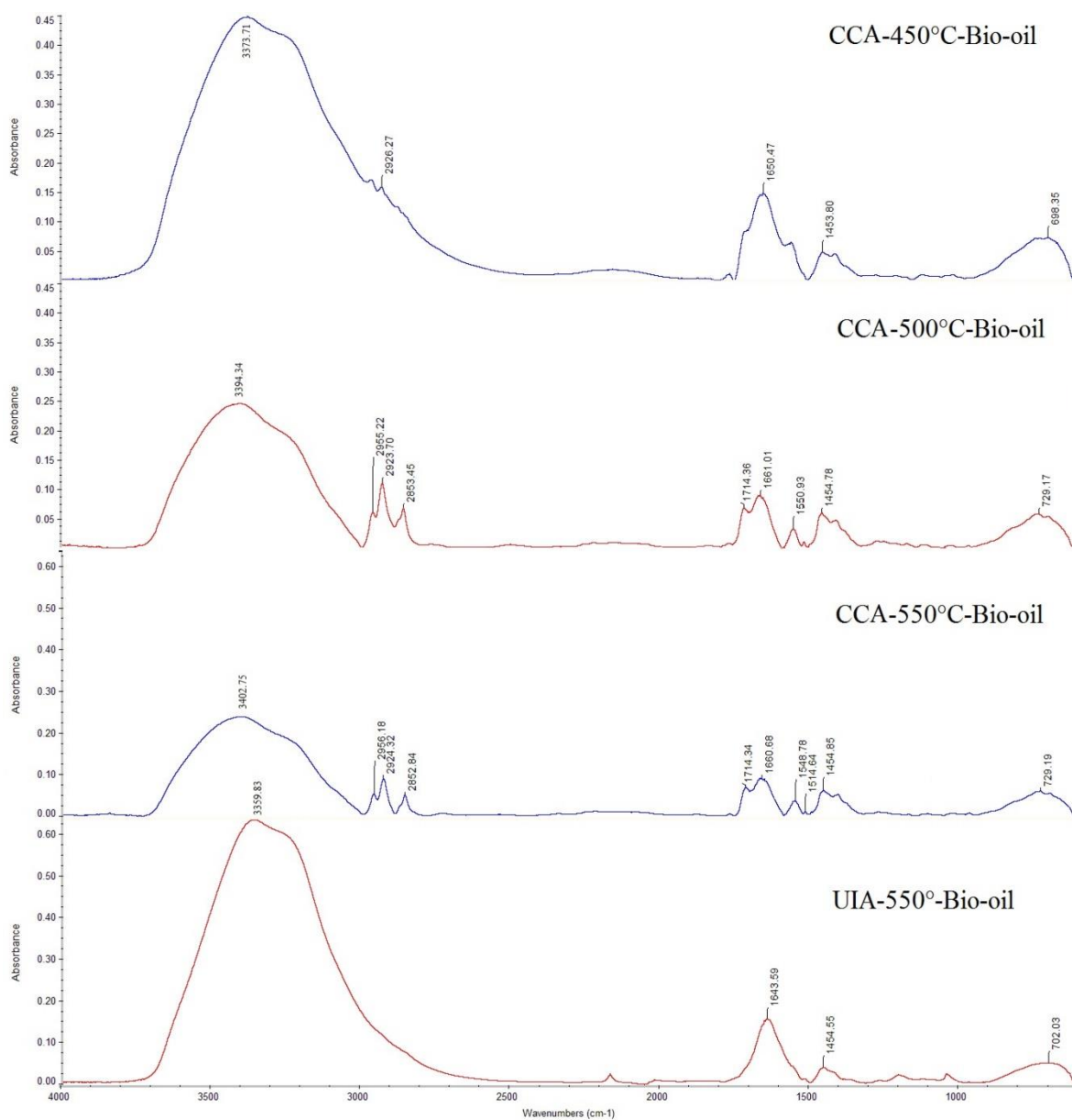
Figure 3.14 FTIR analysis of CCA bio-oil obtained at various pyrolysis temperatures

3.10 ESI-MS of *C. vulgaris* bio-oil

Volatile and semi-volatile compounds are mostly degraded or converted thermally during pyrolysis of CCA, therefore, the generated bio-oil contains a considerable amount of unknown, high-molecular-weight compounds. These high molecular weight compounds cannot be eluted in a GC column. To overcome this issue, positive and negative ion ESI-MS was used to calculate the average molar mass (M_w and M_n) of three bio-oil samples obtained from CCA. The bio-oil obtained from UIA was of very poor quality and was not able to get good spectra and data not presented. Figures 3.15-3.17 illustrate the negative and positive ion ESI-MS spectra of bio-oil samples, obtained from pyrolysis of CCA at various temperatures.

Both the positive and negative ion MS spectra were dominated by <m/z 400 ions for all samples, with a more pronounced dominance in the positive ion mode. The M_w and M_n for all samples are presented in Table 3.9. Polydispersity was calculated for all samples and found to be close to 1.3. These results suggest that the products were mono- to oligomeric compounds. The calculated molar masses were comparable to residual bacterial biomass [79] and higher than other biomass types, i.e., hybrid poplar and potato peel waste [84]. It is worth mentioning that an increase in pyrolysis temperature leads to the generation of bio-oil products with smaller M_w and M_n. This lower average molar mass is a result of the higher degree of degradation during pyrolysis at higher temperatures.

Table 3.9 Molecular weight of compounds in bio-oil, obtained from pyrolysis of CCA at various temperatures, calculated from ESI-MS results.

Pyrolysis bio-oil sample	Positive ion		Negative ion	
	M_n (g/mol)	M_w (g/mol)	M_n (g/mol)	M_w (g/mol)
CCA 450 ℃	263	349	503	647
CCA 500 ℃	259	336	446	606
CCA 550 ℃	252	328	437	588
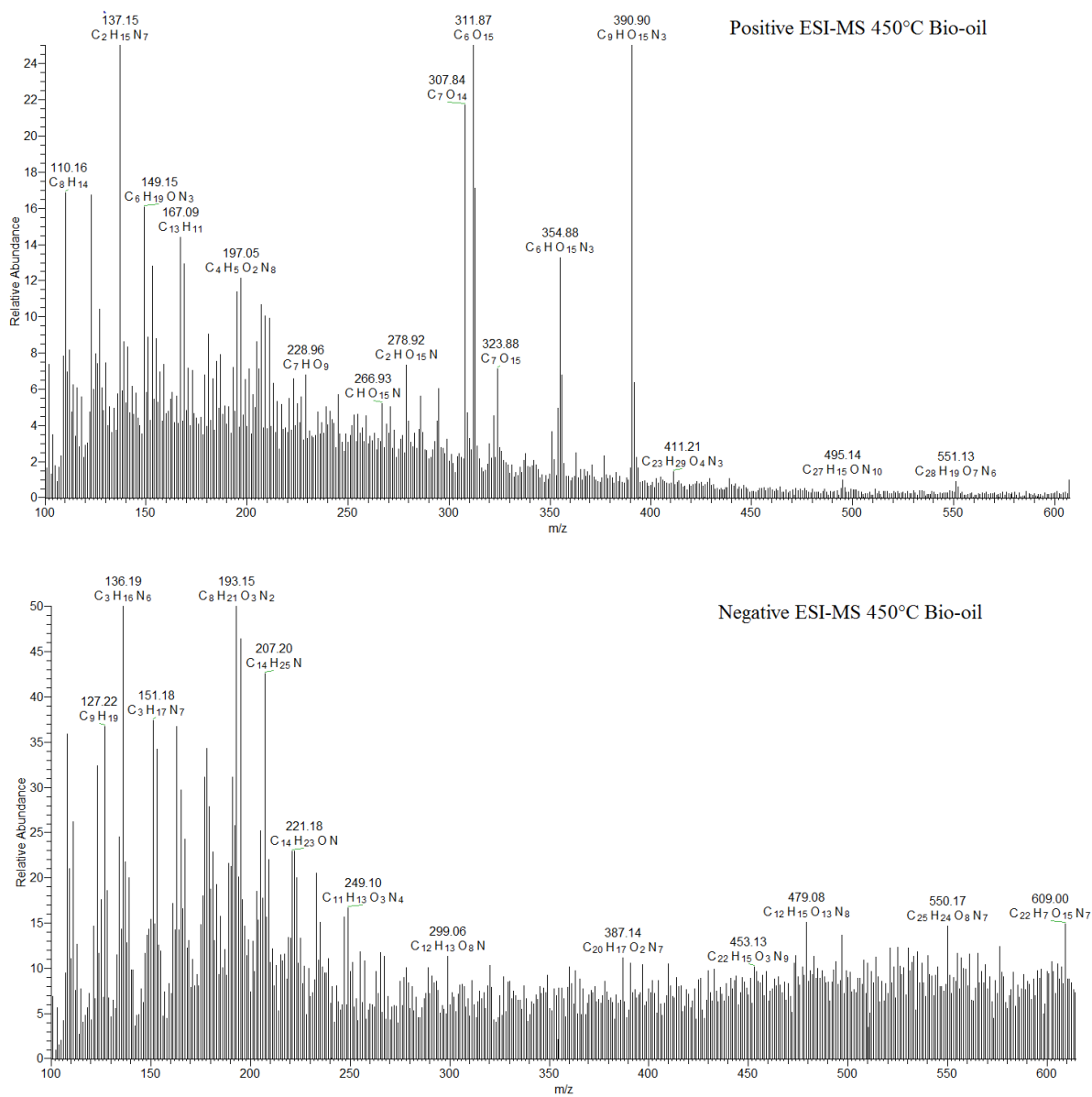
Figure 3.15 Negative and positive ion ESI-MS results of CCA bio-oil obtained at 450℃
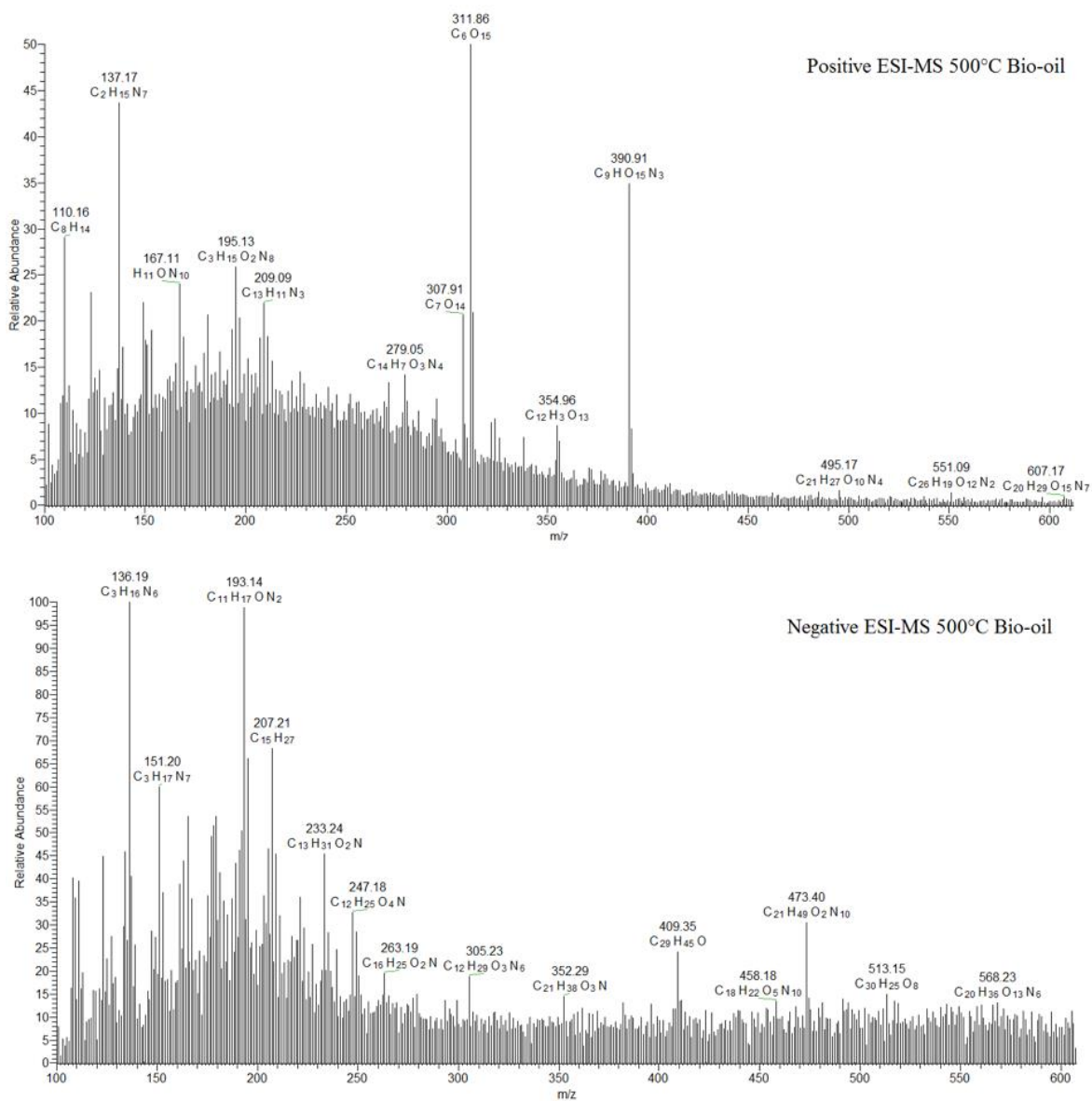
Figure 3.16 Negative and positive ion ESI-MS results of CCA bio-oil obtained at 500℃
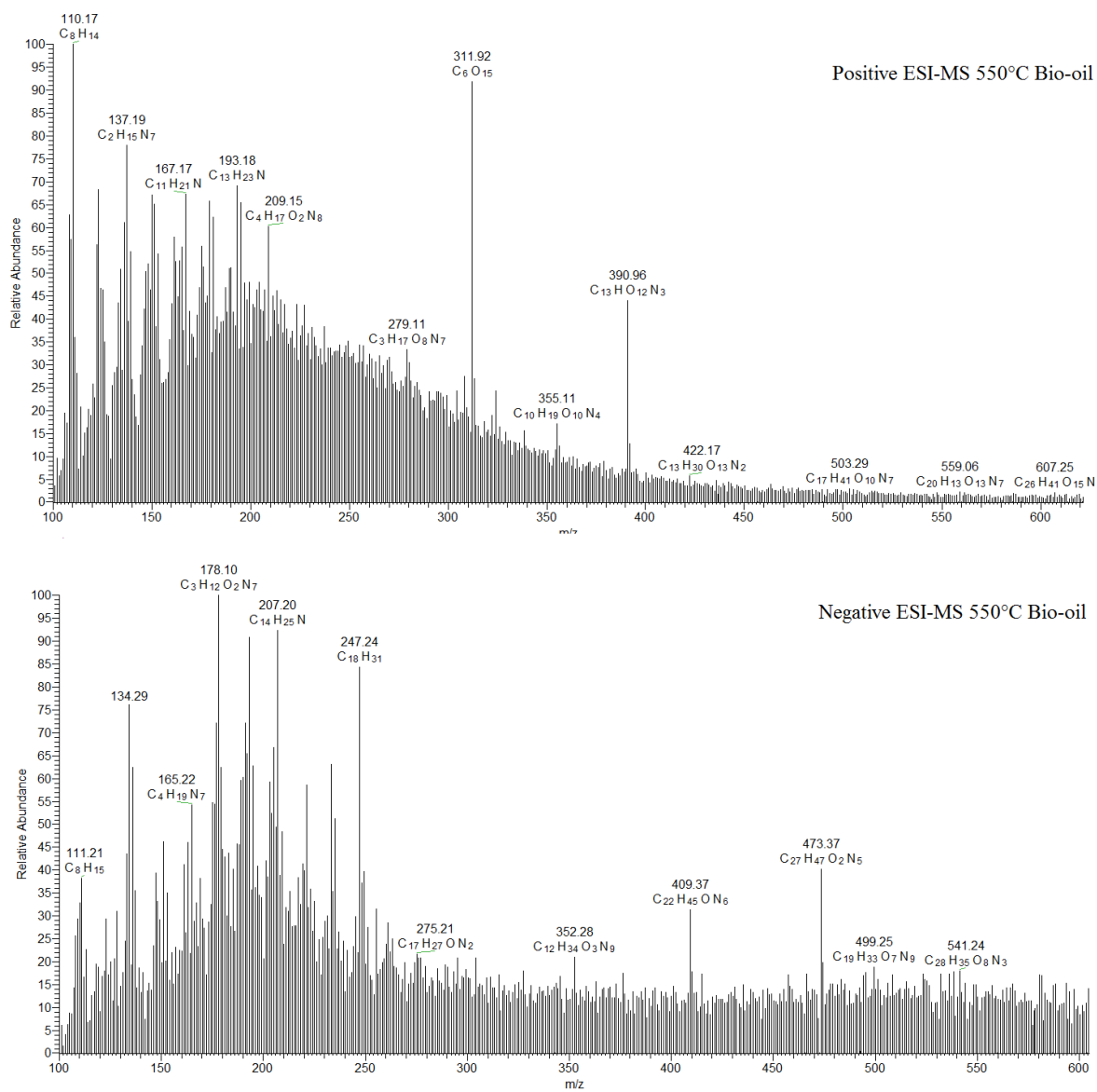
Figure 3.17 Negative and positive ion ESI-MS results of CCA bio-oil obtained at 550°C

3.11 GC-MS of *C. vulgaris* bio-oil

GC-MS was performed on freshly produced bio-oil of commercial *C. vulgaris* (CCA) pyrolyzed at 450, 500, and 550 °C. Thirty-seven potential compounds were identified and are listed in Table 3.10. The chromatograms of all three bio-oil samples exhibit a very complex mixture of organic compounds of C_5 to C_{20} carbons (Figure 3.18). The UIA bio-oil was not analyzed due to its high water content and poor quality.

The samples were mainly composed of phenols, pyrroles, furans, and fatty acids. Nitriles, benzenes, alkanes, alkenes, ketones, and a few nitrogen-containing heterocycles, such as indoles and pyridines, were also identified in the bio-oil samples. The components of CCA bio-oil samples were similar to what was previously reported in the literature for microalgae [113]–[115].

As anticipated by the results of analytical Py-GCMS, reported earlier in this chapter, palmitic acid was the most abundant compound identified in all three CCA bio-oil samples, with an average abundance of 5 µg/mg. Furthermore, in accordance with Py-GCMS results, many types of ketones and phenols were identified. These compounds are thought to have been converted from polysaccharides present in the biomass through chemical reactions such as hydrolysis and dehydration [113].

Multiple alkenes were identified in the bio-oil samples such as 1-tetradecane, 1-tridecane, and 4 cyclopropyl-1-butene. These aklenes have most likely originated from fatty acids in the *C. vulgaris* biomass [113]. Long chain alkanes like n-heptadecane, identified in two of the three CCA bio-oil samples, contribute greatly to the enhancement of combustion properties of bio-oils [113].

The identified nitrogen-containing heterocyclic compounds such as indoles and pyridines are a result of protein degradation [116]. They may have been formed through pyrolysis of peptides, decomposition, or condensation of amino acids. Specifically, the formation of benzene ring structure happens through a polycondensation reaction between aldehydes and ketones, or through decomposition of amino acids.

Since nitrogen in fuels leads to the formation of NOx compounds, which are undesirable for environmental and legislative reasons, it is necessary to remove the nitrogen and oxygen from bio-oils before they can be used as biofuels [113]. Due to the high nitrogen content of the obtained bio-oil samples, they are not good candidates for being used as fuels, however, the high nitrile content makes them suitable for organic synthesis.
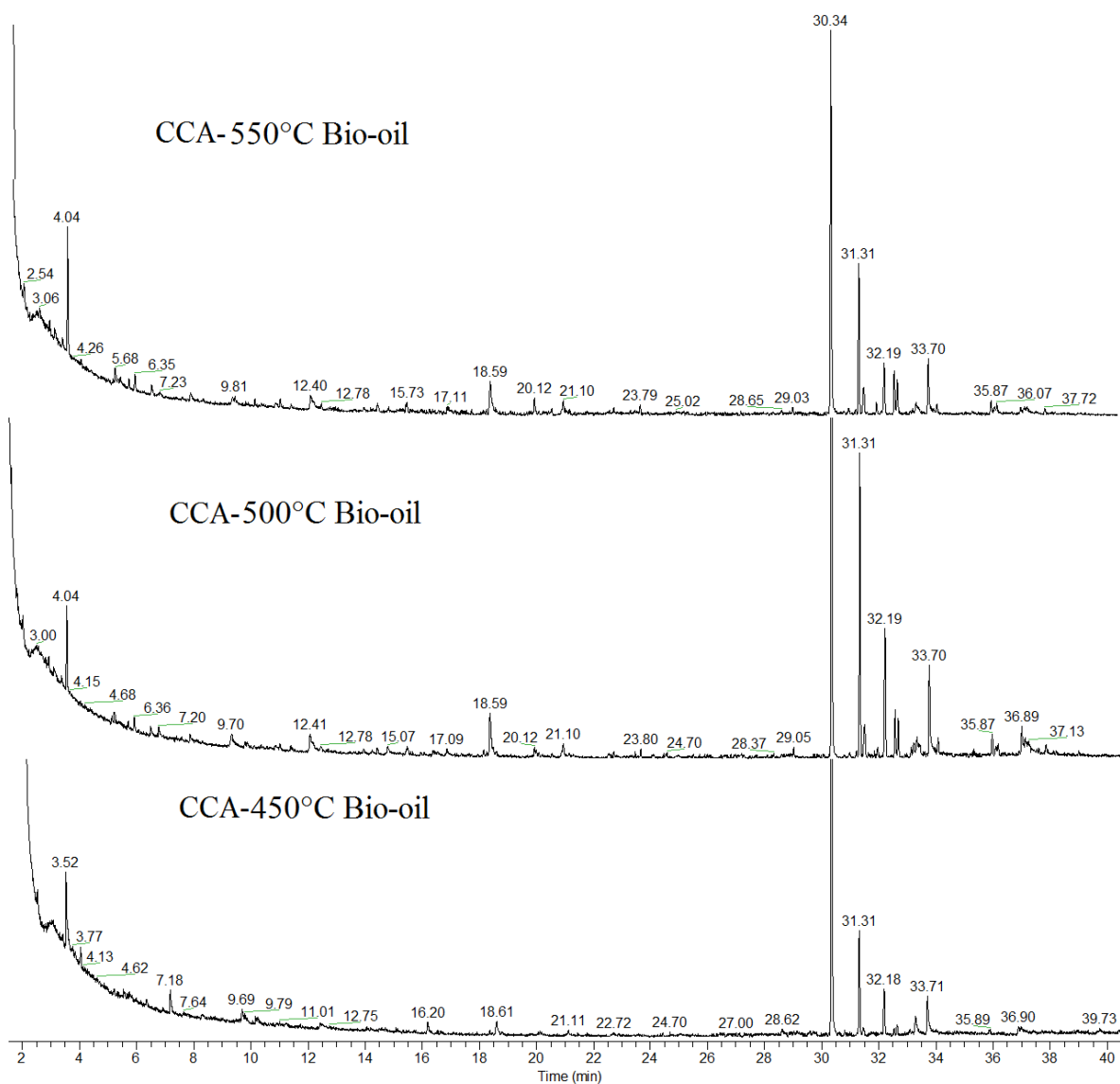
Figure 3.18 Chromatogram of fresh CCA bio-oil samples obtained at various pyrolysis temperatures (450, 500 and 550 °C).

Table 3.10 Compounds identified in CCA fresh bio-oil by GC-MS.

GC-MS	Compound	RT	M+	Formula	CCA 450 °C µg/mg	CCA 500 °C µg/mg	CCA 550 °C µg/mg
1	4-Cyclopropyl-1-butene	4.04	96	$C_5H_4O_2$	0.69	1.7	2.83
2	Xylene	6.15	106	$C_{10}H_{14}$	_	0.26	0.27
3	Benzylnitrile	6.35	106	C_8H_{10}	_	0.32	0.41
4	Styrene	6.93	104	C_8H_8	_	0.24	0.37
5	Phenol	9.81	94	C_6H_6O	0.54	0.56	0.72
6	Methyl-dihydro-(2H)-pyran-2-one	10.49	112	$C_6H_8O_2$	_	_	0.15
7	(3H)-Furan-2-one	11.21	84	$C_4H_4O_2$	0.72	_	0.24
8	2,3,4- trimethylpyrrole	11.37	109	$C_7H_{11}N$	_	_	0.26
9	Phenol,4-allayl-	11.73	134	$C_9H_{10}O$	_	_	0.1
10	Benzyl alcohol	12.40	108	C_7H_8O	0.71	1.08	0.92
11	2,3-dihedrobenzofuran	12.78	120	$C_8H_8O_3$	_	0.19	0.14
12	Benzene, pentyl-	14.71	148	$C_{11}H_{16}$	_	0.19	0.28
13	Guaiacol	15.73	124	$C_7H_8O_2$	_	0.4	0.38
14	Dihydro-methyl-furanone	16.20	100	$C_5H_8O_2$	0.94	_	_
15	Benzene propanenitrile	17.11	131	C_9H_9N	_	0.21	0.39
16	Indole	18.59	117	C_8H_7N	0.94	1.85	1.78
17	Phenol, 3,5-dimethoxy	20.12	154	$C_8H_{10}O_3$	0.18	0.34	0.58
18	Pentanamide, 4-methyl	21.1	115	$C_6H_{13}NO$	0.34	0.56	0.59
19	2-butenethioic acid,3-ethyl	22.88	130	$C_7H_{14}O_2$	0.29	0.12	0.2
20	Cyclopropane, 1-butyl-2-ethyl-	23.44	154	$C_{11}H_{22}$	_	_	0.07
21	Octane, 3,5-dimethyl-	23.61	144	$C_{10}H_{22}$	_	0.08	0.04
22	Benzeneacetic	23.79	152	$C_8H_8O_3$	_	0.22	0.24
23	2-Methyl-2-phenylpropanenitrile	28.65	145	$C_{10}H_{11}N$	0.34	0.28	0.16
24	Cyclotridecane	29.03	182	$C_{13}H_{26}$	_	_	0.16
25	Palmitic acid	31.31	256	$C_{17}H_{34}O_2$	4.28	7.19	4.12
26	1-tetradecene	31.48	196	$C_{14}H_{28}$	_	1.24	1.11
28	1-tetradecene	32.19	196	$C_{14}H_{28}$	2.32	3.89	1.62
29	N-Heptadecane	32.53	240	$C_{17}H_{36}$	0.35	_	1.12
30	N-pentadecanonitrile	32.63	223	$C_{15}H_{29}N$		1.12	0.87
31	7,10-Hexadecadienoic acid	33.29	252	$C_{16}H_{28}O_2$	0.73	_	_
32	Hexadecanamide	33.70	255	$C_{16}H_{33}NO$	1.67	0.95	1.51
33	Hexadecanenitrile	34.01	237	$C_{16}H_{31}N$	_	0.49	0.25
34	Oleic acid	35.87	282	$C_{18}H_{34}O_2$	0.15	0.65	0.36
35	Heptadecadienoic acid	36.07	266	$C_{17}H_{30}O_2$	_	0.65	0.38
36	3-nonadecene	36.88	266	$C_{19}H_{38}$	0.82	2.32	0.18
37	Phytol	37.02	296	$C_{20}H_{40}O$	_	_	0.34

3.12 Analysis of *C. vulgaris* water dispersible (WD) bio-oil fractions

The water dispersible fraction of CCA bio-oil samples obtained at 450, 500, and 550 °C pyrolysis temperatures were further partitioned into ether soluble (ES, 15% w/w) and aqueous (AQ, 85% w/w) fractions, that were respectively analyzed by GC-MS and HPLC to facilitate the identification of generated compounds.

Tables 3.11 and 3.12 list the identified compounds and their corresponding concentrations in the AQ and ES fractions of CCA bio-oil, respectively. Figure 3.19 illustrates the chromatogram of ES fraction of CCA bio-oil obtained at various pyrolysis temperatures. The most abundant compounds in the AQ fraction for 450 °C and 500 °C bio-oil samples respectively, were identified as formic acid (10.80, 16.29 µg/g), propionic acid (6.95, 4.75 µg/g), and 1,6-anhydro-β -D-glucopyranose (4.78, 3.29 µg/g). However, in the 550 °C bio-oil sample, the most abundant compounds were acetic acid at 6.15 µg/mg, followed by propionic acid (4.06 µg/g), and 1,6-anhydro-β -D-glucopyranose (2.79 µg/g). As previously mentioned, the lower molecular weight compounds such as acetic acid were most likely generated by fragmentation reactions at higher pyrolysis temperatures. [68]. Interestingly, no formic acid and glycerol were found in the 550 °C bio-oil samples. The absence of formic acid and glycerol, and the relatively higher abundance of ethanol in the 550 °C bio-oil sample suggests that not only there is a higher degree of degradation at increased pyrolysis temperatures, but new compounds of higher molecular weight may also form through chemical reactions.

The ES fraction bio-oil samples showed a more complex mixture of compounds. As anticipated by Py-GCMS results reported earlier in this chapter, palmitic acid was abundantly found in all three bio-oil samples. Multiple N-based compounds, such as indoles and pyrrole derivatives, were also identified, which further reinforced the results of Py–GCMS analysis.

The profusion of N-based compounds confirms thermal decomposition or recombination of amino acids during pyrolysis [79]. Moreover, in accordance with the Py-GCMS results, some aromatic hydrocarbons were identified, including phenol, methyl phenyls, guaiacol, and toluene derivatives. Previous studies suggest that phenols are the products of thermal fragmentation of free aromatic amino acids such as phenylalanine and tyrosine [117].

Table 3.11 Identified compounds via HPLC for AQ fraction of CCA bio-oil obtained at various pyrolysis temperatures.

Name	RT	Formula	450 °C µg/mg	500 °C µg/mg	550 °C µg/mg
Glucose	12.59	$C_6H_{12}O_6$	0.45	0.35	0.47
1,6-Anhydro-Beta-D-glucopyranose 98%	16.715	$C_6H_{10}O_5$	4.78	3.29	2.89
Lactic Acid	17.283	$C_3H_6O_3$	3.86	1.79	0.62
Glycerol	18.273	$C_3H_8O_3$	2.09	1.30	0.00
Formic Acid	18.507	CH_2O_2	10.80	16.28	0.00
Acetic Acid	20.005	$C_2H_4O_2$	1.48	1.17	6.15
Propionic Acid	23.315	$C_3H_6O_2$	6.95	4.75	4.06
Methanol	24.207	CH_3OH	2.70	2.39	1.82
Ethanol	27.232	C_2H_6O	0.81	0.89	1.06
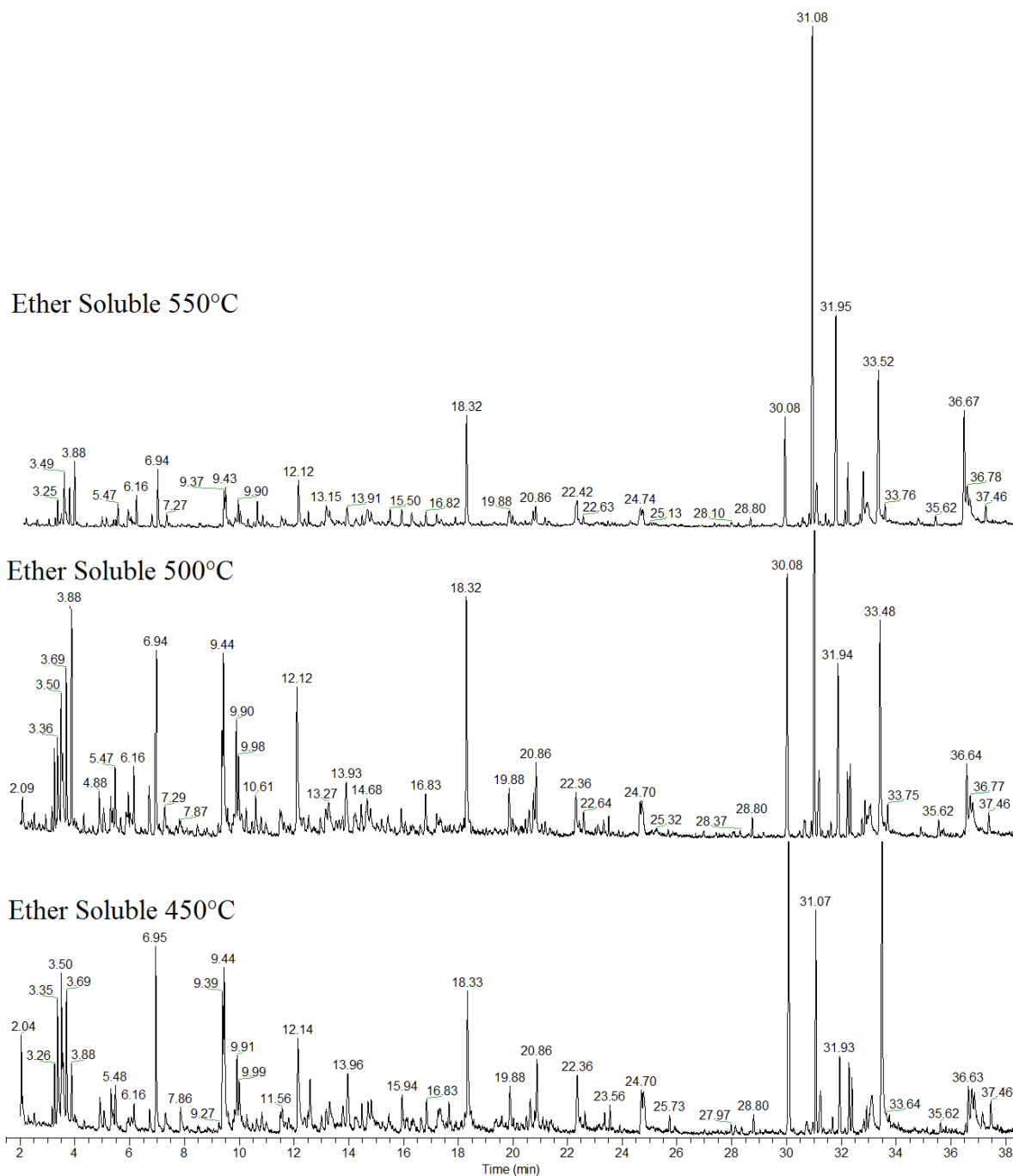
Figure 3.19 Chromatogram of ES fraction of CCA bio-oil samples obtained at various pyrolysis temperatures (450, 500 and 550 °C).

Table 3.12 Identified compounds via GC-MS for ES fraction of CCA bio-oil obtained at
various pyrolysis temperatures.

GC-MS	Compound	RT	M$^+$	Formula	450 °C µg/g	500 °C µg/g	550 °C µg/g
1	2-Furfurayl alcohol	2.93	98	C$_5$H$_6$O$_2$	29.30	55.18	40.07
2	Pyridine	3.16	74	C$_5$H$_5$N	29.54	85.10	64.58
3	3-methylbutanenitrile	3.25	83	C$_5$H$_9$N	90.27	211.00	164
4	2-butenone	3.37	72	C$_4$H$_6$O	238.58	258.28	99.25
5	4-Cyclopropyl-1-butene	3.49	96	C$_5$H$_4$O$_2$	342.67	614.53	356.97
6	3-Methyl-3-buten-2-one	3.56	84	C$_5$H$_8$N			104.11
7	Pyrrole	3.69	67	C$_4$H$_5$N	189.64	407.51	246.33
8	Toluene	3.88	92	C$_7$H$_8$	89.65	738.49	458.07
9	2,5-dimethylfuran	3.99	96	C$_6$H$_8$O	10.20	15.66	14.97
10	3-Methyl-3-buten-2-one	4.32	84	C$_5$H$_8$N	21.29	74.76	31.23
11	Methyl-dihydro-(2H)-pyran-2-one	4.65	112	C$_6$H$_8$O$_2$		26.97	25.11
12	3-Methyl-tetrahydrofuran-2,4-dione	4.83	114	C$_5$H$_6$O$_3$			9.97
13	2-methylpyrazine	4.88	94	C$_5$H$_6$N$_2$	67.71	165.25	78.53
14	Acetylfuran	5.03	110	C$_6$H$_6$O$_2$	37.87	113.33	100.18
15	Acetonitrile, amino	5.31	56	C$_2$H$_4$N$_2$	98.42	87.01	33.62
16	Furan	5.39	68	C$_4$H$_4$O			29.88
17	3-methylpyridine	5.47	93	C$_6$H$_7$N	66.48	47.23	159.63
18	2-methylpyrazine	5.67	81	C$_9$H$_6$N$_2$		54.70	18.11
19	Dihydro-methyl-furanone(Isomer)	5.84	98	C$_5$H$_8$O$_2$			140.99
20	Xylene	5.95	106	C$_8$H$_{10}$	44.40	70.88	31.52
21	Benzylnitrile	6.16	103	C$_{10}$H$_{14}$	38.66	186.97	215.61
22	Styrene	6.72	104	C$_8$H$_8$	52.74	211.51	102.67
23	Unknown:similar to 3-pentanone	6.94	56	C$_4$H$_9$Cl	362.86	914.91	456.59
24	2-Hydroxy-3-methyl-2-cyclopenten-1-one	7.27	112	C$_6$H$_8$O$_2$	69.64	113.33	129.32
25	Anisol=Benzene,methoxy-	7.47	108	C7H8O			12.46
26	Guaiacol	7.67	124	C7H8O2			23.22
27	2,5 dimethylpyridine	7.81	107	C$_7$H$_9$N	65.40	57.46	14.93
28	3-Methyl-1-hexene	8.03	94	C$_7$H$_{14}$			21.41
29	Ethylbenzene	8.1	106	C$_8$H$_{10}$			26.61
30	Propylbenzene	8.47	120	C$_9$H$_{12}$	35.78	56.16	33.53
31	Phenol	9.37	94	C$_6$H$_6$O	16.62	16.80	260.38
32	Unknown	9.58	138		660.33		25.82
33	Pyrimidone	9.79	96	C$_5$H$_6$N$_2$O		39.55	38.15
34	Catechol,3-methyl	9.9	124	C$_7$H$_8$O$_2$	156.62	284.43	163.21

GC-MS	Compound	RT	M⁺	Formula	450 °C µg/g	500 °C µg/g	550 °C µg/g
35	2,3,4-trimethylpyrrole	10.26	109	$C_7H_{11}N$	31.18	88.52	58.60
36	2-Methoxy-3H-azepine	10.48	123	C_7H_9NO	17.02	51.85	51.03
37	2-Cyclopenten-1-one, 2-hydroxy-3-methyl-	10.6	112	$C_6H_8O_2$	37.31	164.67	185.72
38	2-Methylthio-2,3-dimethylbutane	10.8	132	$C_7H_{16}S$	49.03	50.52	96.10
39	2-Cyclopenten-1-one, 2,3-dimethyl-	10.96	110	$C_7H_{10}O$	27.35	81.01	20.93
40	Benzene, butyl-	11.5	134	$C_{10}H_{14}$	93.35	183.44	131.07
41	2-methylphenol	11.64	108	C_7H_7O	26.93	646.11	60.70
42	Phenol, 4-methyl-	12.12	108	C_7H_8O	314.70	65.71	503.36
43	2,5-Dimethyl-4-hydroxy-3(2H)-furanone	12.34	128	$C_6H_8O_3$			86.37
44	Benzofuran, 2,3-dihydro-	12.49	120	C_8H_8O	174.19	36.52	96.73
45	Unknown	12.98	127		38.44	88.95	63.80
46	1H-Imidazole-4-carboxylic acid, methyl ester	13.15	126	$C_5H_6N_2O_2$	47.28	86.57	295.51
47	5-Hydroxymethyl-2-furaldehyde	13.27	126	$C_6H_{13}NO$	81.35	133.58	259.30
48	Benzene, (2-methyl-2-propenyl)-	13.53	132	$C_{10}H_{12}$		39.30	44.87
49	2,5-Pyrrolidinedione, 1-ethyl-	13.79	127	$C_6H_9NO_2$	60.42	70.43	35.35
50	4-ehylphenol	13.91	122	C_8H_7N	170.51	315.56	299.50
51	Phenol,4-allyl-	14.24	134	$C_9H_{10}O$	67.00	170.01	163.23
52	4-methyl guaiacol	14.47	138	$C_{11}H_{16}$	52.70	122.96	82.20
53	3-Pyridinol, 6-methyl-& unknown	14.67	109, 125	C_6H_7	63.56	157.57	272.49
54	2 4 Dimethyl-phenol	14.8	122	$C_8H_{10}O$	59.29	61.18	125.57
55	9-Oxabicyclo[3.3.1]nonan-3-ol	15.06	142	$C_8H_{14}O_2$		50.11	40.17
56	Phenol,4-propenyl-(cis)	15.2	134	$C_9H_{10}O$		63.78	58.67
57	Pyridine, 1-acetyl-1,2,3,4-tetrahydro-	15.41	120	$C_7H_{11}NO$	60.77	101.87	20.88
58	Benzoic acid, 4-hydroxy-	15.5	138	$C_7H_6O_3$			136.19
59	Pyridine, 2-propyl-	15.59	121	$C_8H_{11}N$		22.60	36.78
60	2-Methyl-2-phenylpropanenitrile	15.92	145	$C_{10}H_{11}N$	81.22	110.34	166.91
61	2,3-dihedrobenzofuran	16.28	120	C_8H_8O	54.36	14.71	193.82
62	1H-Pyrrole-2,5-dione, 3-ethyl-4-methyl-	16.62	139	$C_7H_9NO_2$	51.05	60.27	54.97
63	Benzenepropanenitrile	16.82	131	C_9H_9N	66.70	159.26	146.87
64	2-ethylphenol	17.21	122	$C_8H_{10}O$	147.63	78.60	117.43
65	Indole	18.32	117	C_8H_7N	429.35	1000.73	1032.98
66	2-Methoxy-4-vinylphenol	18.86	150	$C_9H_{10}O_2$			35.28
67	Unknown	19.33	132		42.03		69.43
68	Naphthalene, 1,2-dihydro-1,1,6-trimethyl-	19.88	172	$C_{13}H_{16}$	107.43	239.12	246.80
69	Naphthalene, 1,2,3,4-tetrahydro-1,1,6-trimethyl-	20.01	174	$C_{13}H_{18}$	16.53	60.90	88.90
70	Benzene, heptyl-	20.13	176	$C_{13}H_{20}$	13.24		39.12

GC-MS	Compound	RT	M⁺	Formula	450 °C µg/g	500 °C µg/g	550 °C µg/g
71	Guaiacol,4-propyl-	20.33	166	$C_{10}H_{14}$	16.40	44.26	58.15
72	4-Hydroxy-3-methyl-(5H)-furanone	20.63	114	$C_5H_6O_3$	72.39	105.42	15.76
73	1H-Indole, 3-methyl-	20.76	131	C_9H_9N		107.87	111.63
74	Octane, 3,5-dimethyl-	20.86	154	$C_{10}H_{22}$	179.35	216.46	170.78
75	Naphthalene, 1,5-dimethyl-	21.2	156	$C_{12}H_{12}$	17.88	68.00	82.10
76	Isoeugenol(cis)	21.31	164	$C_{10}H_{12}O_2$		179.87	71.60
77	Isoeugenol(trans)	22.41	164	$C_{10}H_{12}O_2$	69.55	27.57	460.74
78	Levoglocosan	22.63	162	$C_6H_{10}O_5$	36.03	86.49	80.80
79	Cyclotridecane	23.55	182	$C_{13}H_{26}$	43.22	65.35	34.78
80	Coniferyl alcohol	24.36	180	$C_{10}H_{12}O_3$		63.37	66.12
81	2,4-Imidazolidinedione, 5-(2-methylpropyl)-, (S)-	24.74	156	$C_7H_{12}N_2O_2$	260.50	94.27	265.69
82	Cyclopropane, 1-butyl-2-ethyl-	27.48	154	$C_{11}H_{22}$		22.05	47.35
83	Furaldehyde phenylhydrazone	28.34	186	$C_{11}H_{10}N_2O$	20.97	27.22	50.96
84	1-tridecene	28.8	168	$C_{13}H_{26}$	37.09	68.80	83.08
85	Myristic acid	30.98	228	$C_{14}H_{28}O_2$	36.24	49.90	110.02
86	Hexadecenoic acid	31.08	256	$C_{16}H_{30}O_2$	393.01	1668.50	4315.77
87	Linoleic	31.25	278	$C_{18}H_{32}O_2$	119.94	332.08	598.63
88	Sinapaldehyde	31.95	208	$C_{11}H_{12}O_4$	181.20	766.75	2195.40
89	Pentadecanenitrile	32.28	296	$C_{15}H_{29}N$	129.44	220.91	127.97
90	3,7,11,15-Tetramethyl-2-hexadecen-1-ol	32.39	278	$C_{20}H_{40}O$	94.08	241.81	534.85
91	Pyrrolo[1,2-a]pyrazine-1,4-dione, hexahydro-3-(2-methylpropyl)-	32.84	210	$C_{11}H_{18}N_2O_2$	49.56	70.27	65.80
92	13-Tetradece-11-yn-1-ol	32.95	208	$C_{14}H_{24}O$	43.99	103.25	453.99
93	N-Heptadecane	33.12	240	$C_{17}H_{36}$	171.08	184.47	294.22
94	Palmitic	33.52	256	$C_{16}H_{32}O_2$	925.54	1019.11	1694.08
95	11,14-Eicosadienoic acid, methyl ester	36.67	322	$C_{21}H_{38}O_2$	82.82	255.28	1107.12
96	Oleic acid(C18:2)	36.78	280	$C_{18}H_{34}O_2$	61.32	272.63	243.80
97	Stearic acid	36.88	284	$C_{18}H_{36}O_2$	44.34	77.85	163.13
98	Hexadecanamide	37.46	255	$C_{16}H_{33}NO$	66.88	85.77	162.98

Chapter 4: Conclusion

4.1 Challenges of pyrolysis

The process of producing fuels from microalgae through pyrolysis is still facing challenges that need to be addressed. The most significant challenge is reducing the cost of various steps of the pyrolysis process. Harvesting microalgae are usually associated with a very high cost and conducting it in an economically feasible way needs a lot of attention. Other main challenges are finding ways to facilitate the process of separating and collecting the liquid product of fast pyrolysis and designing and setting up large-scale commercial installations for fast pyrolysis of microalgae.

Studies have shown that algae in culture are highly dilute and a very energy-intensive drying process is required to prepare the samples before they can be pyrolyzed [34]. This is an on-going challenge for researchers and is the focus of much research. Additionally, bio-oil is a complex mixture of oxygenated compounds. This higher oxygen content of bio-oils compared to fossil fuels leads to their instability and high reactivity, causing challenges for its utilization biofuel can be utilized [20].

Producing biodiesel with a greater flow rate at lower temperatures is another challenge for researchers. Most of the microalgae bio-oil can be converted to biodiesel. The operability of this biodiesel in cold weather is defined as the lowest temperature a vehicle will operate without loss of power due to waxing of the fuel delivery system. The cold flow characteristics of diesel fuels are influenced by the source of the crude oil they are made from, how they are refined, and if they are mixed with dichloromethane. Generally, the better the cold flow characteristics of the base diesel fuel, the greater the effect of blending biodiesel on its cold

flow properties. Blending biodiesel and premium diesel fuels tend to affect cold flow properties more than blending biodiesel.

Selecting an appropriate algal strain is another sensitive step of the process, and it can cause significant challenges. Algae contain up to 40% lipids and fatty acids by weight as membrane components, storage products, metabolites, and sources of energy, and depending on the purpose of the process, it is really important to choose appropriate strain. Studies have shown that *Chlorella vulgaris* and *Chlorella protothecoides* have the most desirable features for pyrolysis. Hu et al. reported that fast pyrolysis of heterotrophic *C. protothecoides* cells yielded 3.4 times more bio-oil than that of autotrophic cells. The bio-oil was characterized by a much lower oxygen content, a higher heating value, and a lower density [36].

The infection of microalgae culture remains an important challenge. There is a high potential for microalgae to be contaminated by natural algae and bacteria from the environment. The solution to this is dense inoculum in a photobioreactor.
Even with all these challenges, microalgae biomass is still a very viable and promising renewable resource, and it has the potential to become an important player in the future energy supply chain [21].

4.2 Conclusion

In this work, chemical and thermal characteristics of *C. vulgaris* microalgae and its pyrolysis products were investigated. Differences were observed between commercial and U of I cultured *C. vulgaris* biomass, which could be attributed to the different cultivation environments. Both samples showed a very high nitrogen content due to the abundance of proteins in microalgae cellular structure. Their calorific values for both samples were

compared to that of residual bacterial biomass and higher than that of lignocellulosic biomass. TGA data showed that thermal decomposition of *C. vulgaris* happens at multiple stages, which further confirms its complex chemical nature. Fatty acids chain lengths in both biomass samples were in the C_{14}-C_{26} range, making *C. vulgaris* a promising contender for production of high-quality biofuel. The high concentration of starch in the biomass samples also contribute to their great biofuel potential. Py-GCMS results reinforced the complex chemical nature of microalgae biomass and its pyrolysis products. Most notable identified compounds were fatty acids (generated through decomposition of lipids), aromatic hydrocarbons (generated from amino acids with aromatic rings), and nitrogenous compounds (generated from proteins).

The highest CCA bio-oil yield (47.7%) was obtained at a pyrolysis temperature of 550 °C. The yield was higher than that of lignocellulosic biomass. The lipids and proteins in the structure of *C. vulgaris* biomass resulted in significant production of fatty acids and aromatic hydrocarbons during pyrolysis that was identified in the bio-oil samples. The GC-MS results of the bio-oil samples suggested that nitrogenous compounds derived from proteins can be converted to aromatic hydrocarbons in the same way that oxygenated compounds of lignocellulosic biomass are converted. CCA bio-oil contained a relatively low number of oxygenated compounds, which enhances the bio-oil stability and refinement process. In general, the increase in pyrolysis temperature improved the quality of the produced bio-oil. The bio-oil generated at 550 °C had the lowest moisture content and the highest calorific value, both of which are desirable traits for bio-oils. Due to their high nitrogen content, the bio-oil samples had high pH values, potentially making them suitable for direct use as boiler fuel.

The highest CCA biochar yield (42%) was obtained at a pyrolysis temperature of 450 °C. The yield was high due to high ash and protein contents of *C. vulgaris*. Analysis of the biochar samples results revealed that the CCA biochar has a reasonable amount of disordered amorphous carbon. This amorphous character promotes mineralization by bacteria and fungi, which is essential for nutrient turnover processes and aggregate formation. Furthermore, considering the high amount of nitrogen, biochar can provide great nutrients for plants, when added to the soil.

Future research should focus on optimizing pyrolysis operational parameters (particle size, temperature, and residence time) to improve the bio-oil or biochar yields and quality. Furthermore, examine different batches of U of I cultured algae to determine why a poor quality bio-oil was obtained by pyrolysis and could this issue be resolved.

4.3 Future research

Most current research on bio-oil extraction is focused on microalgae to produce biodiesel from algal-oil. Algae biomass can play an important role in solving global food and energy challenges in the near future. As previously mentioned, the high cost of producing biofuel through thermochemical conversion of biomass is their limiting factor when it comes to competing with petroleum. Future work on biofuel generation should focus on reducing this cost and further optimize the process to achieve biofuels that are chemically and physically more similar to conventional fossil fuels. Highest costs of thermal conversion of biomass to biofuel are associated with four steps: (i) harvesting microalgae, (ii) separating diluted microalgae from water, (iii) drying, and (iv) extracting the oil from microalgae

considering algae's unique cell walls. To reach large-scale biofuel production, future research should focus on optimizing and reducing the cost of any of these four steps in the process.

The results of this study suggest that improvements can be made in the process to increase the yield of desirable products. The 45% biochar yield obtained at 450°C can be increased to 60% by altering pyrolysis conditions. Considering the high nitrogen content of the biochar, it is a great candidate to be used as soil amendment.

The bio-oil yield was about 50% at the pyrolysis temperature of 550 °C. The dark, brownish, viscous liquid was found to be a complex organic mixture, mainly composed of amides, amines, N-heterocyclic compounds, carboxylic acids, ketones, phenols, hydrocarbons, and other oxygenated compounds. Some of these compounds can cause corrosion, poor thermal and chemical stability, high viscosity and immiscibility with hydrocarbon fuels. These weaknesses can be overcome with catalytic hydrotreatment, which targets the removal of oxygen in the bio-oil obtained from biomass. In hydrodeoxygenation (HDO) the catalyst plays a critical role as the reaction occurs on the surface of the applied catalyst. Therefore, it is possible to develop catalysts that can deoxygenate and reduce active functional groups before compounds undergo polymerization. This will ultimately impair the formation of coke. Ruthenium (Ru), nickel (Ni), and iron (Fe) are examples of catalysts presently used in the HDO process. Some of these catalysts, such as Ru, are rare earth metals and are very costly to obtain, which makes the process economically infeasible for large-scale bio-oil production. There is an eminent need for an affordable and easily-obtainable active HDO catalyst, and finding the right active element to use that can work as well as Ru, is a challenging and exciting future research direction. It is worth mentioning that researchers all

over the world have developed several methods including esterification, catalytic reforming, and ketonization, to upgrade the bio-oil.

There is an exciting future for fast pyrolysis and bio-oil improvements. Microalgae have advantages of higher photosynthetic efficiency, faster growth (than terrestrial crops), and higher carbon and hydrogen contents, which makes it the preferred biomass source for pyrolysis compared to lignocellulosic materials. Studies have shown that they are promising candidates for fuel production. Different species of algae may be better suited for different types of fuel. Developing microalgae with a high lipid content or "bioengineering microalgae" would a new and the promising way for biodiesel production in the future. Fast pyrolysis of microalgae has been the focus of many researchers in recent years. Despite all challenges associated with bio-oil production through fast pyrolysis such as its high cost and the high possibility of contamination, microalgae are one of the most viable contenders for replacing fossil fuels.

References

[1]   E. S. Shuba and D. Kifle, "Microalgae to biofuels: 'Promising' alternative and renewable energy, review," *Renew. Sustain. Energy Rev.*, vol. 81, no. Part 1, pp. 743–755, 2018.

[2]   G. Joshi, J. K. Pandey, S. Rana, and D. S. Rawat, "Challenges and opportunities for the application of biofuel," *Renew. Sustain. Energy Rev.*, vol. 79, no. Supplement C, pp. 850–866, 2017.

[3]   R. Gunawan *et al.*, "Upgrading of bio-oil into advanced biofuels and chemicals. Part I. Transformation of GC-detectable light species during the hydrotreatment of bio-oil using Pd/C catalyst," *Fuel*, vol. 111, no. Supplement C, pp. 709–717, 2013.

[4]   X. Junming, J. Jianchun, S. Yunjuan, and L. Yanju, "Bio-oil upgrading by means of ethyl ester production in reactive distillation to remove water and to improve storage and fuel characteristics," *Biomass and Bioenergy*, vol. 32, no. 11, pp. 1056–1061, 2008.

[5]   L. Ma, T. Wang, Q. Liu, X. Zhang, W. Ma, and Q. Zhang, "A review of thermal–chemical conversion of lignocellulosic biomass in China," *Biotechnol. Adv.*, vol. 30, no. 4, pp. 859–873, 2012.

[6]   P. Alvira, E. Tomás-Pejó, M. Ballesteros, and M. J. Negro, "Pretreatment technologies for an efficient bioethanol production process based on enzymatic hydrolysis: A review," *Bioresour. Technol.*, vol. 101, no. 13, pp. 4851–4861, 2010.

[7]   F. Ma and M. A. Hanna, "Biodiesel production: a review1Journal Series #12109, Agricultural Research Division, Institute of Agriculture and Natural Resources, University of Nebraska–Lincoln.1," *Bioresour. Technol.*, vol. 70, no. 1, pp. 1–15, 1999.

[8]   A. V Bridgwater, "Review of fast pyrolysis of biomass and product upgrading," *Biomass and Bioenergy*, vol. 38, no. Supplement C, pp. 68–94, 2012.

[9]   A. Kumar, D. D. Jones, and M. A. Hanna, "Thermochemical Biomass Gasification: A Review of the Current Status of the Technology," *Energies*, vol. 2, no. 3, pp. 556–581, 2009.

[10] P. Dürre, "Biobutanol: An attractive biofuel," *Biotechnol. J.*, vol. 2, no. 12, pp. 1525–1534, Dec. 2007.

[11] P. D. Patil *et al.*, "Optimization of direct conversion of wet algae to biodiesel under supercritical methanol conditions," *Bioresour. Technol.*, vol. 102, no. 1, pp. 118–122, 2011.

[12] P. C. Smith, Y. Ngothai, Q. D. Nguyen, and B. K. O'Neill, "Improving the low-temperature properties of biodiesel: Methods and consequences," *Renew. Energy*, vol. 35, no. 6, pp. 1145–1151, 2010.

[13] W. Al Maksoud, C. Larabi, A. Garron, K. C. Szeto, J. J. Walter, and C. C. Santini, "Direct thermocatalytic transformation of pine wood into low oxygenated biofuel," *Green Chem.*, vol. 16, no. 6, pp. 3031–3038, 2014.

[14] T. Dickerson and J. Soria, "Catalytic Fast Pyrolysis: A Review," *Energies*, vol. 6, no. 1, pp. 514–538, 2013.

[15] P.-C. Kuo, W. Wu, and W.-H. Chen, "Gasification performances of raw and torrefied biomass in a downdraft fixed bed gasifier using thermodynamic analysis," *Fuel*, vol. 117, no. Part B, pp. 1231–1241, 2014.

[16] D. R. Vardon, B. K. Sharma, G. V Blazina, K. Rajagopalan, and T. J. Strathmann, "Thermochemical conversion of raw and defatted algal biomass via hydrothermal liquefaction and slow pyrolysis," *Bioresour. Technol.*, vol. 109, no. Supplement C, pp. 178–187, 2012.

[17] A. Demirbas and M. F. Demirbas, *Algae Energy: Algae as a New Source of Biodiesel*. 2010.

[18] Z. Wen, "Algae for Biofuel Production." [Online]. Available: http://articles.extension.org/pages/26600/algae-for-biofuel-production.

[19] W.-H. Chen, B.-J. Lin, M.-Y. Huang, and J.-S. Chang, "Thermochemical conversion of microalgal biomass into biofuels: A review," *Bioresour. Technol.*, vol. 184, no. Supplement C, pp. 314–327, 2015.

[20] A. Demirbas, "Use of algae as biofuel sources," *Energy Convers. Manag.*, vol. 51, no. 12, pp. 2738–2749, Dec. 2010.

[21] S. Grierson, V. Strezov, G. Ellem, R. Mcgregor, and J. Herbertson, "Thermal characterization of microalgae under slow pyrolysis conditions," *J. Anal. Appl. Pyrolysis*, vol. 85, no. 1, pp. 118–123, 2009.

[22] R. C. Brown, Ed., "Fast Pyrolysis," in *Thermochemical Processing of Biomass: Conversion into Fuels, Chemicals and Power*, John Wiley & Sons, 2011, pp. 124–156.

[23] X. Miao, Q. Wu, and C. Yang, "Fast pyrolysis of microalgae to produce renewable fuels," *J. Anal. Appl. Pyrolysis*, vol. 71, no. 2, pp. 855–863, 2004.

[24] S.-K. Kim, *Handbook of Marine Macroalgae*. John Wiley & Sons, 2011.

[25] J. Sheehan, T. Dunahay, J. Benemann, and P. Roessler, *Look Back at the U.S. Department of Energy's Aquatic Species Program: Biodiesel from Algae; Close-Out Report*. 1998.

[26] J. R. Benavente-Valdés, C. Aguilar, J. C. Contreras-Esquivel, A. Méndez-Zavala, and J. Montañez, "Strategies to enhance the production of photosynthetic pigments and lipids in Chlorophyceae species," *Biotechnol. Reports*, vol. 10, no. Supplement C, pp. 117–125, 2016.

[27] A. S. Carlsson, J. B. van Beilen, R. Moller, and D. Clayton, "No TitleMicro- and Macro-algae: Utility for Industrial Applications," UK, 2007.

[28] Y. Chisti, "Biodiesel from microalgae," *Biotechnol. Adv.*, vol. 25, no. 3, pp. 294–306, 2007.

[29] V. Das, "Different strains of Microalgae suitable for biodiesel production." 2015.

[30] S. P.S., "Isolation and Characterization green microalgae for Carbon Sequestration Wastewater treatment and biofuel production, International Journal of Bioscience and Biotechnology, Vol.5 (2):17-26, April 2013.," 2013.

[31] M. Hannon, J. Gimpel, M. Tran, B. Rasala, and S. Mayfield, "Biofuels from algae: challenges and potential," *Biofuels*, vol. 1, no. 5. pp. 763–784, Sep-2010.

[32] M. N. Campbell, "Biodiesel: Algae as a Renewable Source for Liquid Fuel," *Guelph Eng. J.*, vol. 1, pp. 2–7, 2008.

[33] E. M. Grima, E.-H. Belarbi, F. G. A. Fernández, A. R. Medina, and Y. Chisti, "Recovery of microalgal biomass and metabolites: process options and economics," *Biotechnol. Adv.*, vol. 20, no. 7, pp. 491–515, 2003.

[34] W. Peng, Q. Wu, P. Tu, and N. Zhao, "Pyrolytic characteristics of microalgae as renewable energy source determined by thermogravimetric analysis," *Bioresour. Technol.*, vol. 80, no. 1, pp. 1–7, 2001.

[35] C. Baskar, S. Baskar, and R. S. Dhillon, *Biomass Conversion: The Interface of Biotechnology, Chemistry and Materials Science*. Springer Berlin Heidelberg, 2012.

[36] Z. Hu, X. Ma, and L. Li, "The characteristic and evaluation method of fast pyrolysis of microalgae to produce syngas," *Bioresour. Technol.*, vol. 140, no. Supplement C, pp. 220–226, 2013.

[37] X. Miao and Q. Wu, "Biodiesel production from heterotrophic microalgal oil," *Bioresour. Technol.*, vol. 97, no. 6, pp. 841–846, 2006.

[38] M. Verma, S. Godbout, S. K. Brar, O. Solomatnikova, S. P. Lemay, and J. P. Larouche, "Biofuels Production from Biomass by Thermochemical Conversion Technologies," *Int. J. Chem. Eng.*, vol. 2012, 2012.

[39] X. Miao and Q. Wu, "High yield bio-oil production from fast pyrolysis by metabolic controlling of Chlorella protothecoides," *J. Biotechnol.*, vol. 110, no. 1, pp. 85–93, 2004.

[40] D. Mohan, C. U. Pittman, and P. H. Steele, "Pyrolysis of Wood/Biomass for Bio-oil: A Critical Review," *Energy & Fuels*, vol. 20, no. 3, pp. 848–889, 2006.

[41] A. Demirbas, "Progress and recent trends in biofuels," *Prog. Energy Combust. Sci.*, vol. 33, no. 1, pp. 1–18, 2007.

[42] J. An, L. Bagnell, T. Cablewski, C. R. Strauss, and R. W. Trainor, "Applications of High-Temperature Aqueous Media for Synthetic Organic Reactions," *J. Org. Chem.*, vol. 62, no. 8, pp. 2505–2511, 1997.

[43] A. Alcalá and A. V Bridgwater, "Upgrading fast pyrolysis liquids: blends of biodiesel and pyrolysis oil," *Fuel*, vol. 109, pp. 417–426, 2014.

[44] A. V Bridgwater, "Review of fast pyrolysis of biomass and product upgrading," *Biomass and Bioenergy*, vol. 38, no. Supplement C, pp. 68–94, 2012.

[45] J. P. Diebold *et al.*, "Proposed Specifications for Various Grades of Pyrolysis Oils," in *Developments in Thermochemical Biomass Conversion: Volume 1 / Volume 2*, A. V Bridgwater and D. G. B. Boocock, Eds. Dordrecht: Springer Netherlands, 1997, pp. 433–447.

[46] T. A. Milne, R. J. Evans, and N. Nagle, "Catalytic Conversion of Microalgae and Vegetable Oils to Premium Gasoline, With Shape-Selective Zeolites," *Biomass*, vol. 21, pp. 219–232, 1990.

[47] H. F. Gerçel, "The Effect of a Sweeping Gas Flow Rate on the Fast Pyrolysis of Biomass," *Energy Sources*, vol. 24, no. 7, pp. 633–642, 2002.

[48] A. E. Pütün, "Biomass to Bio-Oil via Fast Pyrolysis of Cotton Straw and Stalk," *Energy Sources*, vol. 24, no. 3, pp. 275–285, 2002.

[49] H. F. Gerçel, "The Effect of a Sweeping Gas Flow Rate on the Fast Pyrolysis of Biomass," *Energy Sources*, vol. 24, no. 7, pp. 633–642, 2002.

[50] S. Liang, L. Wei, M. L. Passero, K. Feris, and A. Mcdonald, "Hydrothermal liquefaction of laboratory cultivated and commercial algal biomass into crude bio-oil," *Environ. Prog. Sustain. Energy*, 2017.

[51] D. Chen, Y. Zheng, and X. Zhu, "In-depth investigation on the pyrolysis kinetics of raw biomass. Part I: Kinetic analysis for the drying and devolatilization stages," *Bioresour. Technol.*, vol. 131, no. Supplement C, pp. 40–46, 2013.

[52] T. Damartzis, D. Vamvuka, S. Sfakiotakis, and A. Zabaniotou, "Thermal degradation studies and kinetic modeling of cardoon (Cynara cardunculus) pyrolysis using thermogravimetric analysis (TGA)," *Bioresour. Technol.*, vol. 102, no. 10, pp. 6230–6238, 2011.

[53] J. H. Flynn, "The isoconversional method for determination of energy of activation at constant heating rates," *J. Therm. Anal.*, vol. 27, no. 1, pp. 95–102, May 1983.

[54] M. J. Starink, "A new method for the derivation of activation energies from experiments performed at a constant heating rate," *Thermochim. Acta*, vol. 288, no. 1, pp. 97–104, 1996.

[55] A. O. Balogun, O. A. Lasode, and A. G. McDonald, "Devolatilisation kinetics and pyrolytic analyses of Tectona grandis (teak)," *Bioresour. Technol.*, vol. 156, no. Supplement C, pp. 57–62, 2014.

[56] C. D. DOYLE, "Series Approximations to the Equation of Thermogravimetric Data," *Nature*, vol. 207, p. 290, Jul. 1965.

[57] L. Wei, N. M. Stark, and A. G. McDonald, "Interfacial improvements in biocomposites based on poly(3-hydroxybutyrate) and poly(3-hydroxybutyrate-co-3-hydroxyvalerate)

bioplastics reinforced and grafted with [small alpha]-cellulose fibers," *Green Chem.*, vol. 17, no. 10, pp. 4800–4814, 2015.

[58] L. Zhao, X. Cao, O. Mašek, and A. Zimmerman, "Heterogeneity of biochar properties as a function of feedstock sources and production temperatures," *J. Hazard. Mater.*, vol. 256–257, no. Supplement C, pp. 1–9, 2013.

[59] K. Sipilä, E. Kuoppala, L. Fagernäs, and A. Oasmaa, "Characterization of biomass-based flash pyrolysis oils," *Biomass and Bioenergy*, vol. 14, no. 2, pp. 103–113, 1998.

[60] A. M. Rizzo, M. Prussi, L. Bettucci, I. M. Libelli, and D. Chiaramonti, "Characterization of microalga Chlorella as a fuel and its thermogravimetric behavior," *Appl. Energy*, vol. 102, no. Supplement C, pp. 24–31, 2013.

[61] A. Marcilla, A. Gómez-Siurana, C. Gomis, E. Chápuli, M. C. Catalá, and F. J. Valdés, "Characterization of microalgal species through TGA/FTIR analysis: Application to nannochloropsis sp.," *Thermochim. Acta*, vol. 484, no. 1, pp. 41–47, 2009.

[62] L. Pane, E. Franceschi, L. De Nuccio, and A. Carli, "Applications of Thermal Analysis on the Marine Phytoplankton, Tetraselmis Suecica," *J. Therm. Anal. Calorim.*, vol. 66, no. 1, pp. 145–154, Oct. 2001.

[63] A. Marcilla, A. Gómez-Siurana, C. Gomis, E. Chápuli, M. C. Catalá, and F. J. Valdés, "Characterization of microalgal species through TGA/FTIR analysis: Application to nannochloropsis sp.," *Thermochim. Acta*, vol. 484, no. 1, pp. 41–47, 2009.

[64] E. Biagini, A. Fantei, and L. Tognotti, "Effect of the heating rate on the devolatilization of biomass residues," *Thermochim. Acta*, vol. 472, no. 1, pp. 55–63, 2008.

[65] M. A. Lopez-Velazquez, V. Santes, J. Balmaseda, and E. Torres-Garcia, "Pyrolysis of orange waste: A thermo-kinetic study," *J. Anal. Appl. Pyrolysis*, vol. 99, no. Supplement C, pp. 170–177, 2013.

[66] D. Chen, Y. Zheng, and X. Zhu, "In-depth investigation on the pyrolysis kinetics of raw biomass. Part I: Kinetic analysis for the drying and devolatilization stages," *Bioresour. Technol.*, vol. 131, no. Supplement C, pp. 40–46, 2013.

[67] A. M. Rizzo, M. Prussi, L. Bettucci, I. M. Libelli, and D. Chiaramonti, "Characterization of microalga Chlorella as a fuel and its thermogravimetric behavior," *Appl. Energy*, vol. 102, no. Supplement C, pp. 24–31, 2013.

[68] H. N. Almeida *et al.*, "Characterization and pyrolysis of Chlorella vulgaris and Arthrospira platensis: the potential of bio-oil and chemical production by Py-GC/MS analysis," *Environ. Sci. Pollut. Res.*, vol. 24, no. 16, pp. 14142–14150, Jun. 2017.

[69] C. Chen, X. Ma, and Y. He, "Co-pyrolysis characteristics of microalgae Chlorella vulgaris and coal through TGA," *Bioresour. Technol.*, vol. 117, no. Supplement C, pp. 264–273, 2012.

[70] A. Agrawal and S. Chakraborty, "A kinetic study of pyrolysis and combustion of microalgae Chlorella vulgaris using thermo-gravimetric analysis," *Bioresour. Technol.*, vol. 128, no. Supplement C, pp. 72–80, 2013.

[71] B. Kang, K. Honda, K. Okano, T. Aki, T. Omasa, and H. Ohtake, "Thermal analysis for differentiating between oleaginous and non-oleaginous microorganisms," *Biochem. Eng. J.*, vol. 57, no. Supplement C, pp. 23–29, 2011.

[72] P. Das, A. Ganesh, and P. Wangikar, "Influence of pretreatment for deashing of sugarcane bagasse on pyrolysis products," *Biomass and Bioenergy*, vol. 27, no. 5, pp. 445–457, 2004.

[73] C. E. Greenhalf, D. J. Nowakowski, A. B. Harms, J. O. Titiloye, and A. V Bridgwater, "A comparative study of straw, perennial grasses and hardwoods in terms of fast pyrolysis products."

[74] D. Carpenter, T. L. Westover, S. Czernik, and W. Jablonski, "Biomass feedstocks for renewable fuel production: a review of the impacts of feedstock and pretreatment on the yield and product distribution of fast pyrolysis bio-oils and vapors," *Green Chem.*, vol. 16, no. 2, pp. 384–406, 2014.

[75] R. M. Braga, T. R. Costa, J. C. O. Freitas, J. M. F. Barros, D. M. A. Melo, and M. A. F. Melo, "Pyrolysis kinetics of elephant grass pretreated biomasses," *J. Therm. Anal. Calorim.*, vol. 117, no. 3, pp. 1341–1348, Sep. 2014.

[76] M. M. Phukan, R. S. Chutia, B. K. Konwar, and R. Kataki, "Microalgae Chlorella as a potential bio-energy feedstock," *Appl. Energy*, vol. 88, no. 10, pp. 3307–3312, 2011.

[77] A. M. Illman, A. H. Scragg, and S. W. Shales, "Increase in Chlorella strains calorific values when grown in low nitrogen medium," *Enzyme Microb. Technol.*, vol. 27, no. 8, pp. 631–635, 2000.

[78] M. M. Phukan, R. S. Chutia, B. K. Konwar, and R. Kataki, "Microalgae Chlorella as a potential bio-energy feedstock," *Appl. Energy*, vol. 88, no. 10, pp. 3307–3312, 2011.

[79] L. Wei *et al.*, "Production and characterization of bio-oil and biochar from the pyrolysis of residual bacterial biomass from a polyhydroxyalkanoate production process," *J. Anal. Appl. Pyrolysis*, vol. 115, pp. 268–278, 2015.

[80] P. Sannigrahi, A. J. Ragauskas, and G. A. Tuskan, "Poplar as a feedstock for biofuels: A review of compositional characteristics," *Biofuels, Bioprod. Biorefining*, vol. 4, no. 2, pp. 209–226, 2010.

[81] J. Yanik, R. Stahl, N. Troeger, and A. Sinag, "Pyrolysis of algal biomass," *J. Anal. Appl. Pyrolysis*, vol. 103, no. Supplement C, pp. 134–141, 2013.

[82] A. M. Illman, A. H. Scragg, and S. W. Shales, "Increase in Chlorella strains calorific values when grown in low nitrogen medium," *Enzyme Microb. Technol.*, vol. 27, no. 8, pp. 631–635, 2000.

[83] C. E. Brewer, "Biochar characterization and engineering," Iowa State University, 2012.

[84] S. Liang, Y. Han, L. Wei, and A. G. McDonald, "Production and characterization of bio-oil and bio-char from pyrolysis of potato peel wastes," *Biomass Convers. Biorefinery*, vol. 5, no. 3, pp. 237–246, Sep. 2015.

[85] L. M. L. Laurens, M. Quinn, S. Van Wychen, D. W. Templeton, and E. J. Wolfrum, "Accurate and reliable quantification of total microalgal fuel potential as fatty acid methyl esters by in situ transesterification," *Anal. Bioanal. Chem.*, vol. 403, no. 1, pp. 167–178, Apr. 2012.

[86] H. Zheng, J. Yin, Z. Gao, H. Huang, X. Ji, and C. Dou, "Disruption of Chlorella vulgaris Cells for the Release of Biodiesel-Producing Lipids: A Comparison of Grinding, Ultrasonication, Bead Milling, Enzymatic Lysis, and Microwaves," *Appl. Biochem. Biotechnol.*, vol. 164, no. 7, pp. 1215–1224, Aug. 2011.

[87] G. Petkov and G. Garcia, "Which are fatty acids of the green alga Chlorella?," *Biochem. Syst. Ecol.*, vol. 35, pp. 281–285, 2007.

[88] Z. Wang *et al.*, "Oil Crop Biomass Residue-Based Media for Enhanced Algal Lipid Production," *Appl. Biochem. Biotechnol.*, vol. 171, no. 3, pp. 689–703, Oct. 2013.

[89] T. Coward, J. G. M. Lee, and G. S. Caldwell, "Harvesting microalgae by CTAB-aided foam flotation increases lipid recovery and improves fatty acid methyl ester

characteristics," *Biomass and Bioenergy*, vol. 67, no. Supplement C, pp. 354–362, 2014.

[90] Y. A. Tsigie, L. H. Huynh, I. N. Ahmed, and Y.-H. Ju, "Maximizing biodiesel production from Yarrowia lipolytica Po1g biomass using subcritical water pretreatment," *Bioresour. Technol.*, vol. 111, no. Supplement C, pp. 201–207, 2012.

[91] L. H. Huynh, P. L. T. Nguyen, Q. P. Ho, and Y.-H. Ju, "Catalyst-free fatty acid methyl ester production from wet activated sludge under subcritical water and methanol condition," *Bioresour. Technol.*, vol. 123, no. Supplement C, pp. 112–116, 2012.

[92] Q. Hu *et al.*, "Microalgal triacylglycerols as feedstocks for biofuel production: perspectives and advances," *Plant J.*, vol. 54, no. 4, pp. 621–639, 2008.

[93] C.-Y. Chen *et al.*, "Microalgae-based carbohydrates for biofuel production," *Biochem. Eng. J.*, vol. 78, no. Supplement C, pp. 1–10, 2013.

[94] C.-Y. Chen *et al.*, "Microalgae-based carbohydrates for biofuel production," *Biochem. Eng. J.*, vol. 78, no. Supplement C, pp. 1–10, 2013.

[95] S.-H. Ho, S.-W. Huang, C.-Y. Chen, T. Hasunuma, A. Kondo, and J.-S. Chang, "Characterization and optimization of carbohydrate production from an indigenous microalga Chlorella vulgaris FSP-E," *Bioresour. Technol.*, vol. 135, no. Supplement C, pp. 157–165, 2013.

[96] D. W. Templeton, M. Quinn, S. Van Wychen, D. Hyman, and L. M. L. Laurens, "Separation and quantification of microalgal carbohydrates," *J. Chromatogr. A*, vol. 1270, no. Supplement C, pp. 225–234, 2012.

[97] S. Paul-André and M. Norio, *Lipids in Photosynthesis: Structure, Function and Genetics*. 1998.

[98] K. Noda *et al.*, "A Water-Soluble Antitumor Glycoprotein from Chlorella vulgaris," *Planta Med*, vol. 62, no. 5, pp. 423–426, 1996.

[99] K. Wang, "Pyrolysis and catalytic pyrolysis of protein- and lipid-rich feedstock," Iowa State University, 2014.

[100] K. D. Maher and D. C. Bressler, "Pyrolysis of triglyceride materials for the production of renewable fuels and chemicals," *Bioresour. Technol.*, vol. 98, no. 12, pp. 2351–2368, 2007.

[101] Z. Du *et al.*, "Catalytic pyrolysis of microalgae and their three major components: Carbohydrates, proteins, and lipids," *Bioresour. Technol.*, vol. 130, no. Supplement C, pp. 777–782, 2013.

[102] B. M. E. Chagas *et al.*, "Catalytic pyrolysis-GC/MS of Spirulina: Evaluation of a highly proteinaceous biomass source for production of fuels and chemicals," *Fuel*, vol. 179, no. Supplement C, pp. 124–134, 2016.

[103] K. Kebelmann, A. Hornung, U. Karsten, and G. Griffiths, "Intermediate pyrolysis and product identification by TGA and Py-GC/MS of green microalgae and their extracted protein and lipid components," *Biomass and Bioenergy*, vol. 49, no. Supplement C, pp. 38–48, 2013.

[104] M. E. Sánchez *et al.*, "Effect of pyrolysis temperature on the composition of the oils obtained from sewage sludge," *Biomass and Bioenergy*, vol. 33, no. 6, pp. 933–940, 2009.

[105] Z. T. Dobroth, S. Hu, E. R. Coats, and A. G. McDonald, "Polyhydroxybutyrate synthesis on biodiesel wastewater using mixed microbial consortia," *Bioresour. Technol.*, vol. 102, no. 3, pp. 3352–3359, 2011.

[106] V. Anand, V. Sunjeev, and R. Vinu, "Catalytic fast pyrolysis of Arthrospira platensis (spirulina) algae using zeolites," *J. Anal. Appl. Pyrolysis*, vol. 118, no. Supplement C, pp. 298–307, 2016.

[107] A. Ferreira, A. Soares Dias, C. Silva, and M. Costa, "Bio-oil and bio-char characterization from microalgal biomass," *Carbon N. Y.*, vol. 47, p. 50.3, 2014.

[108] K. Wang, R. C. Brown, S. Homsy, L. Martinez, and S. S. Sidhu, "Fast pyrolysis of microalgae remnants in a fluidized bed reactor for bio-oil and biochar production," *Bioresour. Technol.*, vol. 127, no. Supplement C, pp. 494–499, 2013.

[109] A. H. Zacher, D. C. Elliott, M. V Olarte, D. M. Santosa, F. Preto, and K. Iisa, "Pyrolysis of Woody Residue Feedstocks: Upgrading of Bio-oils from Mountain-Pine-Beetle-Killed Trees and Hog Fuel," *Energy & Fuels*, vol. 28, no. 12, pp. 7510–7516, 2014.

[110] L. Zhao, X. Cao, O. Mašek, and A. Zimmerman, "Heterogeneity of biochar properties as a function of feedstock sources and production temperatures," *J. Hazard. Mater.*, vol. 256–257, no. Supplement C, pp. 1–9, 2013.

[111] L. Wei, N. M. Stark, and A. G. McDonald, "Interfacial improvements in biocomposites based on poly(3-hydroxybutyrate) and poly(3-hydroxybutyrate-co-3-hydroxyvalerate) bioplastics reinforced and grafted with [small alpha]-cellulose fibers," *Green Chem.*, vol. 17, no. 10, pp. 4800–4814, 2015.

[112] I. Fonts, M. Azuara, G. Gea, and M. B. Murillo, "Study of the pyrolysis liquids obtained from different sewage sludge," *J. Anal. Appl. Pyrolysis*, vol. 85, no. 1, pp. 184–191, 2009.

[113] Z. Hu, Y. Zheng, F. Yan, B. Xiao, and S. Liu, "Bio-oil production through pyrolysis of blue-green algae blooms (BGAB): Product distribution and bio-oil characterization," *Energy*, vol. 52, no. Supplement C, pp. 119–125, 2013.

[114] Z. Du *et al.*, "Microwave-assisted pyrolysis of microalgae for biofuel production," *Bioresour. Technol.*, vol. 102, no. 7, pp. 4890–4896, 2011.

[115] A. B. Ross, J. M. Jones, M. L. Kubacki, and T. Bridgeman, "Classification of macroalgae as fuel and its thermochemical behaviour," *Bioresour. Technol.*, vol. 99, no. 14, pp. 6494–6504, 2008.

[116] D. Zhou, L. Zhang, S. Zhang, H. Fu, and J. Chen, "Hydrothermal Liquefaction of Macroalgae Enteromorpha prolifera to Bio-oil," *Energy & Fuels*, vol. 24, no. 7, pp. 4054–4061, 2010.

[117] D. Fabbri, A. Adamiano, G. Falini, R. De Marco, and I. Mancini, "Analytical pyrolysis of dipeptides containing proline and amino acids with polar side chains. Novel 2,5-diketopiperazine markers in the pyrolysates of proteins," *J. Anal. Appl. Pyrolysis*, vol. 95, no. Supplement C, pp. 145–155, 2012.

Appendix
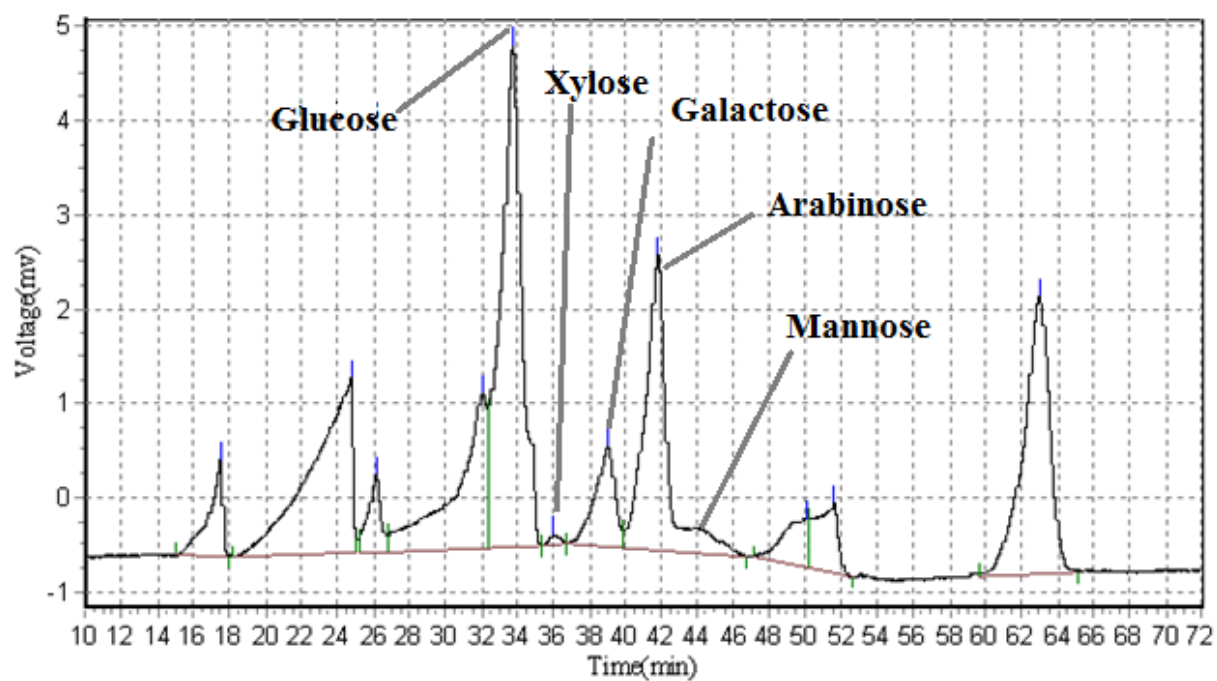
HPLC chromatogram of standard solution.
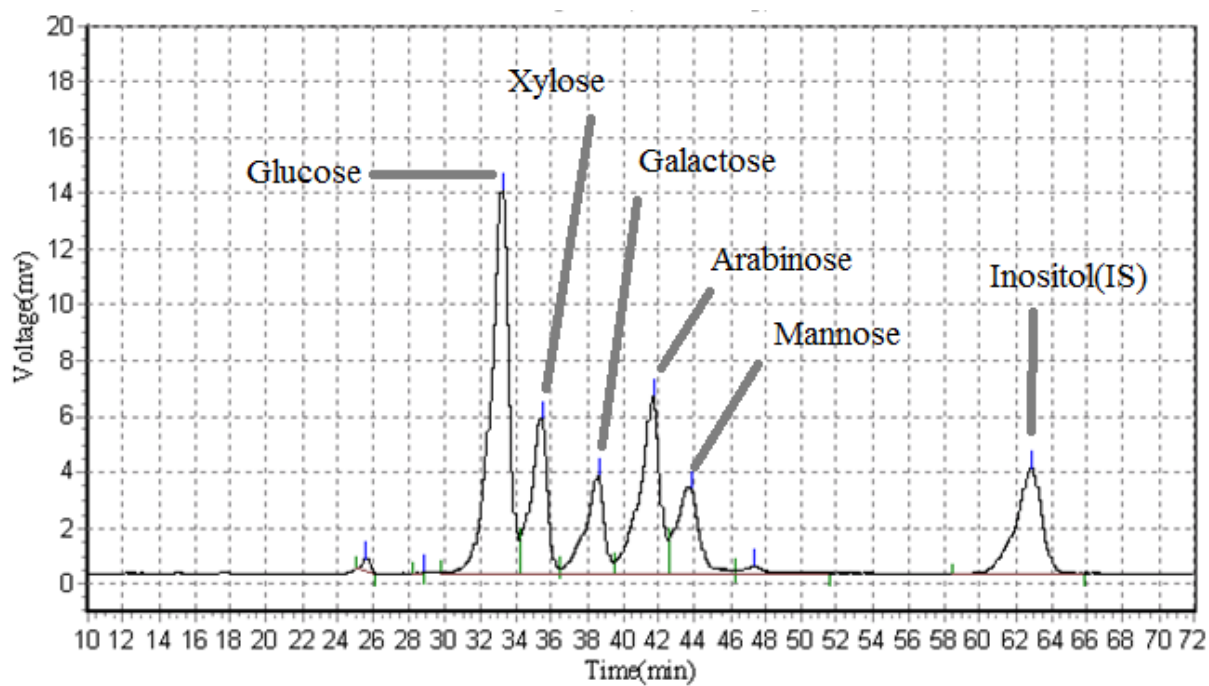
HPLC chromatogram of *C. vulgaris*.